AD_____

Award Number: W81XWH-13-1-0016

TITLE: Underbody Blast Models of TBI Caused by Hyper- Acceleration and Secondary Head Impact

PRINCIPAL INVESTIGATOR: Dr. Gary Fiskum

CONTRACTING ORGANIZATION: University of Maryland
Baltimore, MD 21201

REPORT DATE: February 2014

TYPE OF REPORT: Annual

PREPARED FOR: U.S. Army Medical Research and Materiel Command
Fort Detrick, Maryland 21702-5012

DISTRIBUTION STATEMENT: Approved for Public Release;
Distribution Unlimited

REPORT DOCUMENTATION PAGE

Form Approved
OMB No. 0704-0188

1. REPORT DATE *(DD-MM-YYYY)*	2. REPORT TYPE	3. DATES COVERED *(From - To)*
February 2014	Annual	06January2013–05January2014

4. TITLE AND SUBTITLE

Underbody Blast Models of TBI Caused by Hyper- Acceleration and Secondary Head Impact

5a. CONTRACT NUMBER

5b. GRANT NUMBER
W81XWH-13-1-0016

5c. PROGRAM ELEMENT NUMBER

6. AUTHOR(S)
Dr. Gary Fiskum

Dr. William Fourney
EMAIL: gfiskum@anes.umm.edu

5d. PROJECT NUMBER

5e. TASK NUMBER

5f. WORK UNIT NUMBER

7. PERFORMING ORGANIZATION NAME(S) AND ADDRESS(ES)

University of Maryland,
Baltimore

Baltimore, MD 21201

8. PERFORMING ORGANIZATION REPORT NUMBER

9. SPONSORING / MONITORING AGENCY NAME(S) AND ADDRESS(ES)
U.S. Army Medical Research and Materiel Command
Fort Detrick, Maryland 21702-5012

10. SPONSOR/MONITOR'S ACRONYM(S)

11. SPONSOR/MONITOR'S REPORT NUMBER(S)

12. DISTRIBUTION / AVAILABILITY STATEMENT
Approved for Public Release; Distribution Unlimited

13. SUPPLEMENTARY NOTES

14. ABSTRACT

There is a high incidence of TBI among warfighter occupants of vehicles targeted by underbody blasts but little is known about the unique forces involved or the pathophysiology.

We hypothesize:

- Acceleration experienced during survivable underbody blasts produces dose-dependent, TBI.
- Underbody blast-induced acceleration combined with secondary head impact is also military relevant and can be modeled.
- Neurologic outcome following underbody blast-induced TBI can be improved by force-modifying vehicle hull designs.
- We will expand our underbody blast animal model of TBI to establish full dose-response relationships and to model the combination of acceleration plus head impact. This research will promote development of engineering- and biomedical-based neuroprotective interventions translatable to warfighter TBI.

15. SUBJECT TERMS none provided

16. SECURITY CLASSIFICATION OF:			17. LIMITATION OF ABSTRACT	18. NUMBER OF PAGES	19a. NAME OF RESPONSIBLE PERSON
a. REPORT	b. ABSTRACT	c. THIS PAGE		85	USAMRMC
					19b. TELEPHONE NUMBER *(include area code)*

INTRODUCTION:

There is a high incidence of TBI among warfighter occupants of vehicles targeted by underbody blasts but little is known about the unique forces involved or the pathophysiology. Our goal is to utilize small animal modeling of brain injury caused by underbody blasts to understand the pathophysiology of this uniquely military relevant form of TBI. Through this understanding, we aim to develop engineering- and biomedical-based neuroprotective interventions translatable to warfighter TBI.

Anesthetized and awake animals are being used in experiments where the peak vertical acceleration elicited by an underbody blast will be varied between approximately 20 and 2000 Gs. Anesthetized rats will be used in additional experiments where the top of the head is allowed to strike the surface of the cylinder (cockpit), which models a combined insult typical of underbody blasts.

Comprehensive histopathology, multispectral magnetic resonance imaging, and behavioral tests are being performed at 2 hr to 30 days after these blasts to provide spatiotemporal quantification of diffuse axonal injury, cellular inflammatory responses, cell death, and neurologic outcome that are necessary for understanding and mitigating underbody blast TBI.

We have also made progress in determining if TBI outcomes can be improved by modification to vehicle hull designs, including the use of hull materials that reduce the rate and extent of blast-induced acceleration.

BODY:

ALL PROGRESS IS LISTED UNDER ORIGINAL SOW TECHNICAL REQUIREMENTS AND IS BOLDED AND ITALICISED

1. Statement of Work

1.0 Introduction: The principal purpose of this agreement is to expand development of our novel, small animal model of TBI induced by the hyperacceleration associated with underbody blasts, with the long-term goal of supporting improved primary and secondary preventive strategies. All animal experiments and animal outcome measurements work will be carried out at University of Maryland School of Medicine. Experimental vehicle hull design and construction will be conducted at the University of Maryland School of Engineering.

1.1 Summary of Specific Aims/Objectives:

1.1.1. Establish dose-dependent relationships between G-force/JERK, neuronal/axonal injury, neurochemical alterations, and inflammation in different brain regions at different times after the underbody blast in the absence and presence of secondary head impact.

1.1.2. Eludicate the neurobehavioral alterations that occur after underbody blasts and establish their temporal relationships with the nature and extent of neuropathology present in different brain regions.

1.1.3. Determine if alterations in vehicle hull design, particularly those that reduce both maximal G-force and JERK, reduce histologic, neurochemical, or behavioral indices of brain injury.

2.0 Technical Requirements:

2.1. Quantify physiologic, neurochemical, and neuro-histopathologic TBI outcomes after exposure of rats to underbody blast-induced hyperacceleration. Compare these outcomes to direct measurements of acceleration (G-force) and acceleration rate (JERK) to determine minimal and maximal survivable loads associated with TBI, to establish dose-dependence relationships, and to identify the neurobiologic alterations most closely linked with the pathophysiology of this form of TBI. (Aligned with Objective 1)

2.1.1. Expose anesthetized test animals (rats) to defined degrees of blast-associated acceleration forces while secured on a metal structure that simulates a closed armored vehicle.

Approximately 38 rats have been subjected to underbody blasts resulting in peak vertical accelerations ranging from 10 Gs to 2000 Gs. Accelerometer measurements confirmed target G forces for all but 3 blasts (6 rats). All rats survived these procedures and did not exhibit any external injuries. Two rats that were exposed to the 2000 G underbody blast exhibited evidence of minor lung hemorrhages when perfusion fixed at 7 days post-blast.

2.1.2 Utilize a subset of animals for MRI and MRS measurements performed at one day prior to blast exposure (baseline) and again at several times post-blast.

Eight of the rats exposed to 2000 G underbody blast were used for MRI/MRS measurements performed at baseline (one day prior to blast), and 2 hr, 24 hr and 7 days post-blast. Representative preliminary results from diffusion tensor imaging (DTI) and magnetic resonance spectroscopy (MRS) are shown in Figures 1 and 2. Mean diffusivity of water is reduced at 2 hr post-blast and returns to normal at 24 hr and 7 days. Axial diffusivity appears reduced at 2 hr, 24 hr, and 7 days post-blast but is only significantly lower with n=6 animals at 24 hr. These changes could represent intraxonal molecular alterations which are consistent with the silver staining observed in the internal capsule of animals subjected to underbody blasts. MRS measurements of glutamate plus glutamine indicate a significant reduction in these metabolites in the cerebral cortex at both 2 hr and 7 days post-blast. These changes could represent metabolic alterations in either neurons or astrocytes since most glutamate is present in neurons and most glutamine is in astrocytes. Preliminary DTI and MRS measurements have also been performed in the hippocampus (not shown). The significance of these results is that they provide evidence from non-invasive measurements that exposure of rats to underbody blasts results in both neurochemical and physiological abnormalities.

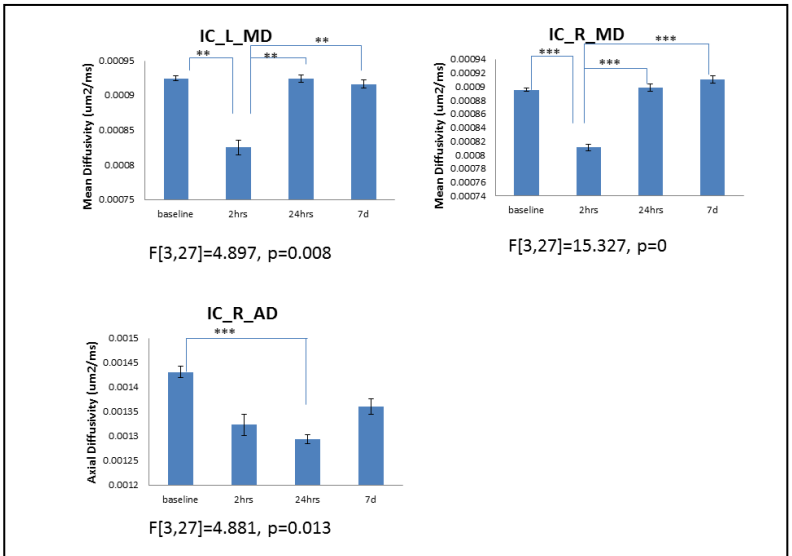

Fig. 1. Diffusion tensor imaging of water diffusion in the internal capsule before and after 2000 G underbody blast. Mean diffusivity changes in the left (L) and right (R) are bisymmetric and observed primarily at 2 hr post-blast. Axial diffusivity is also reduced after blasts. N=6 animals.

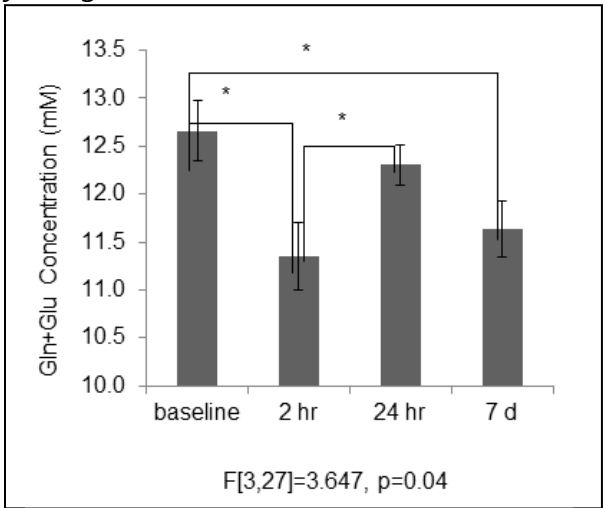

Fig. 2. Magnetic resonance imaging of total glutamine plus glutamate present in the frontal cortex before and after 2000 G underbody blast. Significant reductions were observed at both 2 hr and 7 days post-blast. N=6 animals.

2.1.3. Euthanize anesthetized rats by perfusion fixation within 2 hr after blast exposure, remove brains, and process for electron microscopic analysis of cyto- and axonal ultrastructure and for histochemical evidence of acute neurochemical and neuroanatomic alterations.

No animals have yet been used for electron microscopic analysis of brain cell ultrastructural changes caused by exposure of animals to underbody blasts. These experiments will be performed by the end of the 6th quarter of funding.

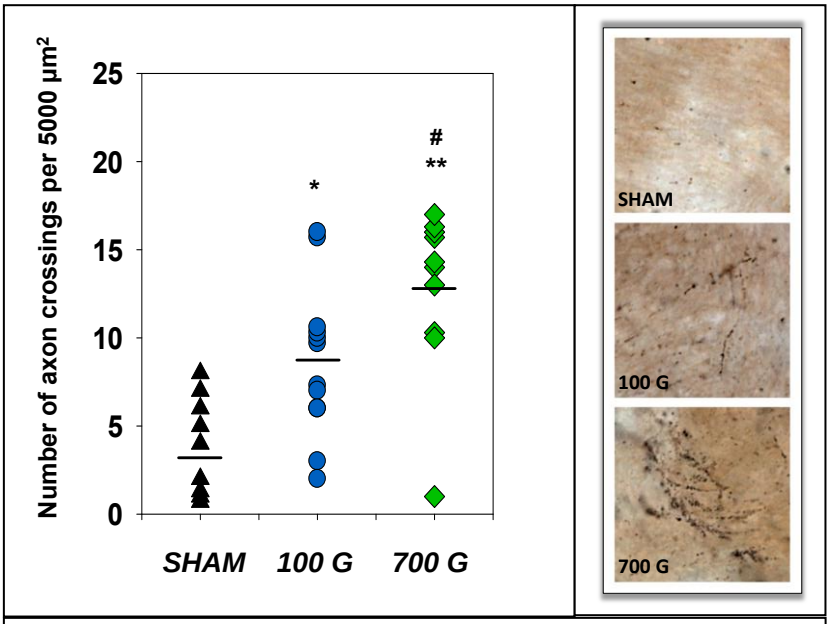

Fig. 3. Silver staining of damaged axonal fibers present in the internal capsule at 7 days after 100 or 700 G blasts or sham anesthesia. *p<0.05 compared to sham. #p<0.05 compared to 100 G. N=8-11 animals per group.

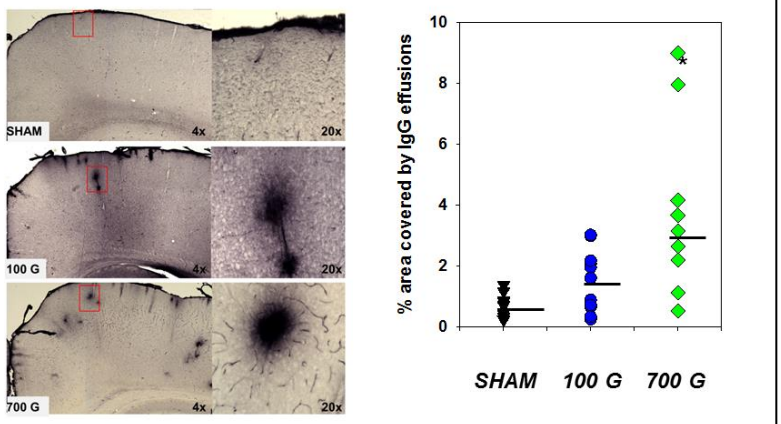

Fig. 4. Immunoglobulin G immuonstaining in the cerebral cortex or rats at 7 days after 100 or 700 G underbody blasts. Percent area covered by perivascular IgG effusions is significantly greater after 700 G blast compared to sham anesthesia controls (*p<0.05). N=7-9 animals per group.

2.1.4 Euthanize anesthetized rats by perfusion fixation at < 2hr and 24 hr, and at 7 and 30 days post-blast, and processed brains for quantitative histochemical and biochemical evidence of subacute and chronic neurochemical and neuroanatomic alterations.

Animals have been perfusion fixed at 2 and 24 hr post-blast and at 7 and 30 days post-blast. At this juncture, most of our quantitative histopathology was generated from animals at 7 days post-blast. As shown in Fig. 3, there was a significant increase in silver staining (de Olmos method) of axon fibers present in the internal capsule of animals exposed to 100 and 700 G underbody blasts compared to ketamine-anesthetized shams. There was also a significant difference between axonal injury in the internal capsule of rats subjected to 700 Gs compared to 100 Gs or to shams. Immunohistochemistry for immunoglobulin G was used as a measure of blood-brain barrier (BBB) disruption since normally IgG is present at only very low levels within the brain parenchyma of sham animals with an intact BBB. Fig. 4 provides the total area of perivascular IgG immunostaining in the frontal cerebral cortex. No significant increase was observed in animals following 100 G underbody blasts; however, there was a significant increase in perivascular IgG effusion area following 700 G blasts.

Additional qualitative findings were obtained at the lower end of the G force range and are included in a manuscript in press in the Journal of Trauma and Acute Care Surgery (see Appendix). These observations include increased axonopathy (silver staining) in the cerebellum and astrocyte activation in the cerebral cortex. The significance of these quantitative histologic measurements is that they strongly suggest that exposure of rats to survivable underbody blasts results in both white matter axonopathy and vascular injury resulting in disruption of the blood brain barrier.

We have also initiated our neurochemical analyses using RNA extracted from hippocampi within unfixed brains. Rats were euthanized, their brains quickly removed, and dissected into regions containing the hippocampus, cortex, internal capsule, and cerebellum, which were stored under -80°C. Total RNA was extracted with TRIzol. The quality and quantity of extracted RNA was further analyzed using Agilent 2100 Bioanalyzer. RNA with integrity number above 7 was used for microarray analysis. All procedures were performed with DNase- and RNase-free tools and reagents.

RNA was amplified and biotin labeled using the two-cycle target labeling kit (Affymetrix) and hybridized to the GeneChip® Rat Gene 2.0 ST arrays (Affymetrix). Samples were processed by the Biopolymer-Genomics Core Facility at the University of Maryland Baltimore. Samples were hybridized using a GeneChip hybridization oven 640 (Affymetrix), processed using a GeneChip Fluid Station 450 (Affymetrix), and scanned using a GeneChip Scanner system 3000 7G (Affymetrix). Microarray data normalization was performed with Affymetrix® Console™ software.

The advantage of using GeneChip® Rat Gene 2.0 ST array over the other related products is the high transcript coverage (every exon of every transcript is probed, and median of 22 probes per gene) that yields accurate detection for genome-wide transcript expression changes. Furthermore, more transcripts are covered (> 27,000 protein coding transcripts, >23,500 Entrez genes) that allows novel target discoveries.

CEL data files were analyzed using Partek Genomics Suite version 6.4 (Partek GS, Partek, Inc.). Data were subjected to filtering by the detection of p-value and Z-normalization. Genes were identified as differentially expressed after calculating the Z-ratio, which indicates the fold-difference between experimental groups, as well as false discovery rate (FDR), which controls for the expected proportion of false rejected hypotheses. ANOVA was performed to evaluate the significance in gene expression alteration between experimental groups. Of the over 7500 genes identified as changing in expression in the hippocampus at 24 hr after 100 G underbody blast, 12 genes were identified as changing in expression very significantly, using rigorous criteria of p value ≤ 0.05, absolute value of z-ratio ≥ 2.0 and FDR ≤ 0.05. These genes are listed in Fig. 5, along with a heat map demonstrating changes in expression between blast animals and shams and the finding that there was excellent agreement between the two animals in each group. Several microRNAs and small nuclear RNAs were identified, which likely play roles in regulating gene expression. Exposure to the blast resulted in a large decrease in Bcl2 expression, which could render brain cells highly vulnerable to apoptotic death. Blast exposure also induced a large increase in expression of the gene coding for VonWillebrand factor, which is known to increase during adverse changes to cerebral endothelial cells and can increase risk for thrombosis. Other gene expression cluster analyses are in progress to determine if changes occur in sets of genes, e.g. those associated with inflammation, oxidative stress, etc. The significance of these results is that significant changes in gene expression occur in the rat hippocampus within 24 hr following even the relatively low level 100 G underbody blast. Studies are in progress to determine gene expression changes following both higher and lower G force blasts.

Fold change ≥ 2, p ≤ 0.05, FDR ≤ 0.05

Gene Symbol	RefSeq	p-value	Fold-Change	Description (100G vs. sham)
Novel miRNA*	ENSRNOT000043523	1.01E-05	-2.06438	down
Bcl2	ENSRNOT00000003768	4.07E-05	-2.59557	down
Fbxw8	reviewed	8.99E-05	2.86312	up
Novel miRNA**	ENSRNOT000000063683	0.000312	2.13415	up
RAB1B	ENSRNOT00000027486	0.000617	2.47881	up
Rps20	NM_001007603	0.000589	2.50095	up
snoRNA##	ENSRNOT000000069073	0.000631	2.00346	up
snoRNA##	ENSRNOT000000069073	0.000631	2.00346	up
-	---	0.000991	2.83156	up
snoRNA#	ENSRNOT000000054102	0.000652	2.28636	up
-	---	0.000988	-2.94326	down
Vwa5b2	NM_001134535	0.001112	2.22691	up

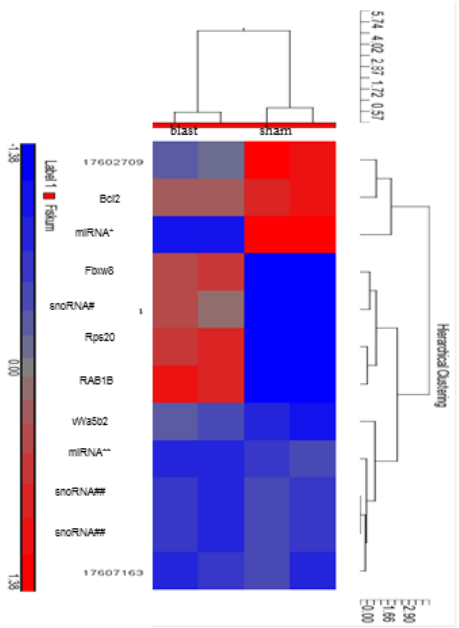

Fig. 5. Major gene expression changes in the hippocampus at 24 hr following exposure to 100 G underbody blast, compared to sham controls. The heat map demonstrates relative differences between blast (left) and sham (right) and also the similarities between the two animals in each group.

2.1.5. Compare quantitative histopathologic measurements of brain injury with accelerometer measurements of maximal G-force and JERK.

At this juncture, most of our histopathologic measurements have been performed on the brains of rats exposed to 100, 700, and 2000 G and perfusion fixed at 7 days post-blast. Additional experiments are in progress to establish quantitative relationships between both G-force or JERK and histopathologic outcome measures.

2.1.6. Milestone: Complete all histopathologic marker/G-force correlations (*timing = 24 months*).
2.1.6.1. Deliverable 1: Determination of whether histopathologic markers of brain injury display a dose-dependent relationship to underbody blast-associated G-forces and whether maximal Gs, JERK or HIC is the best predictor of TBI.
2.1.4.2. Deliverable 2: Determination of minimum G-force associated with any degree of measurable neurohistopathology; determination of the maximum survivable G-force in this experimental system.

2.2. Quantify neurobehavioral alterations after underbody blast-associated acceleration injury, including any evidence of G-force and JERK dose-dependence. (Aligned with Objective 2)

2.2.1. Apply these tests to experiments described by 2.1.1.
2.2.2. In animals surviving to 30 days post-injury, perform behavioral testing with standard methods
2.2.3. Correlate results of neurobehavioral testing with measured G-force and JERK.
2.2.4 Compare results of neurobehavioral testing with MRI/MRS and histologic measurements.
2.2.5. Milestone: Complete all neurobehavioral testing/G-force correlations (*timing = 24 months*).

Initial neurobehavioral test included the balance beam, testing for both latency crossing the beam and the number of foot faults. In addition, a Composite Neuroscore was used for a rough assessment of neurological status. An Open Field test was also used, where distance traveled, time immobile, time in inner zone, and time in outer zone were recorded. Finally, we have recently included the forced swim tests, as a measure of depressive behavior. At this juncture, we have generated preliminary results for animals that were exposed to 700 G underbody blasts (8) compared to the ketamine anesthetized shams (5). In general, no differences have

been observed, except that significantly more foot faults were observed with 700 G blast rats measured at 72 hr compared to shams but by 21 days, the foot faults were significantly lower in the 700 G blast rats. Studies are in progress to compare results from all these behavioral tests between shams and those exposed to 2000 G underbody blasts.

2.2.5.1. Deliverable: Determination of whether neurobehavioral testing results display a dose-dependent relationship to blast-associated G-force or JERK.
2.2.5.2 Deliverable: Identification of the physiologic, neuroanatomic, and neurochemical outcome measures that are most closely related to neurobehavioral indicators of TBI, thus providing insight into the pathophysiology of this form of TBI.

2.3 Perform a limited number of experiments and outcome measures described in 2.1 and 2.2 with rats that are fully awake but restrained during the underbody blast. (Aligned with Objectives 1 and 2)

2.3.1. In addition to standard outcome measurements, determine if rats lose consciousness or ability to walk or right themselves after moderate G force underbody blasts.
2.3.2. Quantitatively compare both short and long-term outcome measurements obtained from rats that are anesthetized and those that are awake.
2.3.3. Milestone: Complete all blasts and outcome measurements with rats awake during the blasts (*timing = 30 months*).

Approval was obtained from the Univ. of Maryland, Baltimore IACUC and the ACURO to expose 16 rats to 700 G blasts, with 8 perfusion-fixed at 24 hr post-blast and 8 perfusion fixed at 30 days post-blast. These experiments will be initiated within the next 4 months.

2.3.3.1. Deliverable: Determination of whether rats that are awake during exposure to underbody blasts demonstrate immediate neurobehavioral alterations and if they exhibit evidence for greater short-term and long-term TBI compared to animals anesthetized during the blast.

2.4. Establish a modified version of the animal model that includes a controlled secondary head impact during the underbody blast-induced hyperacceleration. (Aligned with Objectives 1 and 2)

2.4.1. Develop an articulated rat head holder that allows for the top of the skull to impact the "roof" of the vehicle during the underbody blast.
2.4.2. Expose *anesthetized* rats to a moderate G force underbody blast, allowing for secondary head impact.
2.4.3. Perform all outcome measurements described in 2.1 and 2.2.
2.4.4. Quantitatively compare outcomes obtained from rats with secondary head impact to those without secondary head impact.
2.4.5. Milestone: Complete all blast experiments and outcome measurements with rats exposed to underbody blast plus secondary head impact (*timing = 36 months*).

We are in the process of designing the hardware necessary to combine the underbody blast with head impact. We anticipate that a prototype device will be available the end of 2014 and that results will be presented by the time the second annual report is submitted.

2.4.5.1. Deliverable: A small animal model of TBI caused by the combination of underbody blast-induced hyperacceleration plus secondary head impact that is particularly relevant to many of the warfighters that survive underbody blasts.

2.5. Test the effects of different vehicle hull designs on the loads imparted to the vehicle and to the test animals and determine which design is most effective at reducing TBI. (Aligned with Objective 3)

2.5.1. Test 3 different hull designs (e.g., multiple V-hull and inverted V-hull) for mitigation of maximal G force and JERK loads on the vehicle alone.
2.5.2. Test 3 of these design modifications with *anesthestized* rat occupants at a blast stand-off distance that imparts a moderate G-force with the standard hull design.
2.5.3. Perform all outcome measurements described in 2.1 and 2.2.
2.4.4. Quantitatively compare outcomes obtained from tests using the modified hull designs to those using the standard hull design.
2.4.5. Milestone: Complete all blast experiments and outcome measurements with the modified hull designs (*timing = 44 months*).

We reported in the 3rd quarter progress report that the maximum G force imposed on the hull of our experimental test vehicle could be reduced by approximately 90% by using a double hull with compressible cyclinders located between the two hulls. We now present updated results from experiments demonstrating a nonlinear acceleration mitigation benefit of polymeric coated thin-walled cylinders. No animals were used in these experiments.

In order to tease out the previously hypothesized nonlinear acceleration mitigation benefit of polymeric coated thin-walled cylinders, a series of blast tests was run where the polyurea to aluminum mass ratio was kept constant (along with the other test parameters such as stand-off distance (SOD) and depth of burial (DOB)) while the charge mass was varied. Tests with coated and uncoated cylinders were run to compare how the acceleration varied between the coated and uncoated cylinders as the charge size changes. The test matrix for this series of tests is shown in Table 1.

Table 1: Test matrix for nonlinear study

Charge Mass (g)	DOB (mm)	SOD (mm)	# of Cylinders	Cylinder Material	Cylinder OD Before Coat (mm)*	Cylinder ID (mm)*	Cylinder Height (mm)*	Cylinder Mass (g)*	Polyurea Mass (g)	Mass Ratio (P/S)
2.2	10	40	1	Aluminum	66	65.8	38.1	3	2.37	0.79
2.2	10	40	1	Aluminum	66	65.8	38.1	3	2.58	0.86
1.75	10	40	1	Aluminum	66	65.8	38.1	3	2.75	0.92
1.75	10	40	1	Aluminum	66	65.8	38.1	3	2.02	0.67
1.25	10	40	1	Aluminum	66	65.8	38.1	3	2.63	0.88
1.25	10	40	1	Aluminum	66	65.8	38.1	3	2.27	0.76
0.75	10	40	1	Aluminum	66	65.8	38.1	3	2.46	0.82
0.75	10	40	1	Aluminum	66	65.8	38.1	3	2.47	0.82
0.75	10	40	1	Aluminum	66	65.8	38.1	3	0	0.00
0.75	10	40	1	Aluminum	66	65.8	38.1	3	0	0.00
1.25	10	40	1	Aluminum	66	65.8	38.1	3	0	0.00
1.25	10	40	1	Aluminum	66	65.8	38.1	3	0	0.00
1.75	10	40	1	Aluminum	66	65.8	38.1	3	0	0.00
1.75	10	40	1	Aluminum	66	65.8	38.1	3	0	0.00
2.2	10	40	1	Aluminum	66	65.8	38.1	3	0	0.00
2.2	10	40	1	Aluminum	66	65.8	38.1	3	0	0.00

A total of 16 tests were run, eight tests with cylinders having a polyurea to aluminum mass ratio of about 0.75 and eight tests with uncoated cylinders. Two tests were run for each type of cylinder at charge sizes of 0.75 grams, 1.25 grams, 1.75 grams, and 2.2 grams of explosive. The simplified hull/frame plate combination used in conjunction with a single cylinder was used to collect data. As in the other studies, in order for the data to be reported, the displacement profiles obtained from the high speed camera and the accelerometer must match. The thickness of the coating of polyurea was about three times the thickness of the aluminum cylinder wall thickness. The mass ratio being used here is quite small, less than 1. To put into

perspective for a full size vehicle subjected to 10 pounds of explosive the wall thickness of the cylinder would be 1/2th of an inch and the coating would be about an inch thick.

Nonlinear Effect Results

At the conclusion of the test series to determine the non-linear acceleration mitigation effect on coating thin-walled cylinders with polyurea, two plots were created that show the effect quite clearly. In Fig.6, the difference between the peak acceleration of the coated cylinder and non-coated cylinder is plotted for each charge mass. Figure shows the final recovered height of the cylinder.

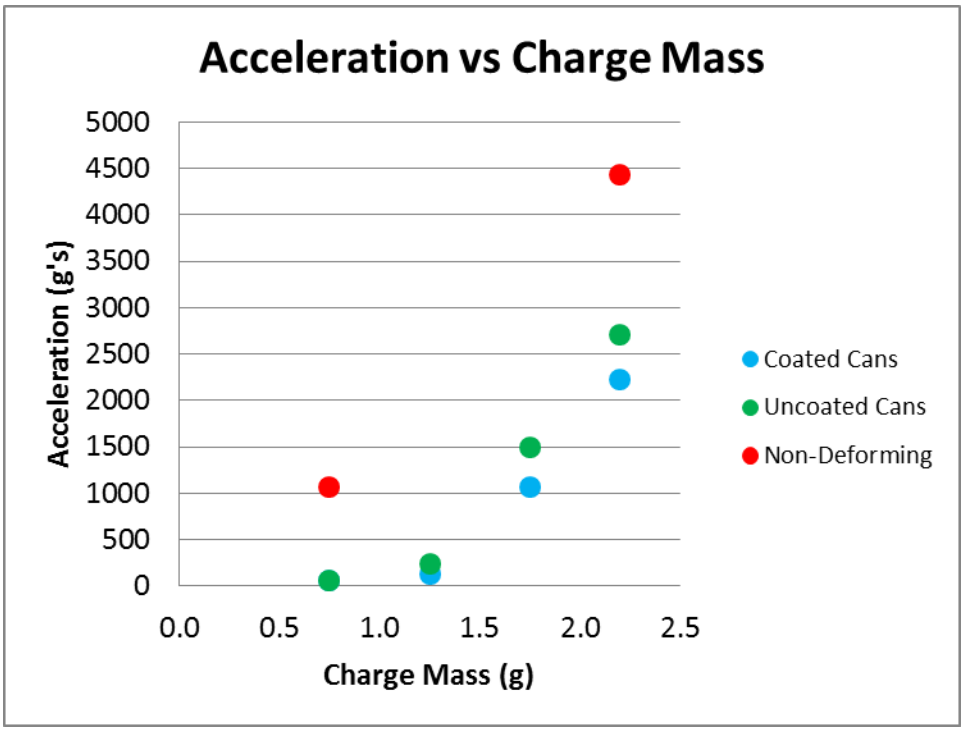

Figure 6: Peak acceleration for coated and uncoated cans versus charge mass

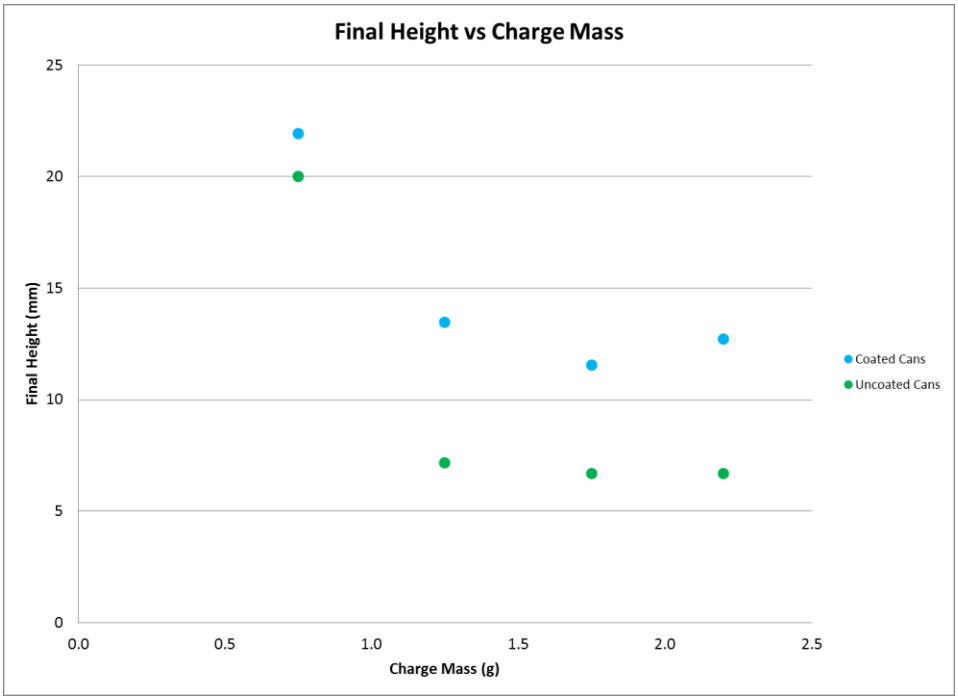

Figure7: Final recovered height of the blast loaded cylinders versus charge mass

Looking at the previous two figures a complete picture of the non-linear effect of polymeric coatings on peak acceleration can be determined. It is seen that as charge mass increases, the recovered height of the polymeric cylinder is steadily greater than the uncoated can. It seems that during maximum crushing scenarios, coated cylinders will recover to around a 13 millimeter height as compared with uncoated cylinders which only recover to around a seven millimeter final height. In terms of acceleration, it is seen that at smaller charge sizes, the acceleration profiles of coated and uncoated cylinders are essentially the same. However as the charge mass increases, the polyurea cylinder acts to better mitigate the acceleration of the frame.

A solid coupling between the hull and frame at 2.2 gm charge results in an acceleration of about 4500 g's. With an uncoated crushing cylinder the acceleration level is reduced to 2700 g's and the cylinder final height is 7 cm compared to an original height of 38 cm. With the same cylinder with a polyurea coating the acceleration level is reduced to 2200 g's and the final height of the cylinder is 13 cm.

Considering these results, we plan on testing uncoated and coated crushing cylinders placed between the inner and outer hulls of the test vehicle used for our underbody blast TBI paradigm. We hypothesize that both will provide protection against TBI, with greatest protection observed with the coated crushing cylinders.

2.4.5.1. Deliverable: Identification of a hull design that both mitigates loads on the vehicle and its occupants and that reduces TBI after underbody blast.

KEY RESEARCH ACCOMPLISHMENTS:

- Quantitative histochemical evidence for damage to brain white matter axon fibers following exposure of rats to underbody blasts resulting in peak vertical accelerations of 100 and 700 Gs, with significant increase in axon injury at 700 compared to 100 Gs.
- Quantitative immunohistochemical evidence for blood brain disruption in the cerebral cortex of rats following exposure to 700 G underbody blasts.
- Quantitative molecular biological evidence for significant differences in hippocampal gene expression following exposure to 100 G underbody blasts. A significant reduction in expression of Bcl2, which could promote brain cell death, and a significant increase in expression of Von Willebrand's factor, which is indicative of vascular injury, were observed.
- Qualitative histological evidence for axonal injury in several brain regions, including the internal capsule, the corpus callosum, and the cerebellum. Also evidence for astrocyte activation.
- Demonstration that the use of crushable cylinders separating an outer and inner hull can dramatically reduce the G force load on the inner hull. Further demonstrations that application of a poly-urea covering to the cylinders can provide further protection at high G forces and allow for at least partial reinstatement of shock-absorbing cylinder structures. This rebound characteristic could increase the chance of the blast-targeted vehicle to remain in operation.

REPORTABLE OUTCOMES:

1. Manuscript in press in Journal of Trauma and Acute Care Surgery providing qualitative histologic evidence for brain injury to rats in our underbody blast TBI model (see Appendix)

2. Results obtained from this project were presented in a poster session at the National Neurotrauma Society meetings in Nashville, TN in August of 2013. The title of the presentation was "Hypobaria Worsens Axonal Injury and Blood Brain Barrier Disruption Induced by Underbody Blast-Induced Hyperacceleration" and an abstract is included in the Appendix.

3. Results obtained from this project were also presented in a platform session at the Military Health System Research Symposium held in Ft. Lauderdale, FL in August of 2013. The title of the presentation

was “Hypobaria Worsens Axonal Injury and Blood Brain Barrier Disruption Induced by Underbody Blast-Induced Hyperacceleration” and an abstract is included in the Appendix.

4. Intellectual property disclosure to the University of Maryland College Park for vehicle hull designs that can mitigate injury caused by underbody blasts (see Appendix).

CONCLUSION: At this early stage of this project we can conclude with confidence that underbody blast induced G forces of as little as 100 Gs cause white matter and vascular damage in the brains of rats. We also conclude that in the absence of secondary head impact, rats survive blast-induce force of at least 2000 Gs, while exhibiting brain injury. We also conclude that even at the log G force of 100 Gs, significant changes in brain gene expression occur that could affect outcomes. Finally, our vehicle hull design efforts have been very successful at demonstrating an unexpectedly large reduction in load placed on the floor of a vehicle, using inner and outer hulls separated by crushable cylinders. Application of such a design to military vehicles could dramatically reduce the extent of injuries to the occupants and even allow the vehicle to keep operating, thus increasing the successful completion of the military mission.

APPENDICES:

APPENDIX

1. Manuscript in press in Journal of Trauma and Acute Care Surgery, including email verifying acceptance

2. Abstract of poster presented at the National Neurotrauma Society meeting in Nashville, TN in August of 2013

3. Abstract of oral platform session presentation at the MHSRS meeting in Ft. Lauderdale, FL in August 2013

4. University of Maryland Intellectual Property Disclosure

Journal of Trauma and Acute Care Surgery

Rat Model of Brain Injury Caused by Under-Vehicle Blast-Induced Hyperacceleration

--Manuscript Draft--

Manuscript Number:	JT-S-13-00245R1
Full Title:	Rat Model of Brain Injury Caused by Under-Vehicle Blast-Induced Hyperacceleration
Article Type:	Original Article
Section/Category:	2013 MHSRS Supplement
Keywords:	axonal injury; astrocyte; inflammation; internal capsule; cerebellum
Corresponding Author:	Gary Fiskum UNITED STATES
Corresponding Author Secondary Information:	
Corresponding Author's Institution:	
Corresponding Author's Secondary Institution:	
First Author:	Julie L. Proctor
First Author Secondary Information:	
Order of Authors:	Julie L. Proctor
	William L. Fourney
	Ulrich H. Leiste
	Gary Fiskum
Order of Authors Secondary Information:	
Manuscript Region of Origin:	UNITED STATES

Level of Evidence: Diagnostic test, Level III

Keywords: axonal injury; astrocyte; inflammation; internal capsule; cerebellum

Title: Rat Model of Brain Injury Caused by Under-Vehicle Blast-Induced Hyperacceleration

Running Title: Hyperacceleration-Induced TBI

Authors: Julie L. Proctor[1], M.S., William L. Fourney[2], Ph.D., Ulrich H. Leiste[2], Ph.D. and Gary Fiskum[1], Ph.D.

Affiliations:
[1] University of Maryland School of Medicine, Dept. of Anesthesiology and the Shock, Trauma, and Anesthesiology Research Center (STAR)
[2]University of Maryland School of Engineering, Dept. of Mechanical Engineering and the Center of Energetics Concepts Development

Email Addresses:

Julie Proctor	jproctor@anes.umm.edu
William Fourney	four@umd.edu
Ulrich Leiste	uleiste@umd.edu
Gary Fiskum	gfiskum@anes.umm.edu

Correspondence and Reprints Address:

Dr. Gary Fiskum
Univ. of Maryland School of Medicine Dept. of Anesthesiology
685 W. Baltimore St., 534 MSTF
Baltimore, MD, USA

Email: gfiskum@anes.umm.edu

Conflict of Interest and Source of Funding Statement: There is no financial, consultant, institutional or relationship conflicts declared by any author. This work was supported in part by US Air Force grant FA8650-11-2-6D04 and the US Army grant W81XWH-13-1-0016.

Content of this manuscript was presented at the 2013 Military Health System Research Symposium meeting in Ft Lauderdale, FL

BACKGROUND

Approximately 25% of all U.S. combat casualties in Operation Iraqi Freedom and Operation Enduring Freedom have been caused by traumatic brain injury (TBI), with most of these injuries caused by explosive munitions such as bombs, land mines, improvised explosive devices and missiles (1,2). Little is known regarding the pathophysiology of "blast TBI". The majority of animal research on blast TBI has focused on one aspect of these explosions, the blast overpressure (3,4,5,6). Most of these studies use a model in which a gas-driven pressure wave was delivered via a long shock tube, either directly to the immobilized animal's head or body. A multitude of physical forces may play a role in blast TBI, including blast overpressure, thermal and chemical components, shockwave, and hyper-acceleration of the brain. We hypothesize that this extreme hyper-acceleration, with subsequent rapid deceleration, is responsible for many aspects of blast TBI.

Acceleration may be particularly important for the large number of soldiers and others injured while occupants of armored vehicles targeted by improvised explosive devices (IEDs). Such explosions result in a very short but very intense acceleration of the vehicle and its occupants. The Dynamic Effects Laboratory at University of Maryland School of Engineering has used small scale testing to evaluate the loads applied to personnel carriers when a buried explosive detonates beneath them (7,8). Adaptation and scaling of this model to allow animal injury in a similar explosive environment could provide a completely new, clinically relevant model of blast TBI that encompasses many of the physical forces including the extreme hyper-acceleration. As a first step toward this goal, this study tested the hypothesis that relatively low underbody blast-induced accelerations of 20 and 50 Gs result in histologic evidence for mild TBI in the absence of obvious injury to other vital organs.

METHODS

A. Underbody blast-induced hyper-acceleration

The device used to induce underbody blast-induced acceleration consists of an aluminum water tank 3 ft long x 2 ft wide x 2 ft deep in which a platform is located that supports two thick aluminum plates, each 15 in square and 1.5 in thick (Fig. 1). The two plates are separated by a styrofoam pad of the same dimensions, which absorbs some of the force transmitted between the plates. The plates and pad travel vertically in response to a blast in the water tank, guided by poles located in holes in each corner of the plates and pad. The two cylinders secured to the top of the plate each house an anesthetized rat that is wrapped in a thick cotton "blanket" to minimize secondary movement within the cylinders. An explosive charge of 0.75 g pentaerythritol tetranitrate (PETN) is placed in the water precisely under the center of the plate at distances that generate precise, maximal G-forces in these experiments of between 20 – 50 Gs. Stand-off distances were determined previously at the Dynamics Effects Laboratory and measured during the animal experiments, using accelerometers. When detonated, the explosion causes the plate containing the two rats to accelerate upwards extremely rapidly to heights of < 4 inches, followed by return down to the original location. Pressure sensors located immediately next to the rat heads indicated that they were exposed to less than 1 psi increase in pressure following the explosion. Fig. 1 provides examples of the accelerometer measurements performed during these tests, demonstrating reproducibility between two different blasts at both 20 and 40 Gs and differences observed at 20, 40, and 60 Gs, with peak accelerations occurring at 5, 4, and 3 milliseconds, respectively.

B. Animal experiments

All animal procedures were performed in accordance with the University of Maryland School of Medicine Institutional Animal Care and Use Committee, the U.S. Army Animal Care and Use Review Office (ACURO), and the U.S. Air Force Animal Use Program Office of Research Oversight & Compliance. At approximately 10 min prior to each blast, two adult male Sprague-Dawley rats (300 – 350 g) were deeply anesthetized by intraperitoneal injection of ketamine (80 mg/kg) and xylazine (10 mg/kg). Immediately following the underbody blast, the rats were removed from the cylinders and their respiratory rates compared to those recorded prior to the blast. No changes in respiration were observed. All animals were fully conscious within 90 min after the blast and appeared unharmed. In addition to the 25 anesthetized rats subjected to blast-induced hyperacceleration, 10 sham rats were anesthetized but not used in blast experiments.

c. *Tissue Preparation*

At different times following the blasts or sham anesthetization, rats were heavily re-anesthetized by intraperitoneal injection of ketamine (160 mg/kg) and xylazine (20 mg/kg) and transcardially perfused with 4% paraformaldehyde plus 2.5% acrolein (9). Brains were removed from the skull and transferred into 30% sucrose. Once brains sunk to the bottom of the container, they were cut (40 μm) on a freezing sliding microtome, yielding 12 series per animal and kept in cryoprotectant (-20C°) until further processing was initiated.

d. Pathology

None of the 25 rats used in the blast experiments exhibited any evidence of injury to the lungs, heart, liver or spleen upon inspection following thoracotomy during perfusion fixation.

Staining of brain sections with Fluoro-Jade B was used to detect dead or dying neurons (9, 10). Free floating brain sections were rinsed free of cryoprotectant with KPBS, mounted on Vectabond treated PLUS superfrost glass slides and dried overnight at 55°C. Slides were sequentially dipped in the following: 100% EtOH (3 min), 70% EtOH (1 min), deionized H_2O (1 min), 0.06% $KMnO_4$ (15 min), H_2O (2 min), and 0.0005% solution of Fluoro-Jade B (30 min). Slides were then dipped in H_2O 4-5 times, and allowed to dry for 30 min at 55°C before being cleared in xylene and coverslipped with DPX mounting media.

The amino cupric silver method of de Olmos was used to stain free-floating 40 μm tissue for the identification of damaged and degenerating axons. Our staining procedure closely followed the detailed protocol described by Tenkova and Goldberg (11). Prior to staining, all glassware was cleaned in 50% nitric acid. Sections were rinsed free from cryoprotectant and incubated in 4% paraformaldehyde (4°C) for 1 week prior to staining to block non-specific labeling of neurons. Sections were then rinsed with deionized H_2O and incubated in pre-impregnation buffer (cupric-silver) for 1 hr at 50°C then at room temperature overnight. The next day, sections were exposed to the following solutions at room temperature: 100% acetone (30 sec), impregnation buffer (silver-diamine) solution for 35 min, reduction agent (formaldehyde with citric acid) for 2 min, bleaching solution (potassium ferricyanide) for 20 min, deionized H_2O for 3 min, and stabilization buffer (thiosulfate solution) for 10 min. All solutions were made fresh immediately before use and sections were carefully shielded from direct light during all staining procedures. After staining, sections were mounted in 50% ethanol onto subbed PLUS slides, dehydrated with ethanol and xylene and subsequently coverslipped with DPX mounting media.

e. Immunohistochemistry

Free-floating sections were single-labeled with antibodies against the astrocyte marker, glial fibrillary acidic protein (GFAP) (9), by rinsing multiple times in 0.05 M KPBS buffer before and after exposure to the following: 1% solution of sodium borohydride for 20 minutes; primary antibody diluted in 0.05M KPBS + 0.4% Triton-X for 48 hrs (Dako Anti-GFAP; 1:150K; biotinylated secondary antibody diluted in 0.05 M KPBS + 0.4% Triton-X 1:600 for 1 hr; and incubation in Vectastain A/B solution (1:222) for 1 hr. Tissue was then rinsed before and after 12 min incubation in Ni-DAB solution with 0.175M sodium acetate buffer. After a final rinse in KPBS buffer, slices were mounted on slides, dehydrated, and coverslipped with DPX mounting media. The sections were examined with Nikon Eclipse E800 microscope and captured using StereoInvestigator software.

RESULTS

Neuronal death is typically observed within one week of injury in most rodent TBI models. Neuronal death or degeneration that occurs in this period is often detected histologically, using a FluoroJade stain, which selectively labels dead or dying neurons (9,10). Figure 2 compares Fluoro-Jade B (FJB) staining present in the frontal cerebral cortex of a sham rat, perfusion fixed 7 days after ketamine anesthesia, to that observed 7 days following moderate injury induced using a controlled cortical impact (CCI) model, which utilizes a pneumatic device to directly impact the cortical surface (12). Representative tissue from the CCI model was obtained from our rodent brain bank and not generated as part of this study. Extensive staining was apparent in the brain from the rat that underwent the CCI, whereas virtually no staining was detectable in the sham rat. In contrast to the staining exhibited by the positive control animal that was previously subjected to cortical impact, no FJB staining was observed

at 7 days in a rat subjected to a 50 G underbody blast. Examination of 12 coronal sections representing the entire brain detected no FJB-stained neurons in 10 rats used in the 50 G underbody blast experiments or in 2 rats used in 20 G underbody blast experiments.

Diffuse axonal injury is often observed in rodent brain injury models and can be detected by staining of axons with silver-containing reagents (10,13). Using the de Olmos silver staining method, widespread staining was evident at 7 days after 50 G blasts. Staining was most striking in the internal capsule, corpus callosum, and cerebellum (Fig. 3). Abnormal axon morphology was represented by undulations and bulb-like swellings (Fig 3, bottom panels). Additional axonal staining was observed in tracts serving the thalamus while very few fibers in the olfactory bulb or anterior commissures showed evidence of axonopathy. Where silver staining was observed in superficial layers of the brain, it occurred more commonly in the ventral rather than dorsal cortical regions. Relatively little axonal silver staining was observed in non-injured sham animals.

Axonal silver staining was detectable in the internal capsule of animals subjected to 20 G underbody blasts and perfusion fixed at either 24 hr or 7 days. Evidence for even earlier axonal injury was obtained with brains fixed 3 hr after 50 G blasts (Fig. 4). In contrast, silver staining was much less obvious at 30 days post-blast compared to 3 hr or 7 days (Fig. 4).

Cellular inflammatory responses are another hallmark of TBI. These responses are characterized by proliferation, migration, and morphological transformation of astrocytes and microglia, which constitute approximately 50% of the mass of the human brain (14). Surprisingly, we obtained no convincing evidence for microglial activation following 20 or 50 G blasts at any outcome times (not shown). Nevertheless, we consistently observed astrocyte accumulation near ventral cortical surfaces, hypothalamic regions and the internal capsule

(Fig. 5). In addition, many astrocytes present in different brain regions exhibited large cell bodies, indicative of activation. Unlike the silver-staining of axons, that declined between 7 and 30 days after the blast, these cellular inflammatory reactions persisted and possibly increased during this period.

DISCUSSION

To the best of our knowledge, these experiments represent the first to test for the effects of specifically underbody blast-induced hyper-acceleration on the brains of lab animals. The blast paradigm was designed to test for the effects of this form of acceleration on the brains of rats in the absence of exposure to any significant blast overpressure. Several conclusions can be made: 1. Adult rats can be subjected to blast-induced hyper-acceleration at maximal G-forces of at least 50 Gs with a 100% survival rate, provided they are protected against secondary impact injuries. 2. FluoroJade-detectable neuronal death does not occur following exposure of rats to either 20 or 50 G underbody blasts. 3. Diffuse axonal injury occurs in several brain regions, as early as 4 hr after 20 or 50 G underbody blasts and is still evident at 7 days, based on silver staining of axonal fibers. 4. Despite the lack of evidence for substantial microglial activation, astrocyte activation occurs within 7 days and persists for 30 days following 20 or 50 G underbody blasts. 5. Based on these qualitative histologic findings, we conclude that rats subjected to 50 G blasts, and possibly even 20 G blasts, suffer mild TBI.

This unique initial approach to understanding the effects of underbody blasts on the brain has several limitations. 1. We specifically designed the device for exposing rats to underbody blasts to test specifically for the effects of acceleration, without secondary effects of potential head impact. Clearly, many victims of TBI who are occupants within vehicles targeted by IEDs detonated underneath the vehicles are subjected to both acceleration, head impact, and

other injuries. Therefore, polytrauma animal models may be more clinically relevant (5, 15). 2. Only two maximal G forces were used that are much lower than maximum survivable G forces experienced by occupants within targeted vehicles. We purposely used relatively low loads in this initial study to avoid mortality and injury to other vital organs. Studies are in progress exposing rats to underbody blasts at much higher G forces in the range of 100 – 2000 Gs. Recently, one study published evidence of head acceleration exceeding 3000 Gs in a blast tube, porcine model of survivable free field blast exposure (16). 3. Neuronal death was only measured using one method, i.e., FluoroJade B tissue staining. It is therefore possible that other methods, such as active caspase 3 immunostaining, could detect neuronal death not detected using FluoroJade B. 4. Diffuse axonal injury was only evaluated using the de Olmos silver staining method. Although this approach is used extensively, additional procedures, e.g., immunohistochemical detection of phosphorylated tau protein and beta-amyloid precursor protein, could provide helpful validation (17, 18). 5. The results obtained from the silver staining of degenerative neurons and the GFAP immunostaining of astrocytes demonstrating activated morphology are at this juncture purely qualitative. Studies are in progress to obtain quantitative results for these and other histologic outcome measures. 6. No quantitative assessment of behavior was performed. Now that we have obtained histologic evidence for mild TBI following low-G underbody blasts, we are developing neurobehavioral tests sensitive enough to detect neurologic alterations at these and higher G forces.

AUTHORSHIP

J.L.P performed all of the histology and generated all of the results presented in the manuscript. W.L.F. and U.H.L designed and built the device used for the underbody blast TBI model, were present at every experiment, and conducted the blasts and performed the accelerometer measurements. G.F. is the principal investigator of the grants that supported the work and conceived the study design. He was also present at every experiment. All authors contributed to the writing of this manuscript.

REFERENCES

1. Okie S (2005) Traumatic brain injury in the war zone. N. Engl. J. Med. 352:2043-2047.
2. Hoge CW, McGurk D, Thomas JL, Cox AL, Engel CC, Castro CA (2008) Mild traumatic brain injury in U.S. Soldiers returning from Iraq. N. Engl. J. Med. 358:453-463.
3. Magnuson J, Leonessa F, Ling GS. (2012) Neuropathology of explosive blast traumatic brain injury. Curr Neurol Neurosci Rep. 12:570-9.
4. Cernak I, Radosevic P, Malicevic Z, and Savic J. (1995) Experimental magnesium depletion in adult rabbits caused by blast overpressure. Magnes Res 8: 249-259.
5. Garman RH, Jenkins LW, Switzer RC 3rd, Bauman RA, Tong LC, Swauger PV, Parks SA, Ritzel DV, Dixon CE, Clark RS, Bayir H, Kagan V, Jackson EK, Kochanek PM (2011) Blast exposure in rats with body shielding is characterized primarily by diffuse axonal injury. J Neurotrauma. 28:947-959.
6. Long JB, Bentley TL, Wessner KA, Cerone C, Sweeney S, Bauman RA. (2009) Blast overpressure in rats: recreating a battlefield injury in the laboratory. J Neurotrauma 26:827-840.

7. Fourney, W.L., Leiste, U., Bonenberger, R., and Goodings, D. (2005) Explosive impulse on plates, FRAGBLAST 9:1-17.
8. Fourney, W.L., Leiste, U., Bonenberger, R.J., and Goodings, D. (2005). Mechanism of loading on plates due to explosive detonation, FRAGBLAST 9:205-217.
9. Hazelton JL, Balan I, Elmer GI, Kristian T, Rosenthal RE, Krause G, Sanderson TH, Fiskum G. (2010) Hyperoxic reperfusion after global cerebral ischemia promotes inflammation and long-term hippocampal neuronal death. J Neurotrauma. 27:753-62.
10. Hall ED, Bryant YD, Cho W, Sullivan PG. (2008) Evolution of post-traumatic neurodegeneration after controlled cortical impact traumatic brain injury in mice and rats as assessed by the de Olmos silver and fluorojade staining methods. J Neurotrauma 25:235-47.
11. Tenkova TI and Goldberg MP. A Modified Silver Technique (de Olmos Stain) for Assessment of Neuronal and Axonal Degeneration. Methods in Molecular Biology 399:31-39 (2007).
12. Robertson CL, Puskar A, Hoffman GE, Murphy AZ, Saraswati M, Fiskum G. (2006) Exp Neurol. 97:235-43. Physiologic progesterone reduces mitochondrial dysfunction and hippocampal cell loss after traumatic brain injury in female rats.
13. Kochanek PM, Dixon CE, Shellington DK, Shin SS, Bayır H, Jackson EK, Kagan VE, Yan HQ, Swauger PV, Parks SA, Ritzel DV, Bauman R, Clark RS, Garman RH, Bandak F, Ling G, Jenkins LW. (2013) Screening of biochemical and molecular mechanisms of secondary injury and repair in the brain after experimental blast-induced traumatic brain injury in rats. J Neurotrauma 30:920-37.
14. Kumar A, Loane DJ (2012) Neuroinflammation after traumatic brain injury: opportunities for therapeutic intervention. Brain Behav Immun. 26:1191-201.

15. Hicks RR, Fertig SJ, Desrocher RE, Koroshetz WJ, Pancrazio JJ. (2010) Neurological effects of blast injury.J Trauma. 68:1257-63.

16. Shridharani JK, Wood GW, Panzer MB, Capehart BP, Nyein MK, Radovitzky RA, Bass CR. (2012) Porcine head response to blast. Front Neurol. 8;3:70.

17. Goldstein LE, Fisher AM, Tagge CA, Zhang XL, Velisek L, Sullivan JA, Upreti C, Kracht JM, Ericsson M, Wojnarowicz MW, Goletiani CJ, Maglakelidze GM, Casey N, Moncaster JA, Minaeva O, Moir RD, Nowinski CJ, Stern RA, Cantu RC, Geiling J, Blusztajn JK, Wolozin BL, Ikezu T, Stein TD, Budson AE, Kowall NW, Chargin D, Sharon A, Saman S, Hall GF, Moss WC, Cleveland RO, Tanzi RE, Stanton PK, McKee AC. (2012) Chronic traumatic encephalopathy in blast-exposed military veterans and a blast neurotrauma mouse model. Sci Transl Med. 16;4(134):134ra60.

18. Risling M, Plantman S, Angeria M, Rostami E, Bellander BM, Kirkegaard M, Arborelius U, Davidsson J. (2011) Mechanisms of blast induced brain injuries. Experimental studies in rats. Neuroimage. 54 Suppl 1:S89-97.

FIGRURE LEGENDS:

Figure 1. Device used for underbody blast-induced hyperacceleration experiments and accelerometer recordings obtained during the blasts. Tracings show highly reproducible accelerations generated by duplicate blasts at both 20 and 40 G and a single blast at 60 G.

Figure 2. Fluoro-Jade B staining for dead or dying neurons after exposure of rats to head impact or underbody blast. Sham animal was anesthetized with ketamine and perfusion fixed 7 days later. One rat was used in a controlled cortical impact (CCI) model of mod-

erate TBI and perfused 7 days later. One ketamine-anesthetized rat was subjected to a 50 G underbody blast and perfused 7 days later.

Figure 3. de Olmos silver staining of rat brain 7 days following a 50 G underbody blast. Widespread staining demonstrates axonopathy in white-matter structures of the cerebellum in rats exposed to underbody blast (A) as compared to Sham controls (B). High magnification confirms the presence of abnormal swellings and varicosities present in silver stained axons within the internal capsule (C,D) following blast exposure.

Figure 4. de Olmos silver staining of rat brain internal capsule at early and late time points following 20 and 50 G generated blasts. Intense internal capsule staining is induced with 50 G forces (B-D) which appears to dissipate with time as compared to ketamine-anesthetized sham controls (A). Sham (A), 50 G at 3 hours post-blast (B), 50 G at 7 days post-blast (C), 50 G at 30 days post-blast (D).

Figure 5. Astrocyte activation near hypothalamic regions at 7 days after a 50 G under-body blast. Intensities of GFAP-stained astrocytes were greater in animals exposed to under-body blasts compared to sham-treated rats. Astrocyte activation was observed in the internal capsule (B), and regions of the hypothalamus (D) as compared to these regions in shams (A,C).

Figures

Click here to download high resolution image

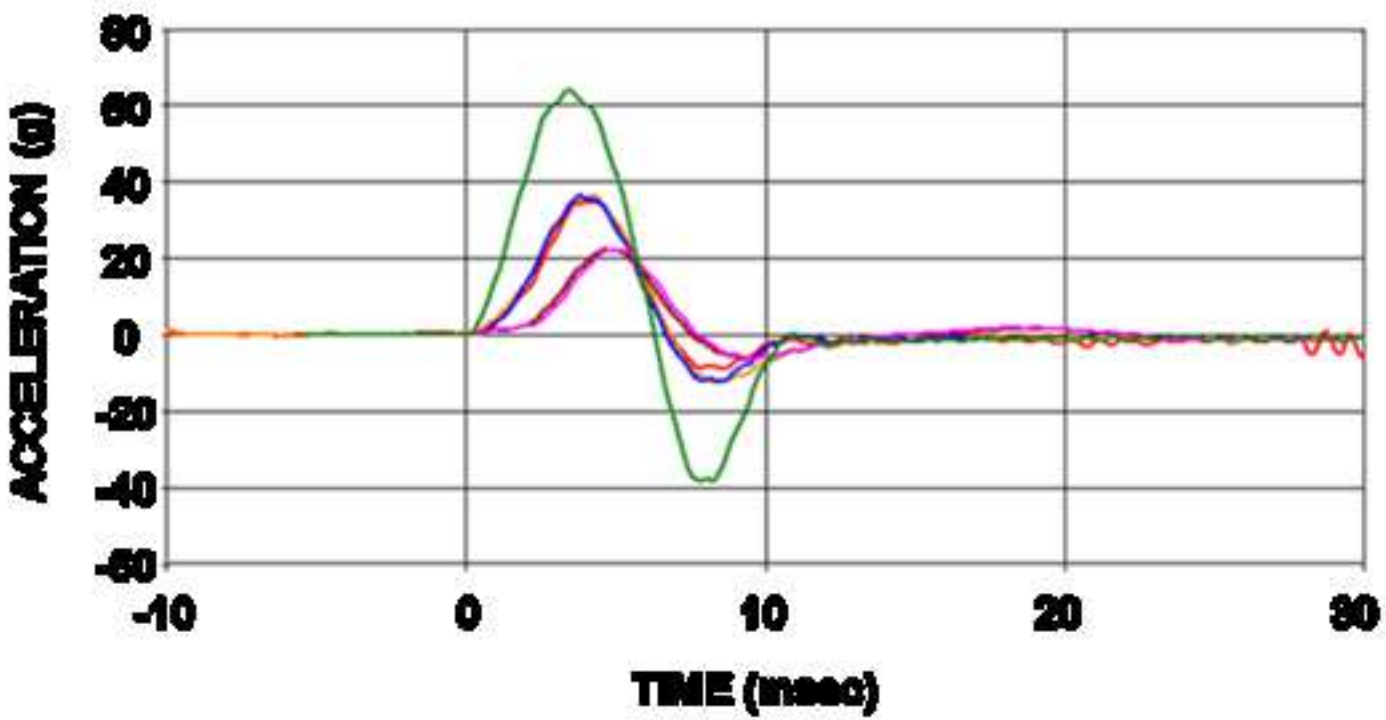

Figures
Click here to download high resolution image

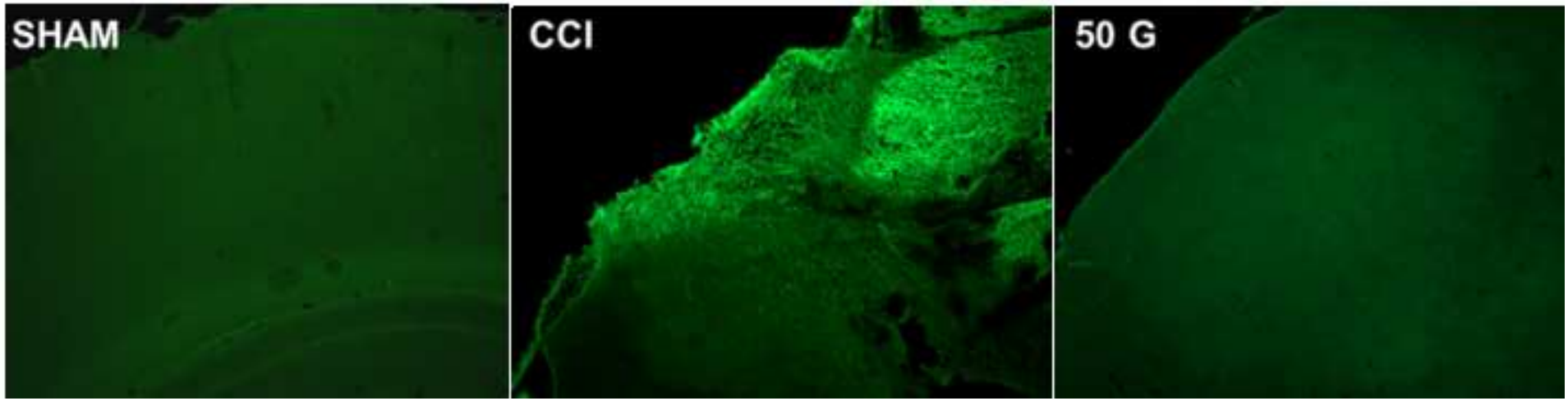

Figures

Click here to download high resolution image

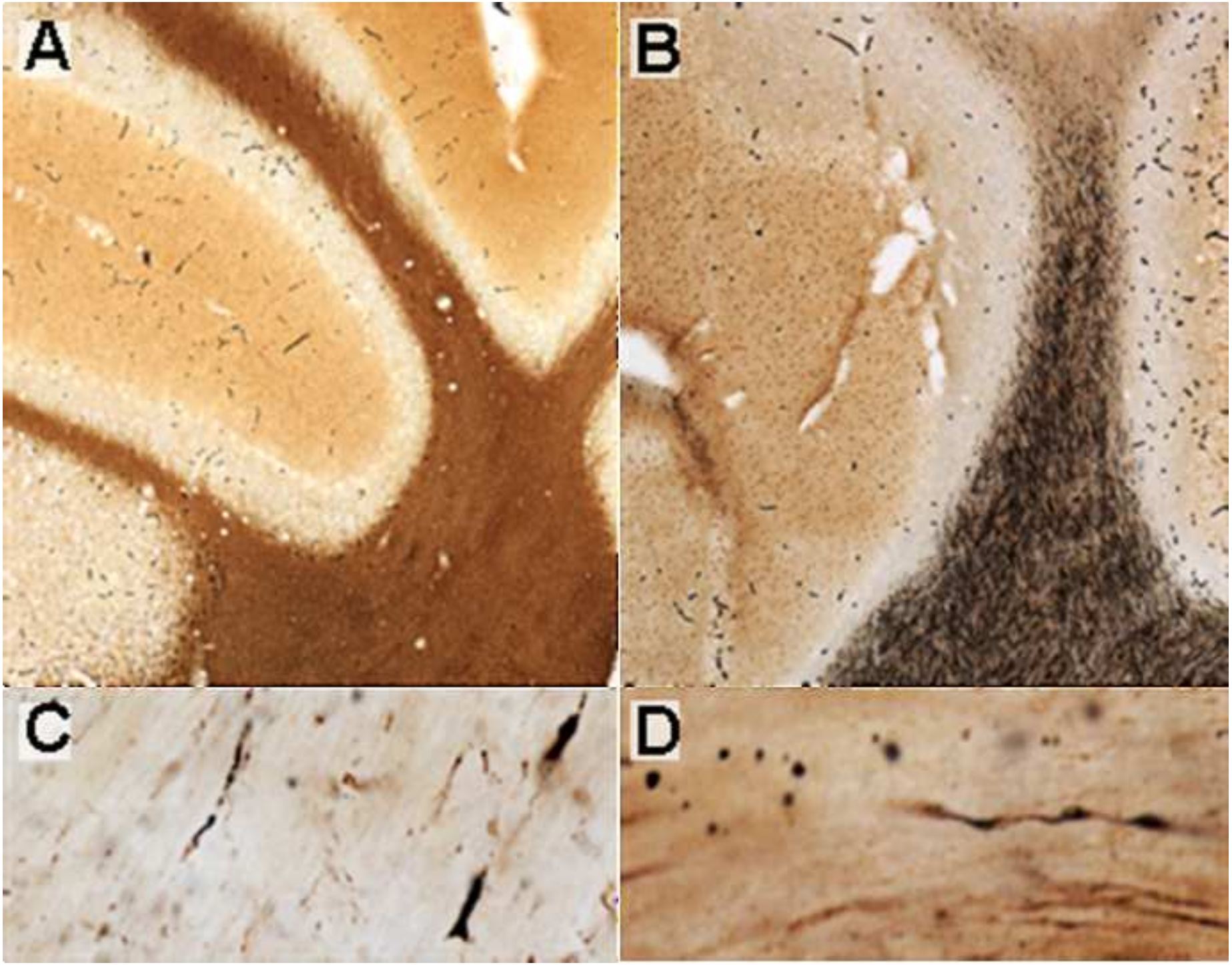

Figures

Click here to download high resolution image

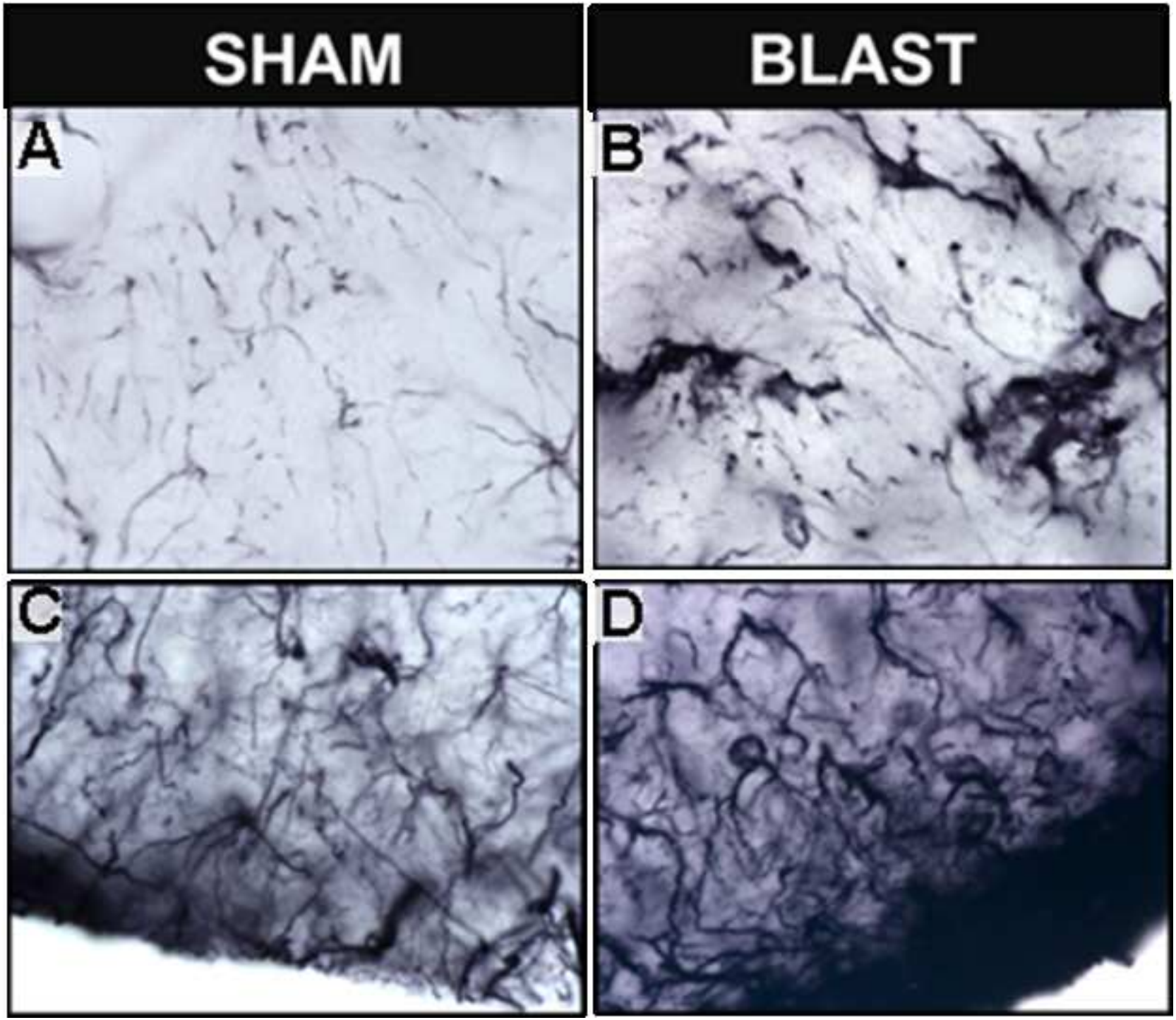

Figures

Click here to download high resolution image

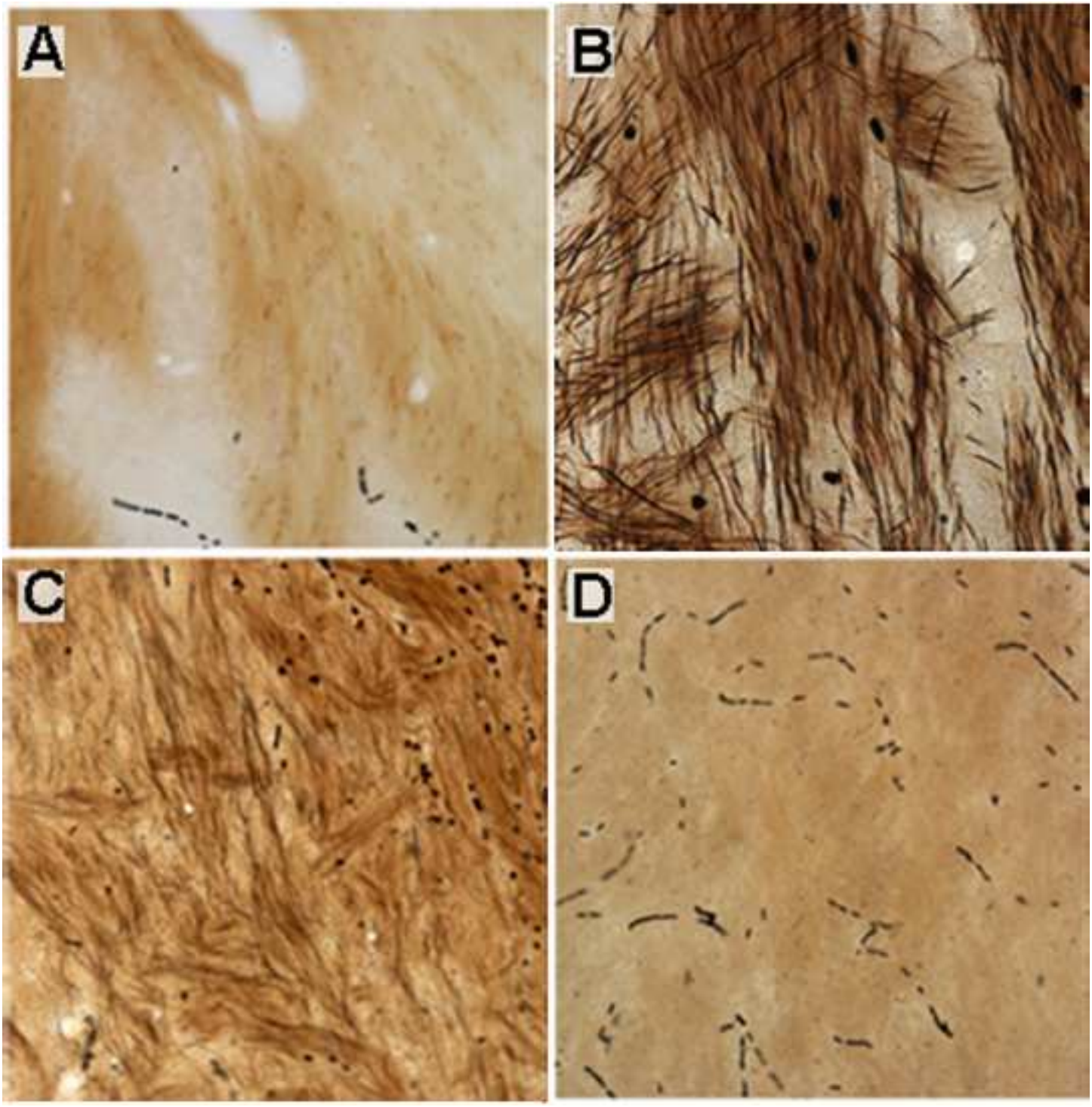

From: em.jt.1df.39d5fa.2f7b41a8@editorialmanager.com on behalf of Steven R. Shackford <shackford.steven@scrippshealth.org>
Sent: Monday, March 17, 2014 1:40 PM
To: FISKUM, GARY
Subject: Manuscript #JT-S-13-00245R1

Re: JT-S-13-00245R1
"Rat Model of Brain Injury Caused by Under-Vehicle Blast-Induced Hyperacceleration"

Dear Dr. Fiskum:

Thank you again for submitting your work to the Journal of Trauma's Military Health System Research Symposium supplement. We are pleased to inform you that your manuscript has been approved by the MHSRS editors.

As you know, your manuscript's files will now be sent to the Journal of Trauma's editorial office to determine whether further peer review is warranted.

In the meantime, please note that the Journal must have signed Copyright Assignment and Financial Disclosure forms from each author associated with this paper before your manuscript can be processed.

To access these forms, please visit the Journal's home page at www.editorialmanager.com/jt. The links to these forms are located under the 'Files & Resources' heading. Please download, complete, sign, and return these forms at your earliest convenience.

If you have any questions, please contact me or the Journal's editorial office at 303-602-1815 or 303-602-1816 any time.

Best regards,

Steven R. Shackford, MD
Associate Editor, Journal of Trauma and Acute Care Surgery

Col. Todd E. Rasmussen, MD
Guest Editor, Journal of Trauma and Acute Care Surgery

Presented at the 2013 National Neurotrauma Society Symposium

Hypobaria Worsens Axonal Injury and Blood Brain Barrier Disruption Induced by Underbody Blast-induced Hyperacceleration

Julie Proctor, Irina Balan, Yi-Chun Hsieh, William Fourney, Adam Puche, Alan I. Faden, Robert Rosenthal, Raymond Fang, Parissa Rangghran, and Gary Fiskum
University of Maryland Schools of Medicine and Engineering

Introduction

Occupants of vehicles targeted by buried IEDs often sustain TBI. Warfighters that experience underbody blasts are aerially evacuated (AE) to a regional military medical center usually within a few days after injury. This study tested the hypothesis that exposure of rats to AE-relevant hypobaria worsens TBI caused by underbody blasts.

Methods

The underbody blast device consists of a water tank in which a platform is located that supports a thick aluminum plate located above the water line. The plate can travel vertically, guided by poles located in holes in each corner of the plate. The two cylinders secured to the top of the plate each house an anesthetized, immobilized male rat. An explosive charge is placed in the water precisely under the center of the plate at various stand-off distances that generate peak G-forces of from 100 - 700 Gs within 2 msec after the explosion. At 7 days after the blast, rats were perfusion-fixed and their brains analyzed for evidence of axonal fiber injury (de Olmos silver staining), and cerebrovascular injury (IgG for blood brain permeability (BBB) disruption). Quantification of silver-stained axons and number of IgG effusions employed a stereologic approach and StereoInvestigator software.

Results

The number of silver-stained axonal fibers (line crossings per 5000 μm^2) in the internal capsule was significantly greater in animals (n = 10/group) exposed to 100 G blast than in shams (8,0 ± 1.2 vs 3.9 ± 1.0), and three-times greater following 700 G blasts (12.5 ± 1.3). Animals exposed to 6 hr hypobaria (= 8000 ft altitude) at 6, 24, or 72 hr after the 100 G blasts all exhibited significantly more silver-stained fibers than those not exposed to hypobaria (14.7 ± 0.9; 19.8 ± 1.4; 15.3 ± 1.2, respectively). The number of perivascular IgG effusions present in the hippocampus (per mm^2) was also greater in animals (n=5/group) exposed to either 100 or 700 Gs (7.2 ± 1.4; 21.2 ± 3.9), compared to shams (3.0 ± 0.8). Preliminary results also suggest that exposure to hypobaria at 24 hr following exposure to 700 Gs blasts further increases the number of hippocampal IgG effusions (30.4 ± 5.7).

Conclusions

1. Underbody blast-induced acceleration loads of 100 – 700 Gs produce region-selective axonopathy quantifiable by silver staining. 2. BBB disruption occurs in the hippocampus after exposure of rats to blast-induced high G-forces. 3. Exposure to hypobaria similar to that experienced during AE causes an increase in axonopathy and blood brain barrier disruption. 4. These results represent the first quantitative evidence that blast-induced acceleration alone, in the absence of exposure to blast overpressure, results in white matter and cerebrovascular injury. 5. The increase in injury caused by exposure to AE-relevant hypobaria raises concerns about when it is safe-to-fly warfighters with TBIs. Further studies will determine the minimum delay before AE that is necessary to avoid exacerbation of different forms of brain injury.

Acknowledgments

Support from US Air Force Medical Service FA8650-11-2-6D04 and US Dept. of Defense W81-xWH-13-1-0016

Presented at the 2013 Military Health Services Research Symposium

Hypobaria Worsens Axonal Injury and Blood Brain Barrier Disruption Induced by Underbody Blast-Induced Hyperacceleration

Julie Proctor, Irina Balan, Yi-Chun Hsieh, William Fourney, Adam Puche, Alan I. Faden, Robert E. Rosenthal, Raymond Fang, Parissa Rangghran, and Gary Fiskum
University of Maryland Schools of Medicine and Engineering

Occupants of vehicles targeted by IED-generated blasts often sustain TBI. This study tested the hypothesis that exposure of rats to aerial evacuation (AE)-relevant hypobaria worsens TBI caused by underbody blasts. A PETN explosive was used to vertically accelerate rats secured to an aluminum plate at maximal G forces of 100 or 700 Gs. Rats were exposed to 6 hr hypobaria (=8000 ft) at 6, 24, or 72 hr post-blast. At 7 days post-blast the silver-stained axonal fibers in the internal capsule were significantly greater in animals exposed to 100 G blast than in shams, and three-times greater following 700 G blasts. Animals exposed to 6 hr hypobaria at 6, 24, or 72 hr after 100 G blasts exhibited significantly more silver-stained fibers than those not exposed. The perivascular IgG effusions in the hippocampus were also greater in animals exposed to either 100 or 700 Gs, compared to shams. Hypobaria at 24 hr following 700 G blasts further increased hippocampal IgG effusions. We conclude that 1. Underbody blast loads of 100 or 700 Gs produce region-selective axonopathy. 2. Blood brain barrier disruption occurs in the hippocampus after exposure of rats to blast-induced G-forces. 3. Exposure to AE-relevant hypobaria increases damage to axonal fibers and blood vessels. 4. The increase in injury caused by exposure to hypobaria raises concerns about when it is safe-to-fly warfighters with TBIs. Support by the US Air Force FA8650-11-2-6D04 and US Dept. of Defense W81-xWH-13-1-0016.

UNIVERSITY OF MARYLAND

CONFIDENTIAL

University of Maryland Intellectual Property Disclosure Form
(Patent, Copyright, Trademark and/or Tangible Research Property)

ATTENTION: If an invention is to be presented or published within a week, please contact the Office of Technology Commercialization (OTC) immediately (301-405-3947)

Guidelines and instructions for this form may be found at http://www.otc.umd.edu/documents/Guidelines and Instructions.doc
(Please review these instructions before signing the form)

Intellectual Property Disclosure Number: (to be assigned by OTC)

1. **Title of Invention/Work** Acceleration mitigation utilizing shape memory polymeric-coated metallic thin-walled cylinders

2. **Inventor/Creator Data** (*List inventors in order that they should appear on official documents; primary contact will be responsible for all communications regarding this invention.)*

Primary Contact Inventor/Creator Name: William Fourney

Inventor/Creator #1:
Dr. Name: William Fourney Percentage of Inventor Royalty (UM only) 50 %
Title: Professor Department: AE/ME U ID #: 104211647 Citizenship: USA
Full Business Address: 1131 U Martin Hall, University of Maryland, College Park, MD 20742
Full Home Address: 8710 Teresa Lane, Laurel, MD 20723
Direct Business Phone: 301 405 1129 Dept. Business Phone: Fax: Home Phone: 301 725 4108
Email: four@umd.edu UM Affiliation: ☒Faculty ☐Staff ☐Grad Student ☐Undergrad Student ☐Other
UM Appointment(s) at time of invention:
Institution Name: UMC 100% College Name: Engineering 100% Department Name: AE/ME 100%
Institution Name: % College Name: % Department Name: %

Inventor Signature: W Fourney **Date Signed:** 3/19/14

Inventor/Creator #2:
Dr. Name: Jarrod Bonsmann Percentage of Inventor Royalty (UM only) 50 %
Title: Lecturer Department: ME U ID #: 112043858 Citizenship: US
Full Business Address: 3181 Glenn L. Martin Hall, College Park, MD 20742
Full Home Address: 1115 Old Cedar Road, McLean, VA 22102
Direct Business Phone: 301-405-5339 Dept. Business Phone: Fax: Home Phone: 407-923-3554
Email: bonsmann@umd.edu UM Affiliation: ☒Faculty ☐Staff ☐Grad Student ☐Undergrad Student ☐Other
UM Appointment(s) at time of invention:
Institution Name: UMC 100% College Name: % Department Name: %
Institution Name: % College Name: % Department Name: %

Inventor Signature: J Bonsmann **Date Signed:** 03-19-14

Inventor/Creator #3:
Dr. Mr. Ms. Mrs. Name: Percentage of Inventor Royalty (UM only) %
Title: Department: U ID #: Citizenship:
Full Business Address:
Full Home Address:
Direct Business Phone: Dept. Business Phone: Fax: Home Phone:
Email: UM Affiliation: ☐Faculty ☐Staff ☐Grad Student ☐Undergrad Student ☐Other
UM Appointment(s) at time of invention:

Institution Name: % College Name: % Department Name: %
Institution Name: % College Name: % Department Name: %

Inventor Signature: _____ Date Signed: _____

(Please attach extra page(s) with information on additional inventors)

3. **Date of Invention** *(Provide the date the invention was first conceived. This date should be documented in your lab records. Give reference numbers and physical location of the lab records, but do not enclose them.)* 08/08/2013

4. **Brief Description of Invention** *(attach description if necessary)* abstract attached

5. **Detailed Description of Invention** *(Please attach a complete enabling description of the technology describing the specific novelty of the invention. The description may be by reference to a separate document such as a copy of a report, preprint, grant application, manuscript and the like.)*

6. **Sponsorship**
Funding Source: ☒Federal ☐State ☐Corporate ☐UM ☐MIPS ☐Other: ☐ None

Contracting Agency/Commercial Entity	Grant/Contract Number	Funding Amt.	UM FRS#	MIPS #
UMB(USArmy Contract)	SR00002574	400K	4305830	

7. **Publication**
(a) Submitted to a Journal: ☐Yes ☐No Date: Journal Name:
(b) Published: ☐Yes ☐No Date: Journal Name:
(c) Oral Disclosure: ☐Yes ☐No Date: Location: Handouts? ☐Yes ☐No
(d) Poster Presentation: ☐Yes ☐No Date: Published Abstract: ☐Yes ☐No
(e) Thesis or Dissertation: ☒Yes ☐No Date: 11/2014
(f) Other Disclosure: ☐Yes ☐No Date: Describe:

8. **Technology Significance** *(choose one)*
☐ Modification to existing technology ☐Substantial advancement in the art ☒Major breakthrough

9. **Technology Stage** *(choose one)*
☐Concept ☐Design ☒Prototype ☐Modification ☐Production Model
☐Used in current work ☐Ready to license final product

10. **Future Research Plans** What additional research is needed to complete development and testing of the invention?
(a) Is this research presently being undertaken? ☒Yes ☐No If yes, identify sponsor:
(b) Actively pursued by faculty/staff? ☒Yes ☐No If yes, identify faculty/staff:
(c) Actively pursued by corporate partner? ☐Yes ☐No If yes, identify corporate partner:
(d) Should corporate sponsorship be pursued, other than the corporate partner? ☐Yes ☐No
(e) Do you wish to form a "start-up" company based on this technology? ☐Yes ☒No

11. **Commercial Potential**
(a) List all products, processes and/or services you envision resulting from this invention and whether they can be developed in the near term (less than two years) or long term. -Vehicle protection systems, near term
(b) Software inventions: If this is a modification or improvement to an existing work or incorporates elements that are not original to the creator(s), please identify that work and its creator(s). n/a

12. **Competition and Potential Users and Manufacturers**
(a) Describe alternate technology or products, processes and/or services currently on the market of which you are aware that accomplish the purpose of this invention. Collapsible Bumpers
(b) Please identify any related technologies or devices which are used for other purposes.
(c) List any companies you believe may be interested in this technology. Provide contact(s), address(es) and phone number(s) for each, if available.

13. **Marketing**
Once the OTC staff accepts this disclosure, marketing of this technology will begin. Please acknowledge whether or not you believe the technology is ready for marketing to commence:
☒Begin marketing ☐Delay marketing until further notice (provide reason)
☐Company interested (identify company) ☐ Specifically contact persons and entities identified in 12(c)

Signatures All UM inventors must sign and date this Intellectual Property Disclosure Form which certifies that all information provided herein is complete to the best of the inventor's knowledge. Signatures further certify that inventors have reviewed and understand the University of Maryland Policy on Intellectual Property [IV-3.20 (A)]; Approved by the President on March 13, 2003, approved by the Chancellor on July 18, 2005 and the University of Maryland Intellectual Property Disclosure form General Guidelines and Information.

Completed Intellectual Property Disclosure Forms may be sent by email or mail to the Office of Technology Commercialization:
Postal Address: Office of Technology Commercialization, 2130 Mitchell Bldg., College Park, MD 20742
Email: otc@umd.edu

Incomplete Intellectual Property Disclosure forms cannot be processed and will delay the technology transfer process.

OTC Review and Acceptance of the Invention Disclosure (for OTC use only):

Printed Name: _____ Title:_____

Signature: _____ Date:_____

Guidelines and instructions for this form may be found at http://www.otc.umd.edu/inventors2/disclosures.html or contact the Office at Technology Commercialization at 301-405-3947

Acceleration mitigation utilizing shape memory polymeric-coated metallic thin-walled cylinders

Abstract

This paper investigates various means for mitigating acceleration experienced by passengers in vehicles subjected to blast loading. In order to complete this study, small-scale testing of simulated vehicles was used. The explosives designated for this research are exclusively buried in saturated sand, which will act as the loading media for the simulated vehicles. In addition to explosive testing, various tests were performed dynamically using a high-pressure gas gun. Test plates used in this study vary in both size and geometry. When necessary, simple plate geometries are employed to investigate various mitigation parameters. Ultimately, much of the testing was conducted on simplified scaled versions of vehicles likely to be subjected to attack. This paper focuses mainly on mitigation through crushing of thin-walled cylinders, but also investigates the advantages of applying polymeric coatings to dynamically loaded structures. Piezoelectric accelerometers are used in conjunction with high speed videography to collect test data. The ultimate goal of this research is to help create a vehicle that will increase the probability that the passengers will survive a blast event with minimal long-term damage to the brain.

Acceleration mitigation utilizing shape memory polymeric-coated metallic thin-walled cylinders

Introduction

Over the past decade, the increase in fatalities due to use of buried explosives has created a demand for expanded knowledge in the field of target response to blast loading. When a vehicle experiences a blast load from a buried explosive, it is speculated that the damage mechanisms for a passenger in the vehicle result from rapid accelerations [1] and large changes in momentum [2]. Blast loading results in traumatic brain injury (TBI) and violent injuries such as broken limbs due to rapid accelerations and large changes in momentum respectively. In recent years a growing number of people involved in buried explosive attacks have been diagnosed with TBI in what is speculated to have resulted from the rapid acceleration of the targeted vehicle. This research aims to help design vehicles that will minimize the amount of damage to a passenger traveling in a vehicle that undergoes explosive loading.

In order to accomplish the goals of the research, the primary experimental testing technique employed is small-scale explosive testing. This testing method is used to investigate means of acceleration mitigation including crushing of thin-walled cylinders. A number of geometric properties of thin-walled cylinders, such as height, wall thickness and outer diameter are all studied. In addition to geometric properties, the number of cylinders and to a minor degree, the cylinder material is also studied. The majority of the aforementioned tests were conducted on plates fabricated to be simplified scaled down versions of vehicles likely to undergo blast scenarios.

On top of using explosive testing to study mitigation properties of crushing of thin-walled cylinders, the mitigation properties of polymeric coatings of structures are also examined. Steel and aluminum bars coated with polyurea were tested dynamically using a pressurized gas gun to determine the effect of increasing the mass and thickness of polymeric coatings on acceleration. Thin-walled cylinders were also coated in polyurea and crushed by explosively loaded plates to determine the benefits of adding polyurea to the previously tested mitigation technique.

At the conclusion of the research it was determined that there are great benefits to using thin-walled cylinders to mitigate the acceleration of a passenger travelling in an explosively loaded vehicle. In addition to this, polymeric coatings were determined to be of use in the crushing of thin-walled cylinders and coated beams but the effects depend greatly on the amount of polyurea applied to the metallic structure.

Background

In answer to the demand for knowledge pertaining to vehicle response under blast loading, the Dynamic Effects Lab at the University of Maryland has spent much time and many resources investigating this event. Research has been conducted to better understand the mechanisms of the vehicle loading [3] and to determine various methods of reducing impulse and acceleration on these structures [4, 5]. The main mechanism of the vehicle loading for a buried charge is the impact on the vehicle bottom by the soil that is thrown up by the detonated charge. This soil has been

shown to be traveling in excess of Mach one, and when it is brought to rest on the bottom of the vehicle very large pressures develop [6].

As a result of the increased understanding of vehicle response to blast loading, the number of injuries and deaths as a consequence of buried explosive attacks has steeply declined as seen in Figure 1[7]. The most important development in vehicle design has been the utilization of Mine-Resistant Ambush-Protected vehicles which have angled bottoms that deflect the ejected soil in a sidewise direction.

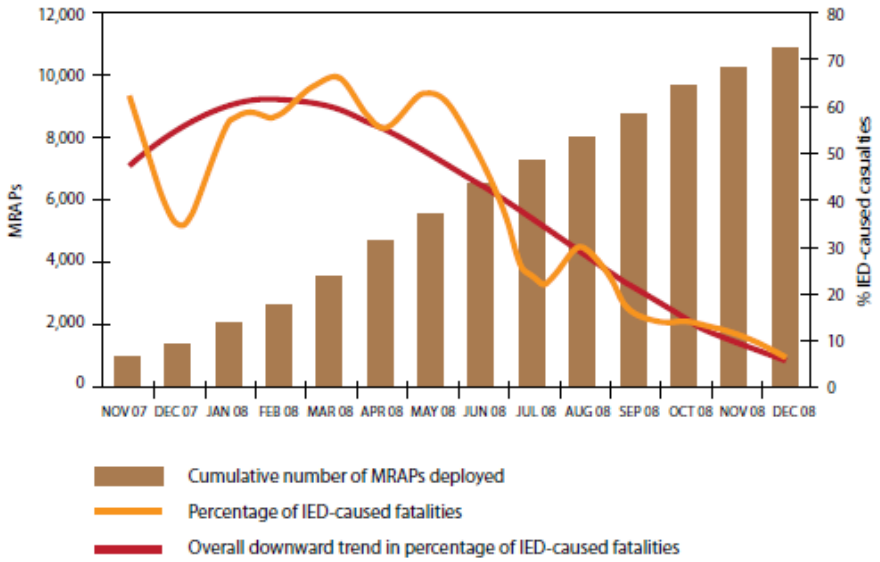

Figure 1: MRAPs deployed in the field versus IED casualties

By shaping the bottom of the blast loaded vehicles, violent injuries and deaths due to the change in the impulse have steeply declined. However, since the passenger of the vehicle is surviving beyond the initial blast, the incidences of TBI have risen. For this reason, further knowledge is needed in the area of acceleration mitigation on blast loaded vehicles.

The studies mentioned above place a good deal of emphasis on blast mitigation due to vehicle shaping. One of the primary focuses in this paper is to study the acceleration mitigation effects of localized buckling (crushing) of thin-walled cylinders. Thin-walled cylinders have long been studied in the field of energy absorption. There exists a plethora of research detailing the benefits of adding tubes to structures to absorb impact energy. For lower speed impacts both Alghamdi and Yuen et al. give an overview of a multitude of collapsible structures for use as energy absorbers [8, 9]. A number of studies have been performed characterizing the benefits of crushing tubes laterally for impact protection [10, 11]. Quite a few studies have been conducted to classify the energy absorption of composite tubes [12, 13, 14]. Additionally there have even been some studies, both numerical and experimental, where tubes or thin-walled structures of multiple geometries made of various materials (both metallic and composite) have been studied for use as sacrificial claddings for structures that undergo blast loading [15, 16, 17]. All of this research points to the fact that thin-walled structures, in a variety of geometrical patterns made

of all kinds of materials, have numerous benefits to offer when it comes to protecting structures from blast loads. There is a dearth of information, however, involving the benefits of using thin-walled cylinders as a technique for mitigating acceleration.

Much effort has been spent [18, 19] in researching the mechanical behavior of polymeric materials used for coatings in blast applications, especially the material polyurea. It has been found that under very high strain rates the polymer loses its "rubbery" mechanical behavior and begins acting more like leather. This characteristic allows the polymer to increase toughness under high strain rates, making it more effective at absorbing blast loads. In addition to characterizing the high strain rate mechanical properties of polyurea, the polymeric coating has been applied to panels that undergo blast loading in order to determine what benefits it has as a protective layer to prevent deformation and damage to structures. Major benefits in protection of structures due to polymeric or elastomeric coatings have been found when applied to composite structures [20]. On the contrary, when applied to steel plates, keeping the areal density constant, it was found that plain steel plates absorb the blast more efficiently than those coated with polyurea [21]. Finally, some preliminary work has been performed in previous years in the Dynamic Effects Lab that shows that coating the hull of a vehicle that undergoes blast loading is an effective means for acceleration mitigation, though it should be noted that the areal density of the plate was not kept constant in this study [22].

Small-Scale Testing

The testing facilities at the University of Maryland are equipped to perform small-scale explosive testing. Small-scale testing has a number of advantages over large-scale testing, costing less in both time and money to perform. In addition to these advantages, it has been shown [23, 24] that small-scale testing can accurately represent the response of a target to an explosion.

The scaling factor is determined by taking the cubed root of the ratio of the full-scale mass of the explosive over the small-scale mass of the explosive.

$$SF = \left(\frac{mass_{full-scale}}{mass_{small-scale}}\right)^{\frac{1}{3}}$$

In this work a geometry that will scale to 4.536 kilograms of explosive was used. In the majority of the research in this paper, the small-scale tests use an explosive mass of 4.4 grams, resulting in a scaling factor of approximately ten. All length and time dimensions are scaled using this factor. The small-scale lengths and times are determined by dividing the full-scale values by this factor while the small-scale accelerations are determined by multiplying the full-scale values by this factor.

Test Equipment

In order to perform a successful explosive experiment, a wide array of equipment is needed. Instrumentation to obtain measurements of acceleration, displacement, and time are all required to generate the data necessary for proper analysis. On top of that, equipment is needed for the blasting itself. In addition to the blasting apparatus,

equipment necessary for conducting dynamic testing using a pressurized gas gun is also required.

The accelerometers used in this series of tests were manufactured by PCB Piezotronics Inc. The accelerometers chosen were model 350B04 with a measurement range of ±5000g's. A PCB Piezotronics Inc. signal conditioner, model 483A and two LeCroy oscilloscopes, model numbers 9314AM and 9315AM, were employed alongside the accelerometers for data acquisition.

For obtaining displacement and time data for the blast tests, a Phantom v12.1 high speed camera equipped with a Tamron 28-75mm variable focus lens was used. The video was analyzed in the Phantom software. Microsoft Excel was used to create displacement versus time plots.

To create the blast, plastic explosive sheet (Deta Sheet from Omni Explosives) is used in conjunction with an Exploding Bridge Wire Detonator manufactured by Teledyne Technologies. The detonator has a small amount of explosive located inside of it that, when combined with the plastic deta sheet, sums up to a total mass of explosive reported for each test. The plastic explosive charge is formed and placed in a plastic sleeve to insure repeatability in charge geometry from test to test. The firing system responsible for detonation is connected to the explosive, high speed camera and oscilloscopes so that when the firing system is discharged each of the recording devices trigger so that they may record the explosive event simultaneously.

The actual blast test takes place in a tank constructed to outer dimensions of 1.5 meters long by 1.5 meters wide by 0.6 meters deep. The tank is filled with sand and is capable of being flooded with water from the bottom up. A schematic of the blast testing equipment is shown in Figure 2.

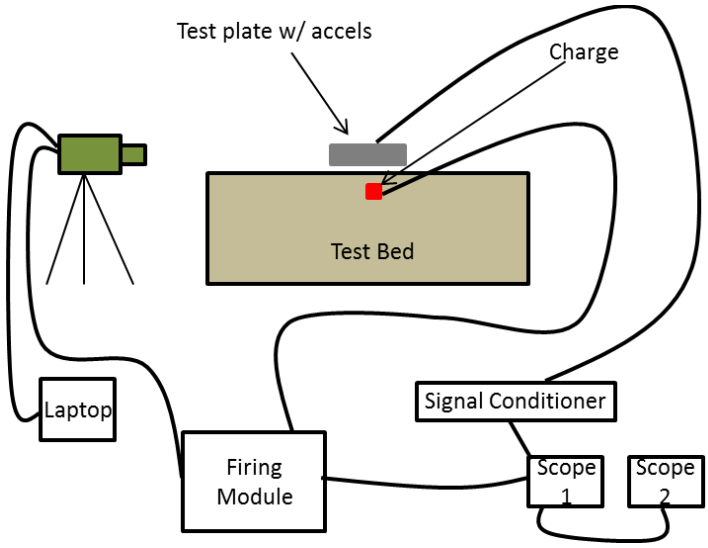

Figure 2: Schematic detailing blast test equipment set-up

Specific equipment is also necessary for dynamic testing using a pressurized gas gun. A high-pressure gas gun from a Split-Hopkinson bar is used in this research to provide dynamic loading to cantilevered beams. In addition to the gas gun, a cantilever support is created capable of providing a true cantilever boundary condition to a beam.

Blast Test Set-Up

There are a number of steps that must be taken in order to prepare for each blast test. Because the small-scale nature of the test, test preparation is performed with the utmost care as a small variation in any value may result in large variation in the test data. Each of the steps mentioned in the next paragraph are explained in more detail in previously published papers [29, 30].

The initial sand bed preparation consists of creating a 1.2 meter by 1.2 meter elevated and compacted sand platform in the center of the test bed. The height and compaction of the sand bed is controlled and repeatable. Once created, the explosive charge is buried in the sand platform at a location directly under the center of any specific test plate.

For all of the tests in this study a depth of burial (DOB) corresponding to ten centimeters large-scale is used. The small-scale DOB is ten millimeters since, as previously mentioned, the scaling factor for this series of tests was determined to be approximately ten. DOB is defined here as the distance between the top surface of the charge and the surface of the sand.

The next step is to locate the plate and set its stand-off distance (SOD). SOD is defined as the distance between the top of the sand and the bottom of the target plate. Depending on the plate characteristics, the test plate may either be placed on a set of blocks that are machined to have the exact height of the specified SOD, (Figure 3), or suspended above the sand on chains attached to the ceiling.

Once prepared, the test bed is saturated from the bottom up. The water height is controlled and repeatable. The final test set-up for a blast test is shown in Figure 3.

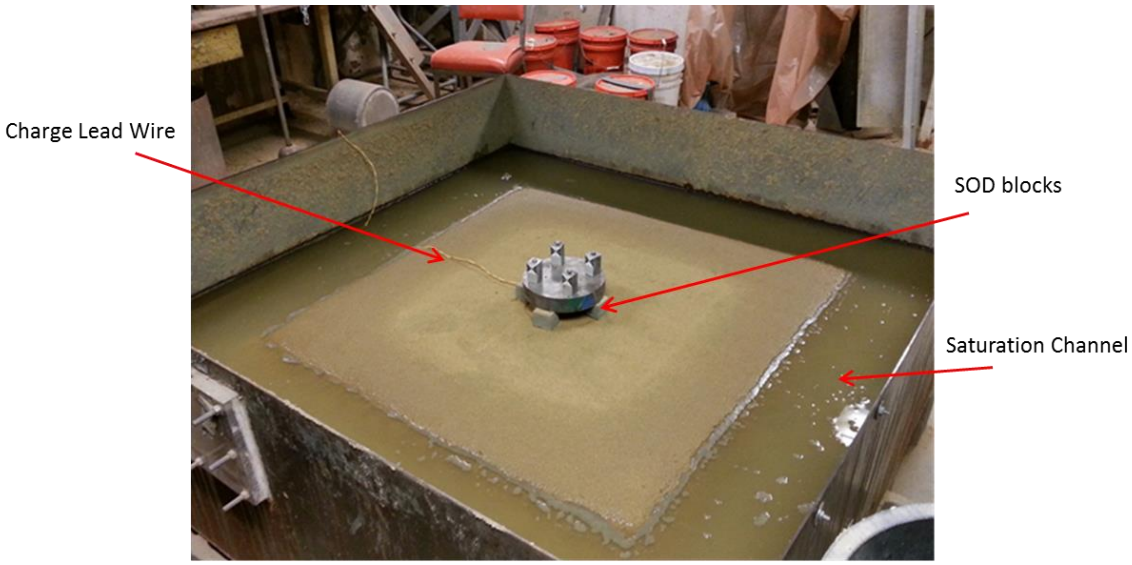

Figure 3: Fully prepared blast test sand bed

Once the bed has saturated fully, the accelerometer cables are connected to each accelerometer on the plate. The high speed camera is set-up and the image adjusted, following which a dummy charge is fired to make sure all data acquisition systems are functioning properly. After the dummy round, the charge lead wires are connected to the firing module and the charge is detonated. Upon detonation the video is examined and saved using the Phantom software. The acceleration signal is downloaded from the scopes and viewed in the UERDTools program to ensure proper recording; the signals are then saved and analyzed.

Gas Gun Test Set-Up

The cantilever beam tests are set-up by first placing a beam in the cantilever support mentioned in the section on gas gun test equipment. Care is taken to place the center of the beam in line with the striker projectile path. The beam is clamped such that it cannot move in the support.

Once the beam has been placed in the testing position, the gas gun projectile is loaded and the pressure chambers primed. For the beam testing the pressure is in the neighborhood of 75 kilopascals, and will be described in more detail later. Once the gun is pressurized, the oscilloscopes and high speed camera are made ready and are triggered simultaneously by the firing of the gas gun. The data is then downloaded from the oscilloscopes and saved for processing using the Phantom high speed camera software.

Mitigation Study on Small-Scale Vehicle Shapes

Ideally, the plates under study should reflect the geometric properties of the vehicles that are regularly targeted by explosive devices. As such, for the upcoming portion of this research, rectangular plates having the scaled down dimensions of some of those vehicles are used. Specifically, each plate has outer dimensions of 45.72 centimeters by 30.48 centimeters.

This series of tests utilizes a hull/frame combination to represent the vehicle. The hull, or bottom, of the simulated vehicle is responsible for capturing all of the ejecta. The frame, or top, of the simulated vehicle represents where the passengers of an actual vehicle would sit; this is where the accelerometers and tracking targets are placed, as this is the portion of the vehicle for which the mitigation needs to have the most effect. The hull to frame mass ratio is kept close to one. If the mass of the hull is much greater than the mass of the frame, it can be postulated that that the acceleration of the frame will be very high. On the other hand, if the frame is much more massive than the hull, this set-up might result in unrealistically low acceleration values.

Before going into any detail regarding the test series, it is necessary to describe the general test set-up used for the mitigation study. As previously mentioned, this series of tests employed a hull/frame combination small-scale vehicle. In between the hull and frame, there is at any given time either a series of thin-walled cylinders made from metal of various geometric properties, or air. The combination of the hull and frame resulted in a vehicle mass in the neighborhood of 15 kilograms.

It was mentioned previously that there are two methods for setting the SOD of a test plate – the stand-off blocks and hanging the plate from chains. The chains are normally used for heavier plates. For the mitigation tests, a combination of the two methods was used. The first portion of the mitigation study involved creating baseline data where the only air separates the hull and the frame. For these tests, the hull rested on stand-off blocks and the frame hung on the chains a specific distance away from the hull. In later tests when mitigation was added in between the hull and the frame only one of two SOD scenarios is used.

The first and most common set-up involves attaching the thin-walled cylinders only to the hull. In this situation, as in the air gap tests, the hull rests on the blocks and the frame is lowered on the chains until the frame just makes contact with the thin-walled cylinders. This set-up prevents the stand-off block from supporting too much weight – causing them to sink in the saturated sand and changing the SOD. For a few tests, the thin-walled cylinders are attached to both the hull and the frame. These tests only require the use of the chains to set the SOD of the test plate.

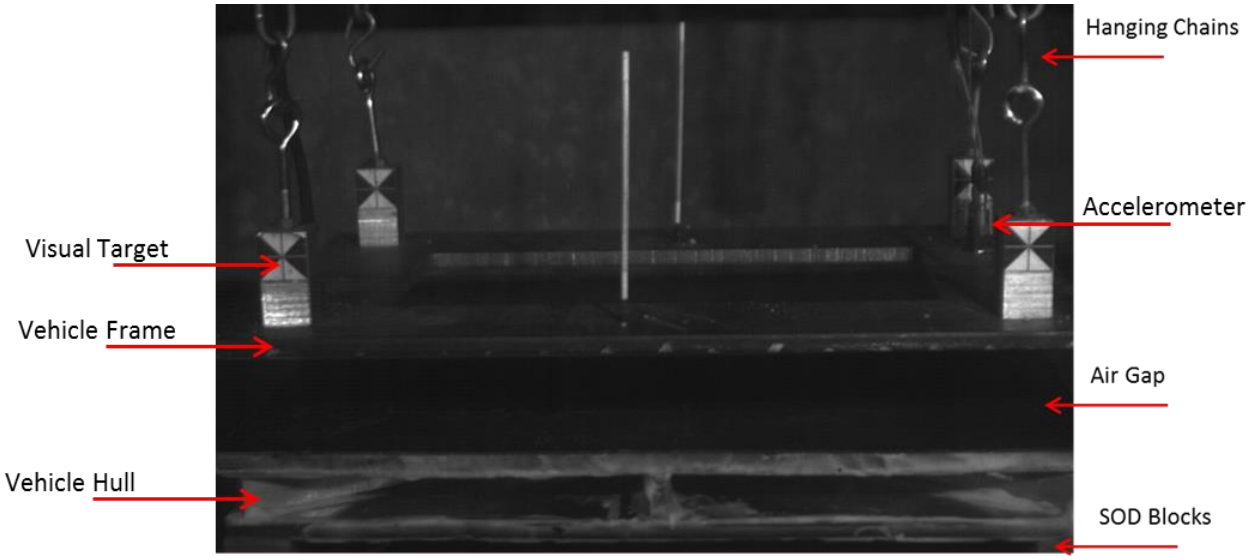

Figure 4: Test set-up for no mitigation tests

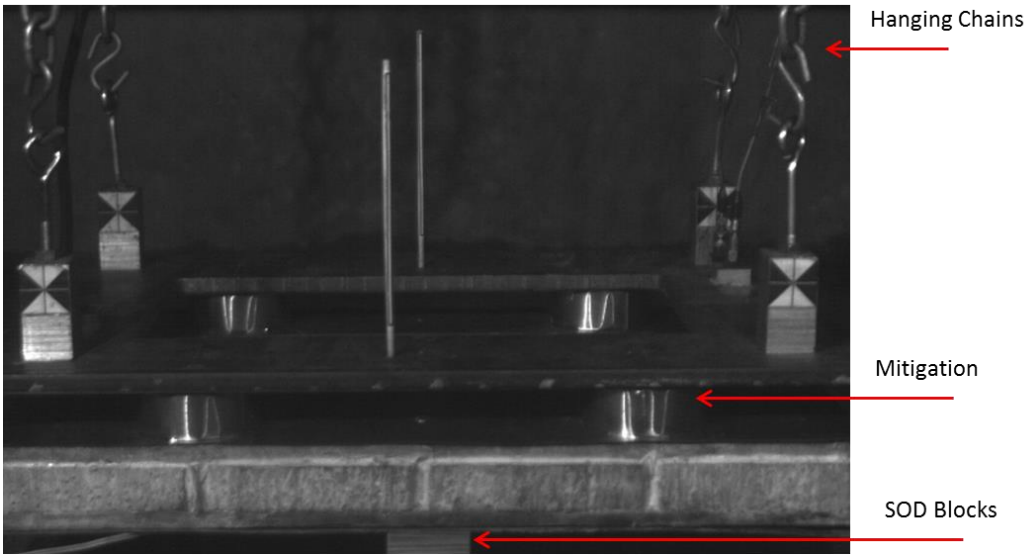

Figure 5: Test set-up with mitigation attached to hull only

A couple of minor things need to be mentioned in this section. The first is that each test plate will have four targets attached to the frame. One target will be located on each corner of the frame so that it may be tracked using the high speed camera. The second is that each test frame, much like those in the previous studies, will have two or three accelerometers located along a diagonal line connecting the left front portion of the frame with the rear right portion. These acceleration signals are averaged to give the final readings reported in the results section. The accelerometers and the visual targets can all be seen in Figure 4, Figure 5.

Height of Target Study

The first series of complete tests run to study the effect of adding thin-walled cylinders to mitigate acceleration was executed to determine how changing the height of the cylinders changes the peak acceleration recorded on the frame. The initial tests

in this series were conducted with no mitigation between hull and frame. Following this, four tests were run with standard aluminum beverage cans separating the hull and the frame by distances of 25, 38, and 50 millimeters.

The cylinders for the first round of mitigation tests were attached only to the hull. The second round of mitigation tests consisted of the same geometry cans tested with the cans attached to both the frame and the hull, resulting in an accordion type stretching following the initial crushing. One test was repeated to demonstrate test repeatability. The test matrix can be seen in Table 1.

Table 1: Test matrix for HOT test study

Test Number	Charge Mass (g)	DOB (mm)	SOD (mm)	# of Cylinders	Cylinder Material	Cylinder OD (mm)	Cylinder ID (mm)	Height of Target (mm)
1	4.4	10	40	-	-	-	-	50
2	4.4	10	40	-	-	-	-	25
3	4.4	10	40	-	-	-	-	38
4	4.4	10	40	4	Aluminum	66	65.8	50
5	4.4	10	40	4	Aluminum	66	65.8	25
6	4.4	10	40	4	Aluminum	66	65.8	38
7	4.4	10	40	4	Aluminum	66	65.8	25
8*	4.4	10	40	4	Aluminum	66	65.8	25
9*	4.4	10	40	4	Aluminum	66	65.8	38
10*	4.4	10	40	4	Aluminum	66	65.8	50
Note: Test numbers with an * were conducted with the cylinders attached to both frame and hull								

Height of Target Study Test Results

At the end of the test series described in Table 1, the acceleration signals were analyzed and averaged for each test. It is of interest to view how the acceleration signal changes from a test with no mitigation, to mitigation attached the hull only, to mitigation attached to both the hull and the frame. A plot of this can be seen in Figure 6. This plot compares the signals from the accelerometers from the tests for each scenario at a HOT of 25 millimeters. Following this plot, a full summary is given of how the acceleration changes with HOT for the three different test scenarios: No mitigation, mitigation attached to the hull, and mitigation attached to the hull and the frame. This plot is presented in Figure 7. A zoomed in view of the benefit of attaching the cylinders to the frame and the hull can be seen in Figure 8.

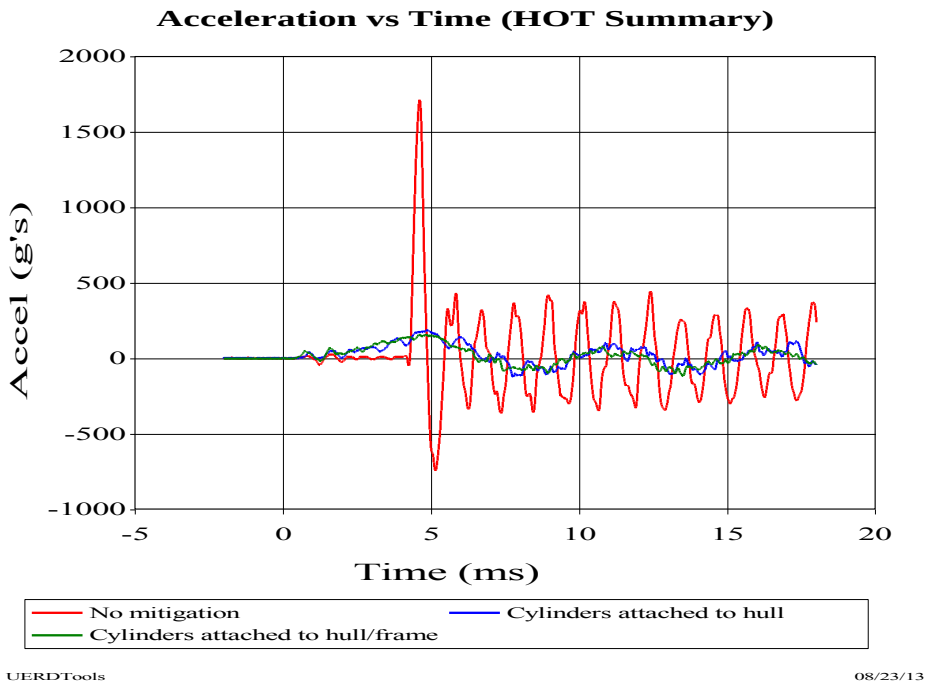

Figure 6: Comparison of acceleration signals for HOT study

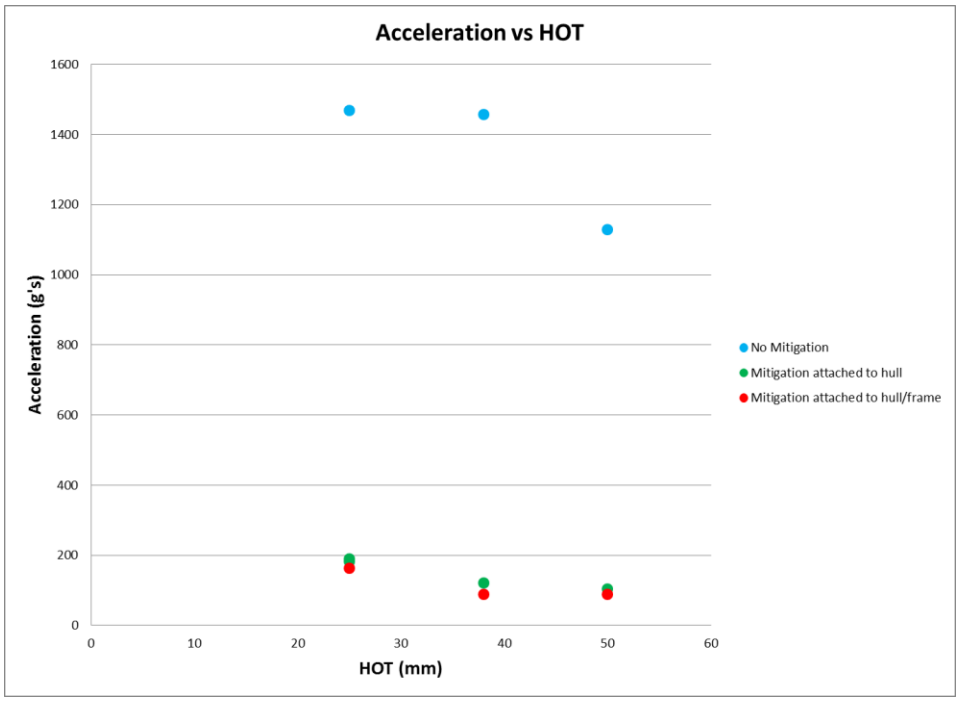

Figure 7: Acceleration versus height of target for no mitigation and mitigation

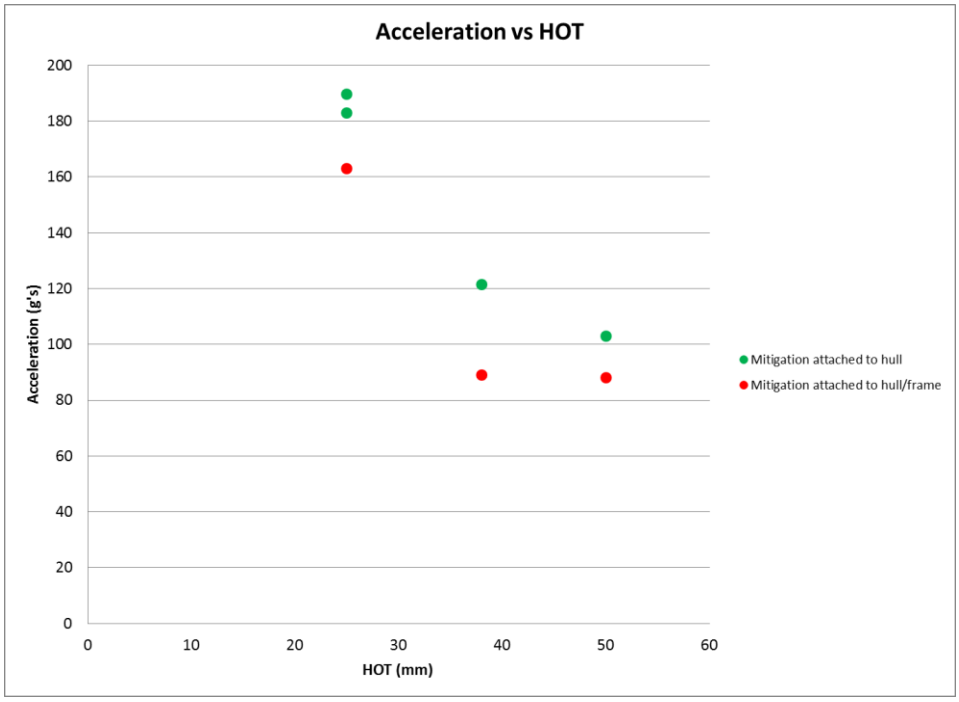

Figure 8: The effect of attaching cylinders to the hull and the frame

The first and primary take-away from the graphs in this section is that the crushing of thin-walled cylinders as a source of mitigation of acceleration can have a tremendous effect. At a height of target of 25 millimeters, the peak frame acceleration is decreased from close to 1500g's to around 190g's. Going a step further, if the cylinder height is increased by a factor of two, and the accordion stretching of the cans is added to the initial crushing by attaching the can to the frame, the acceleration level can be decreased to around 90 g's.

To put this into perspective, using the cube-root scaling law and scaling this result up to full-scale, for this series of testing, in the worst case scenario (no mitigation, 25 centimeter HOT full-scale) a passenger would experience an acceleration of 150g's – a fatal level. Using the hull/frame attached cans at a HOT of 50 centimeters full-scale, a passenger in the vehicle would experience around 9g's. This is around the same level of acceleration experienced by a fighter pilot in an ejection seat.

Number of Thin-Walled Cylinders Study

In order to determine the effect of adding more cylinders between the hull and the frame, a test series was run for four different scenarios. Initially a control test containing no cylinders was run. After which the number of cylinders was increased to four, then six, then eight. A summary of the important test parameters is listed in Table 2. Each test will be run with the cylinder attached only to the hull.

Table 2: Test matrix for the number of thin-walled cylinder study

Test Number	Charge Mass (g)	DOB (mm)	SOD (mm)	# of Cylinders	Cylinder Material	Cylinder OD (mm)	Cylinder ID (mm)	Height of Target (mm)
Control	4.4	10	40	0	-	-	-	25
1	4.4	10	40	4	Aluminum	66	65.8	25
2	4.4	10	40	6	Aluminum	66	65.8	25
3	4.4	10	40	8	Aluminum	66	65.8	25

As can be seen in Table 2, the thin-walled cylinders used for this study are of the same outer diameter and wall thickness of the cylinders used for the HOT study. Namely, a typical aluminum beverage can is used. It was decided to test the worst-case HOT in every instance for this study. This decision was made for two reasons. The primary reason for determining that a 25 millimeter height of target should be used comes as the fact that vehicles in the field face situations where vehicle roll-over is a very real concern. To combat this, it is often desired that the vehicle center of gravity be as low as possible. By testing the 25 millimeter high cylinders, a determination of the effectiveness of the mitigation techniques for a low center of gravity vehicle can be made.

Another reason for testing the 25 millimeter cylinders comes as the fact that the acceleration levels of the 50 millimeter HOT tests are simply too low to be easily measured. Upon examining the acceleration signals from the 50 millimeter HOT tests (Figure 9) it is not too difficult to imagine that the peak acceleration comes from the low frequency vibrations of the frame as opposed to a sharp acceleration peak resulting from hull to frame contact. Because of the extremely low acceleration levels of the 50 millimeter HOT, a more effective study of the effect of increasing the number of cylinders can be made at the 25 millimeter HOT. A comparison of the two different HOT test accelerations can be seen in Figure 9.

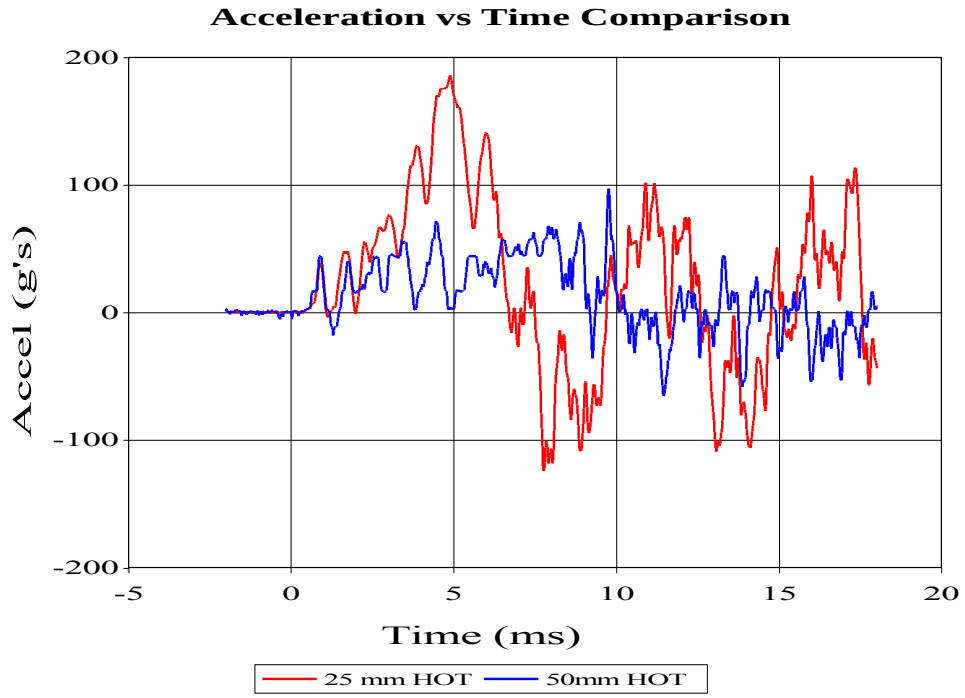

Figure 9: Comparison of acceleration signals for 25mm HOT and 50mm HOT

Number of Thin-Walled Cylinders Study Test Results

One of the initial interesting results coming from increasing the number of cans happens to be the general shape of the acceleration pulse. From looking at the test with four cylinders separating the hull and the frame, it appears as if there is a strong element of low frequency frame vibration that adds an element to the acceleration signal. When the cylinder number increases, that low frequency vibration seems to be eliminated. An illustration of this is seen in Figure 10. The red signal represents the four can test, with the blue and green signals representing six and eight cans respectively. After the initial peak acceleration, the four can test has a substantial vibration signal at a defined frequency. This vibratory characteristic does not appear in either of the other tests.

The overall effect of increasing the number of cylinders is also presented here. As in other tests, the average peak acceleration for each test is determined and plotted versus number of cans. The results can be seen in Figure 11.

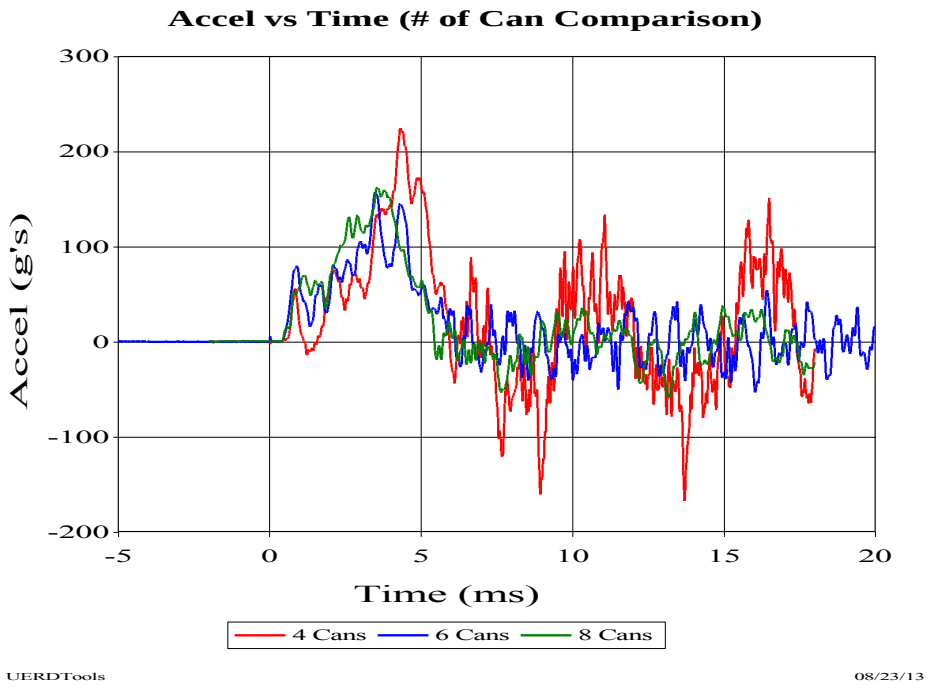

Figure 10: Comparison of acceleration signals for four, six, and eight cans

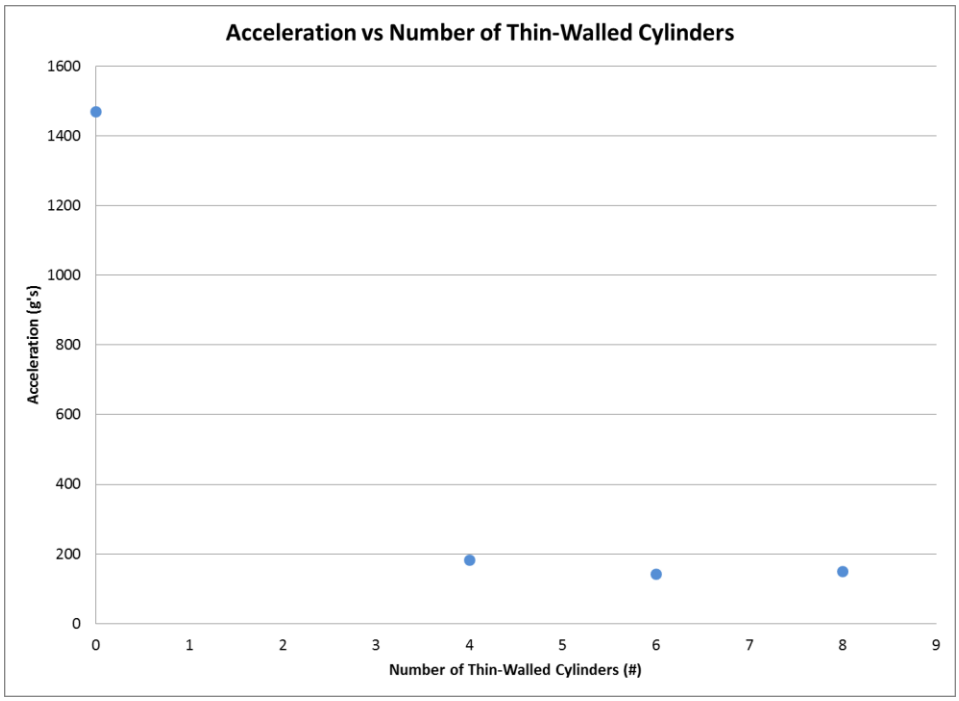

Figure 11: Acceleration versus number of thin-walled cylinders

From looking at Figure 11 some general remarks should be made. It appears as if there is a slight benefit to be realized in peak acceleration by increasing the number of cylinders to six and eight. Full-scale acceleration levels decrease from around 18 g's to somewhere in the neighborhood of 14 to 15 g's. While not a drastic drop the benefit is definitely there. Additionally, as mentioned previously, it looks like

increasing the number of cans may damp out low frequency frame vibration; significantly reducing the duration of time a passenger might experience high levels of acceleration.

Outer Diameter Study

To study the effect of an increased and decreased outer diameter of the mitigating cylinders, a series of four tests was run. In this series, in addition to the control test where no mitigation was present, tests were run with the outer diameter varying from 53 to 73 millimeters. The cylinders used for this test are beverage containers having the same wall thickness made from the same material, but of different outer diameters. The test matrix can be viewed in Table 3.

Table 3: Test matrix for outer diameter study

Test Number	Charge Mass (g)	DOB (mm)	SOD (mm)	# of Cylinders	Cylinder Material	Cylinder OD (mm)	Cylinder ID (mm)	Height of Target (mm)
Control	4.4	10	40	0	-	0	0	25
1	4.4	10	40	4	Aluminum	66	65.8	25
2	4.4	10	40	4	Aluminum	73	72.8	25
3	4.4	10	40	4	Aluminum	53	52.8	25

As in the number of thin-walled cylinder study, a height of target of 25 millimeters is used for this series of tests; for the same reasons as listed in that section. From examining Table 3, it should also be noted that only four cylinders were used in each of these tests. The final note before discussing test results is that the cylinders were only mounted to the hull.

Outer Diameter Study Test Results

As in the previous series of tests, a comparison between the actual acceleration signals is presented (Figure 12) along with the trend of acceleration versus outer diameter (Figure 13). When comparing the three tests with cylinders it is seen that each acceleration signal has the same low frequency vibrations present. This backs up the previous hypothesis that, when excited from the four points of contact of the thin-walled cylinders, the frame vibrates at a low frequency resulting in a relatively high acceleration level. The red line represents the smallest outer diameter, the blue line represents the middle outer diameter size, and the green line portrays the acceleration of the simulated vehicle frame that utilized the cans with the largest outer diameter.

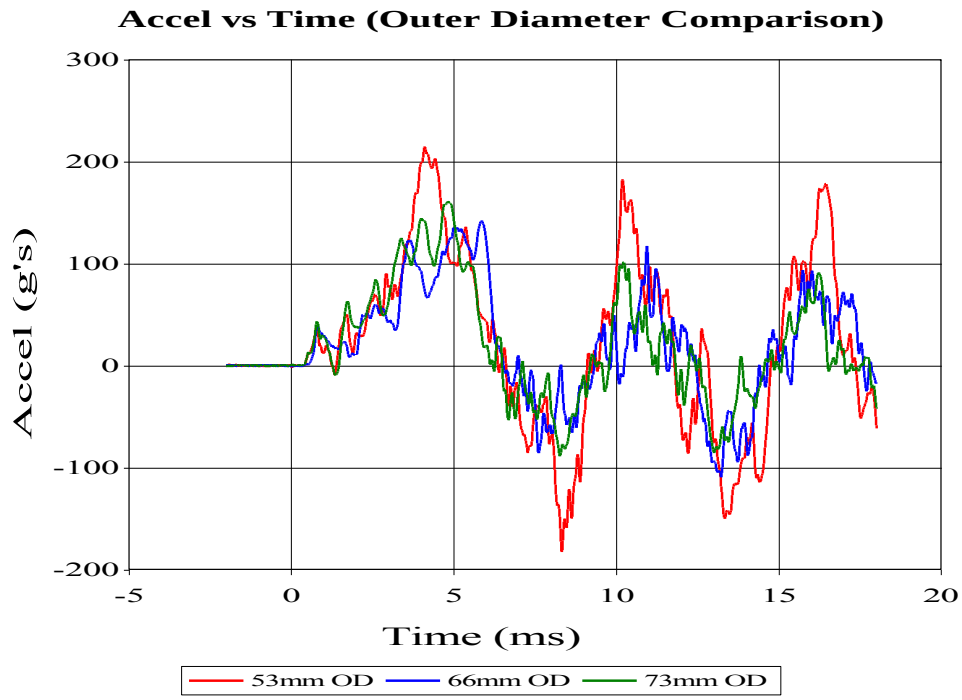

Figure 12: Acceleration signal comparison for outer diameter study

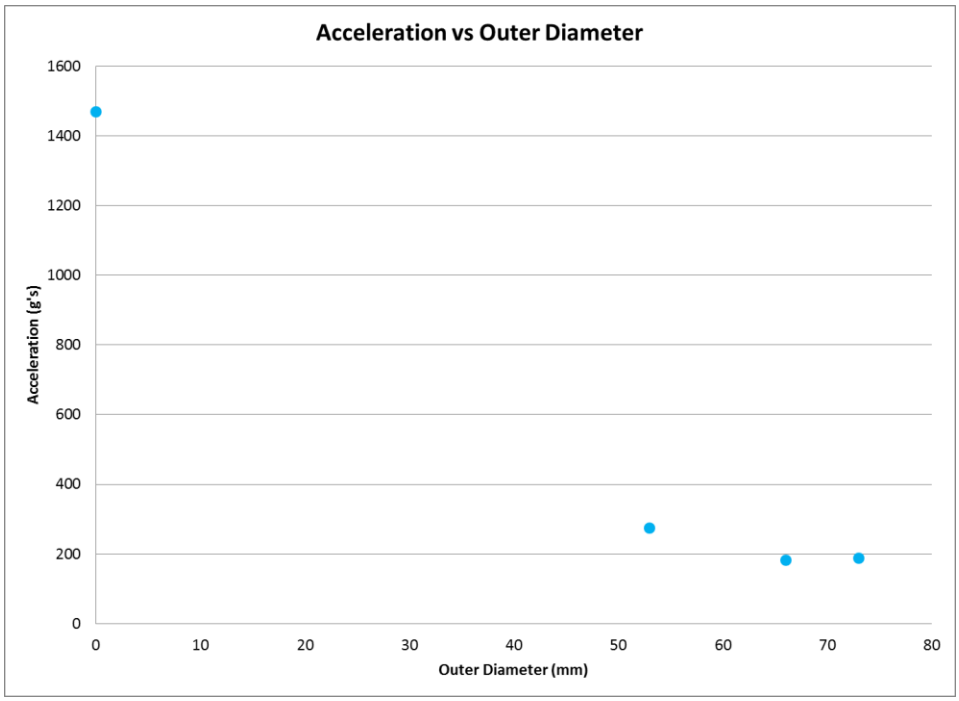

Figure 13: Acceleration versus outer diameter of mitigation cylinders

After examination of Figure 13 a few observations are in order. Starting with the graph displaying acceleration, it is seen that at the 53 millimeter outer diameter, the acceleration of the frame decreases from the baseline value of 1470 g's to around 275 g's. The sharp decline of acceleration continues at 66 millimeter outer diameter where the acceleration drops to around 180 g's. After which it appears as if the

acceleration value levels off somewhat, and a drastic change is not noted when moving from a 66 millimeter outer diameter to a 73 millimeter outer diameter..

Wall Thickness Study

To test the effect of wall thickness on acceleration, the test preparation is a bit more involved. In previous tests, beverage cans with the necessary geometric characteristics were used as the mitigation material. This provided a cylinder, uniform in wall thickness, with a seamless construction. Beverage cans of varying wall thicknesses could not be found, so thin-walled cylinders of varying wall thicknesses had to be constructed out of shim stock.

The initial test of this series involved replicating a previously performed test, but this time performing the test with a shim stock cylinder as opposed to a commercially produced cylinder. In addition to this comparison, two additional tests were completed with different wall thicknesses from the original test. The test matrix for the wall thickness study can be seen in Table 4.

Table 4: Test matrix for wall thickness study

Test Number	Charge Mass (g)	DOB (mm)	SOD (mm)	# of Cylinders	Cylinder Material	Cylinder OD (mm)	Cylinder Wall Thickness (mm)	Height of Target (mm)
Control	4.4	10	40	0	-	0	0	25
1	4.4	10	40	4	Aluminum (commercial)	66	0.1	25
2	4.4	10	40	4	Aluminum (shim)	66	0.1	25
3	4.4	10	40	4	Aluminum (shim)	66	0.15	25
4	4.4	10	40	4	Aluminum (shim)	66	0.2	25

From the test matrix note that these test were performed at a height of target of 25 millimeters; done for previously stated reasons. Also, for each of the tests only four thin-walled cylinders were used for mitigation. The cylinders were only attached to the hull and not the frame.

Wall Thickness Study Test Results

Before delving into the effects of wall thickness on acceleration, the results from the two tests comparing commercially produced aluminum cans to the shim stock cans will be analyzed. It was observed that there was no splitting of the shim stock cans at the seam. The cans crumpled as effectively as a commercially produced can as well. The test results for acceleration and velocity from the first integration of the acceleration are shown in Table 5.

Table 5: Test results for commercial versus shim stock cylinders

Test Number	# of Cylinders	Cylinder Material	Cylinder OD (mm)	Cylinder Wall Thickness (mm)	Height of Target (mm)	Avg Peak Accel (g's)	Avg Peak Velocity (m/s)
1	4	Aluminum (Commercial)	66	0.1	25	183	4.225
2	4	Aluminum (Shim)	66	0.1	25	182.75	4.235

From looking at Table 5 it is very clear that the thin-walled cylinders produced from shim stock perform the same as the commercially produced, seamless cans. As such, the test series studying the effects of wall thickness can be directly compared to the tests studying the effects of height of target, number of cans, and outer diameter. It is also beneficial in that, as will be seen later, cylinders from other materials might be made in a similar method and compared to the earlier mitigation studies.

The next graph will highlight the differences in the acceleration signal. Similar to the instance when the number of cylinders was increased, as the wall thickness increases, the low frequency frame vibration seems to diminish. Though not as drastic of a damping effect as increasing the number of cans, it is still recognizable. The easiest way to highlight this low frequency frame vibration damping effect is to study the Fourier Spectra for each of the three wall thicknesses. Refer to Figure 14 to witness the weakening of the low frequency frame vibrations as the walls of the cylinder become thicker.

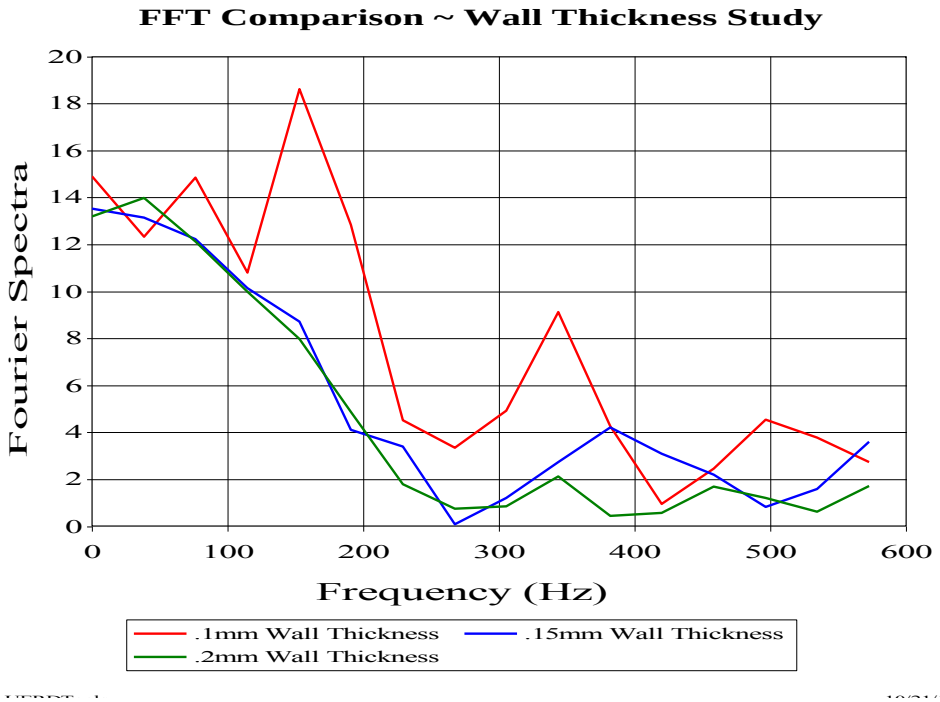

Figure 14: Fourier Spectra comparison for tests in the wall thickness study

In addition to the dampening of the low frequency frame vibrations, it appears as if increasing the wall thickness of the mitigation cylinders hold other benefits as well. To illustrate, the plots showing the acceleration of the frame for all of the tests

performed are reported here. Figure 15 displays the three test outputs as a function of increasing wall thickness of each mitigation cylinder.

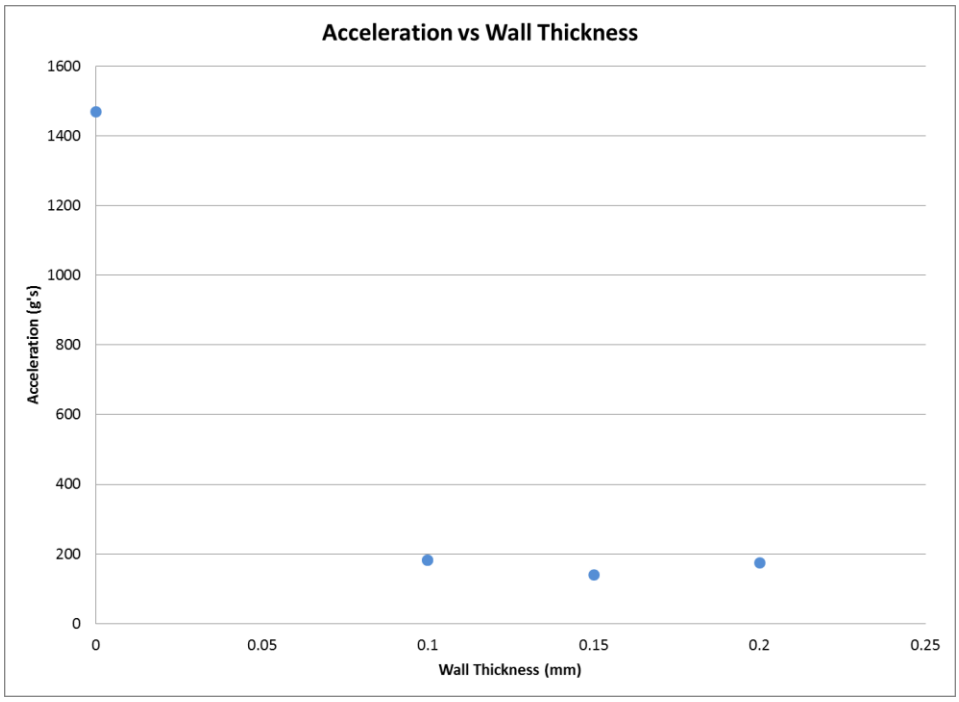

Figure 15: Acceleration versus wall thickness of mitigation cylinders

The initial indication from viewing Figure 15 is that the cylinder wall thickness has little notable effect. A minor decrease in acceleration accompanying the increase in wall thickness from .1 to .15 millimeters is directly followed by an increase of the same magnitude with an increase in wall thickness from .15 to .2 millimeters.

The final result stemming from the wall thickness study comes as a visual observation. After each test the cylinders are inspected to make sure no tearing of the can occurred. At this point it was noted that the cans crushed in significantly different ways as the wall thickness increased. Pictures of each platform of cylinders (post-test) are shown in Figure 16. From these photos it is noted that the .1 millimeter thick cylinders crushed completely with many folds in the material. The .15 millimeter can underwent semi-complete crushing with nice folds in the material as well. At the point when the wall thickness reached .2 millimeters, it is noted that the cylinder does not undergo complete crushing and that there are a few larger areas on the surface of the can that show little or no plastic deformation.

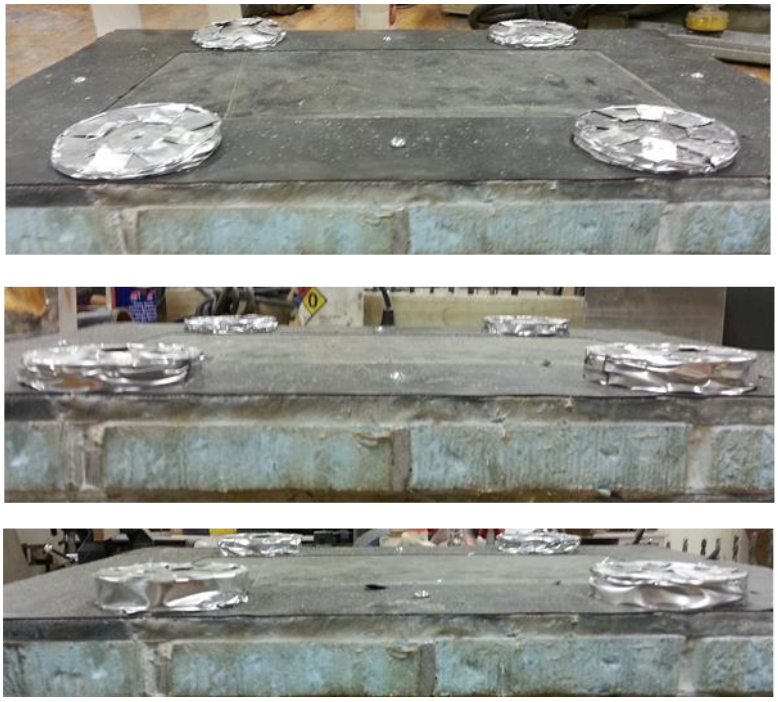

Figure 16: Crushing characteristics of .1mm (top) .15mm (middle) and .2mm (bottom) wall thickness cylinders

Cylinder Material Study

The next series of tests conducted was very brief. The series aimed at viewing the effects of changing the metal material of the thin-walled cylinders. To achieve this, steel cylinders with the same wall thickness and outer diameter as the aluminum cylinders were created. The test results are shown below in Table 6.

Table 6: Test results for cylinder material study

Test Number	# of Cylinders	Cylinder Material	Cylinder OD (mm)	Cylinder Wall Thickness (mm)	Height of Target (mm)	Avg Peak Accel (g's)	Avg Peak Velocity (m/s)
1	4	Aluminum (shim)	66	0.1	25	183.0	4.2
2	4	Steel (Shim)	66	0.1	25	203.3	3.8

From viewing the results in Table 6, it is seen that the difference between the two types of cylinders is minor. Due to the fact that the steel cylinders did not make a remarkable difference, for better or for worse, it was decided to spend effort studying other areas as opposed to creating cylinders out of various other materials. This concludes the portion of the research involving using thin-walled cylinders for mitigation of acceleration on small-scale vehicles.

Effects of cylinder geometry and number of impulse and kinetic energy

Though not covered in detail in this paper, the change in kinetic energy and impulse of the target plate should be mentioned briefly.

Regardless of the various HOT scenarios tested, the impulse imparted to the frame saw a decline in the neighborhood of 15 percent when compared with the baseline (no mitigation) tests. Kinetic energy decreased by close to 30 percent, compared with the corresponding test with no mitigation present, for each HOT.

With six cylinders used as mitigation, the impulse decreased by approximately 25 percent of the value of impulse resulting from a test with no mitigation. A larger decrease in kinetic energy of approximately 50 percent occurred when using six cylinders as opposed to no mitigation.

The largest outer diameter cylinder had a decrease of 15 percent compared with the impulse value obtained with no mitigation. The kinetic energy of the simulated vehicle with the largest outer diameter cylinders declined by 30 percent compared to the kinetic energy from the test with no mitigation.

The final series of tests studied the effect of changing the wall thickness of the cylinders. The minimum impulse occurs at a wall thickness of .2 millimeters and dropped 27 percent in relative to the maximum value of impulse when no mitigation is present. Similarly, the kinetic energy is lowest for a cylinder wall thickness of .2 millimeters and reduced the value of the no mitigation case by 48 percent.

Coated Cylinder Blast Test Study

To better understand the dynamic effects of coating structures with polyurea, a number of thin-walled cylinder crushing tests were run. Since crushing of thin-walled cylinders has already been proven to be an effective means of mitigation using small-scale vehicle shapes, a more practical means of comparison between non-coated and coated cylinders was developed. This series of tests utilized a single thin-walled cylinder in between two circular aluminum plates. The aluminum plates are termed the hull (bottom) and the frame (top); the same as the scaled vehicle testing. The plate characteristics are listed in Table 7.

Table 7: Polyurea coated cylinder test plate characteristics

Frame Material	Frame Diameter (cm)	Frame Thickness (cm)	Frame Mass w/ Targets and accels (kg)	Hull Material	Hull Diameter (cm)	Hull Thickness (cm)	Hull Mass (kg)	Total Plate Mass (kg)
Alum 6061	16.51	2.74	1.43	Alum 6061	16.51	2.82	1.27	2.74

The thin-walled cylinder was created from aluminum shim stock with a polyurea coating applied onto the outer walls. A specific mass of polyurea for each test is mixed and applied to the prepared shim stock surface using a small paint brush. Each test was conducted with a pre-determined mass ratio of polyurea to aluminum substrate.

The polyurea used for this portion of the research is manufactured by Specialty-Products, Inc. and is designated HM-VK. It is an ultra-high strength hand-mixable polyurea elastomer. This specific polyurea was chosen for its high gel-time of 18 minutes and lower viscosity. These two properties allow the polyurea to be used in a mold to accurately create test specimens for this study. A description of the dry

properties of the polyurea (as obtained from the HM-VK technical data sheet) is shown in Table 8.

Table 8: Polyurea dry properties for HM-VK [27]

DRY PROPERTIES @ 125 mils (1.67 mm)*	
Tensile Strength ASTM D412	6671 PSI (46.36 mpa) Average
Elongation ASTM D412	506% Average
Hardness (Shore A) ASTM D2240-81	95 (0s)
Hardness (Shore D) ASTM D2240-81	48 (0s)
Modulus 300% ASTM D412	1395 psi (9.7 mpa)
Service Temperature	-30°F - +250°F (-34°C - +121°C)

Tests for this study are conducted using stand-off blocks set to 40 millimeters in height. A 2.2 gram charge is buried at ten millimeters in a saturated sand bed prepared as previously described. The thin-walled cylinders are connected to the hull only, and the frame is equipped with four targets for high speed video tracking and two accelerometers on opposite sides of the plate. A sample test plate is seen in Figure 17.

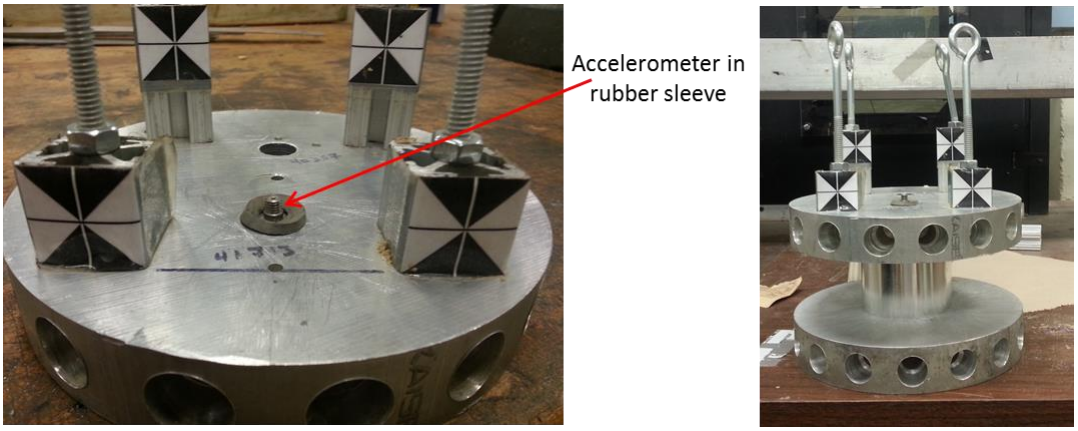

Figure 17: Accelerometer placement (left) and plate set-up (right) for coated can tests

Before describing the tests conducted for this study it should be noted that this series of tests aims only at describing the differences in acceleration of the frame that arise from coating thin-walled cylinders with polyurea. The charge mass has been decreased to result in manageable acceleration signals but the other test characteristics have remained the same. As such the test results are not meant to be indicative of full-scale levels experienced by a passenger in a vehicle that experiences blast loading. The variable that changed and is reported here is the mass ratio of polyurea applied to the thin-walled cylinder. The test matrix for this study is seen below in Table 9.

Table 9: Test matrix for polyurea coated can study

Test Number	Charge Mass (g)	DOB (mm)	SOD (mm)	# of Cylinders	Cylinder Material	Cylinder OD (mm)*	Cylinder ID (mm)*	Cylinder Height (mm)*	Cylinder Mass (g)*	Polyurea Mass (g)	Mass Ratio (Poly/Alum)
2	2.2	10	40	1	Aluminum	66	65.8	38.1	3.07	0	0.00
3	2.2	10	40	1	Aluminum	66	65.8	38.1	2.89	0	0.00
4	2.2	10	40	1	Aluminum	66	65.8	38.1	6.95	3.88	1.27
5	2.2	10	40	1	Aluminum	66	65.8	38.1	7.1	4.03	1.32
6	2.2	10	40	1	Aluminum	66	65.8	38.1	10.65	7.58	2.48
7	2.2	10	40	1	Aluminum	66	65.8	38.1	11.28	8.21	2.68
10	2.2	10	40	1	Aluminum	66	65.8	38.1	18.12	15.05	4.92
11	2.2	10	40	1	Aluminum	66	65.8	38.1	18.75	15.68	5.12
*Note: Values reported with an * denote those takes of the shim stock cylinder before the coated in polyurea											

Coated Cylinder Study Test Results

Similar to the mitigation studies conducted with the thin-walled cylinders, the initial test for test validity is the comparison of the displacement curve developed from the tracking of the targets using high speed video with that of the double integrated acceleration signal. It should be mentioned that due to the small size and weight of the test plate, slight offsets in charge location or plate placement resulted in significant rotation of the frame. As such the accelerometer displacement was plotted alongside all four target displacement curves to make sure it fell in among them. Samples of the acceleration signal along with the displacement curve comparison are shown in Figure 18 and Figure 19. The displacement signals from the high speed camera and the accelerometer match very nicely. This same level of agreement is required for the test results to be considered valid and worthy of reporting.

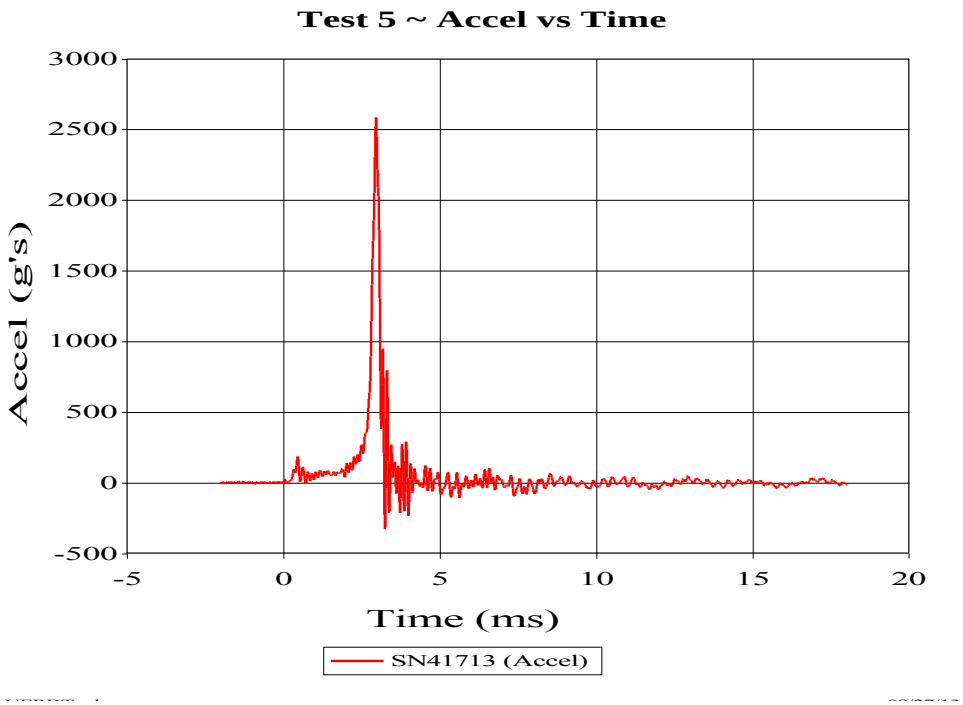

Figure 18: Acceleration signal from a polyurea coated cylinder test

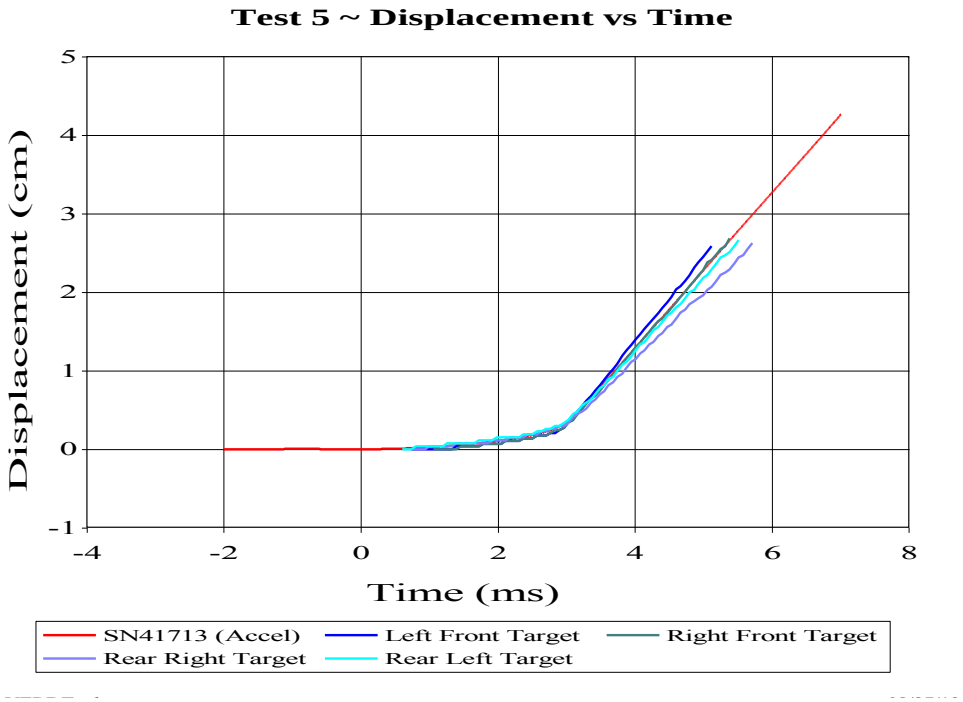

Figure 19: Accompanying displacement versus time curve comparison for accelerometer and camera data

Another area of interest is viewing how the acceleration signal changes with the increasing mass of polyurea applied to the thin-walled cylinder. To this end a sample

signal from one accelerometer for four testing scenarios is plotted on the same graph. The result is shown in Figure 20.

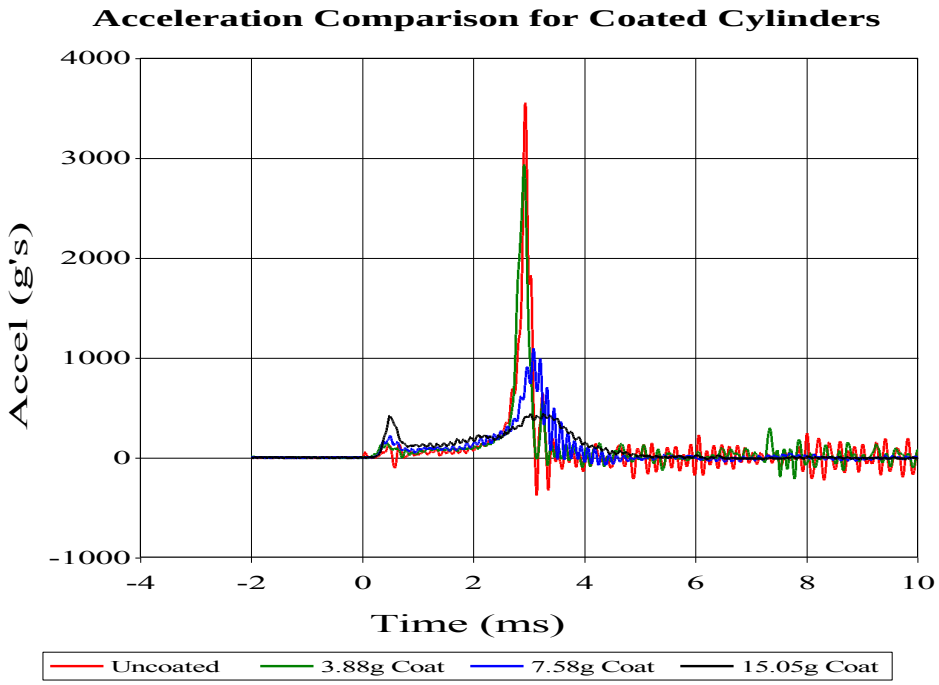

Figure 20: Acceleration signal comparison for various coatings

From studying Figure 20 a couple of observations can be made. The first and most obvious is how the peak acceleration decreases as the mass of polyurea applied to the cylinder increases. The second is that the time over which the acceleration pulse is delivered stretches out as the mass of the coat increases. So though the acceleration signal is lower it is delivered over a significantly larger period of time.

It might be helpful to view the final deformed state of each of the testing scenarios. At the end of each test, the cylinder was detached from the hull and compared with the other test cylinders. It was noted that as the mass of the polyurea coating increased, the recovered height of the cylinder also increased. A visual of the final cylinder deformations (post-test) is presented in Figure 21.

Figure 21: Front view of crushed cylinders increasing in polyurea mass from left to right

From Figure 21 it is clearly seen that as the mass of polyurea applied to the aluminum base increases, the final deformation of the can decreases. It should be noted that each cylinder underwent severe crushing in every test. After the initial crushing, the cylinders with the polyurea coating rebounded and recovered a portion of their initial

height. There was no delamination of polyurea from the metal substrate noted in the thinner coats, and only minor delamination of the polyurea from the aluminum as the mass of the polyurea increased. A measurement of the height of the crushed cylinder was made in each scenario and averaged to determine how much height each cylinder recovered after the blast event. These results are shown in Table 10.

Table 10: Recovered height of blast-tested polyurea-coated cylinders

Test Number	Approximate Mass Ratio (Polyurea/Aluminum)	Initial Cylinder Height (mm)	Post-Test Cylinder Height (mm)
2 & 3	0	38	6.7
4 & 5	1.3	38	16
6 & 7	2.5	38	31
10 & 11	5	38	35

Finally a comparison between the acceleration is made by plotting against the mass ratio of polyurea to aluminum of each cylinder. This plot is shown in Figure 22.

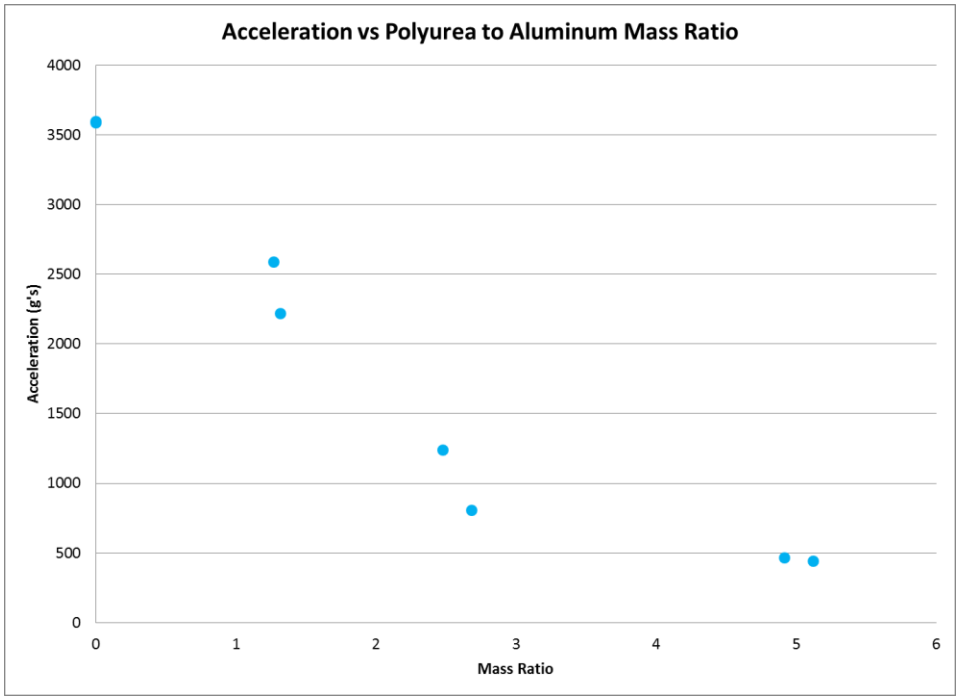

Figure 22: Acceleration versus mass ratio for coated cylinders

From viewing the graph a few observation can be made. The first and most important is how much of a decline in acceleration is obtained through coating thin-walled cylinders with polyurea. Studying Figure 22 it is noted that by adding the mass of the metal substrate in the form of a polyurea coating (resulting in a 1:1 mass ratio), the acceleration levels of the frame can be reduced by 30 percent of the value experienced by the frame that utilized only an uncoated cylinder. In the wall thickness study it was noted that only marginal gains were made by doubling the wall thickness, and thus the cylinder mass. Also it should be noted that the mass of the cylinders is negligible compared to the mass of the hull/frame combination. Though

not reported in detail here it was found that increasing the mass ratio on the thin-walled cylinders did not affect the impulse and kinetic energy of the frame.

Polyurea Coated Cantilevered Beam Test Study

This section of this research aims at developing a better understanding of the effects of polyurea coatings structures subjected to dynamic loading. Cantilevered beams coated in polyurea were tested using a high-pressure gas gun. Beams with varying thicknesses and mass ratios of polyurea were all tested.

In addition to being viewed by high speed camera, each beam test was conducted with an accelerometer mounted to the end of the beam for data collection purposes. A photograph of the final beam configuration is seen in Figure 23.

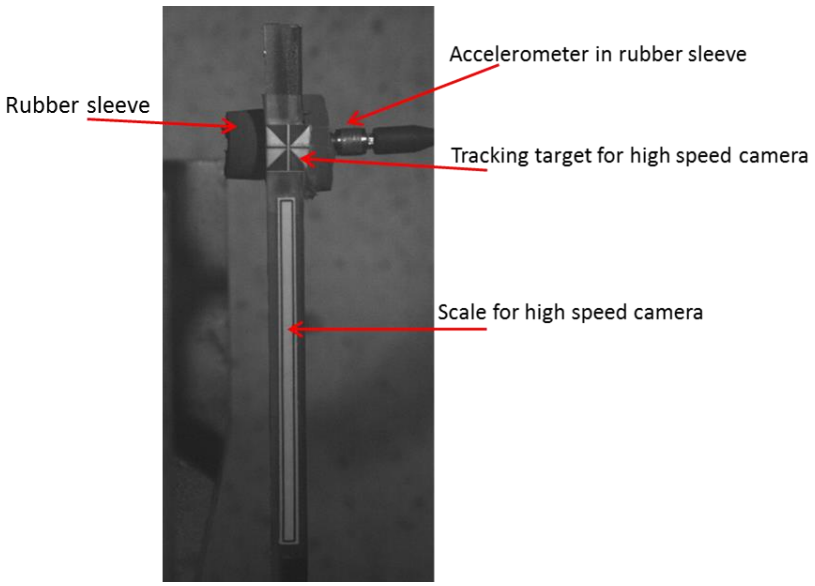

Figure 23: Beam set-up for cantilever beam tests

By mounting the accelerometer in the rubber sleeve as shown in Figure 23, the accelerometer moves with the neutral axis of the beam and does not incur any transverse motion during the test. As a result, it was discovered that the displacement curves determined from the accelerometer and high speed camera match perfectly (Figure 24). In order for test results to be reported, the displacement versus time curves developed from the double integrated accelerometer data and the high speed camera must match similarly.

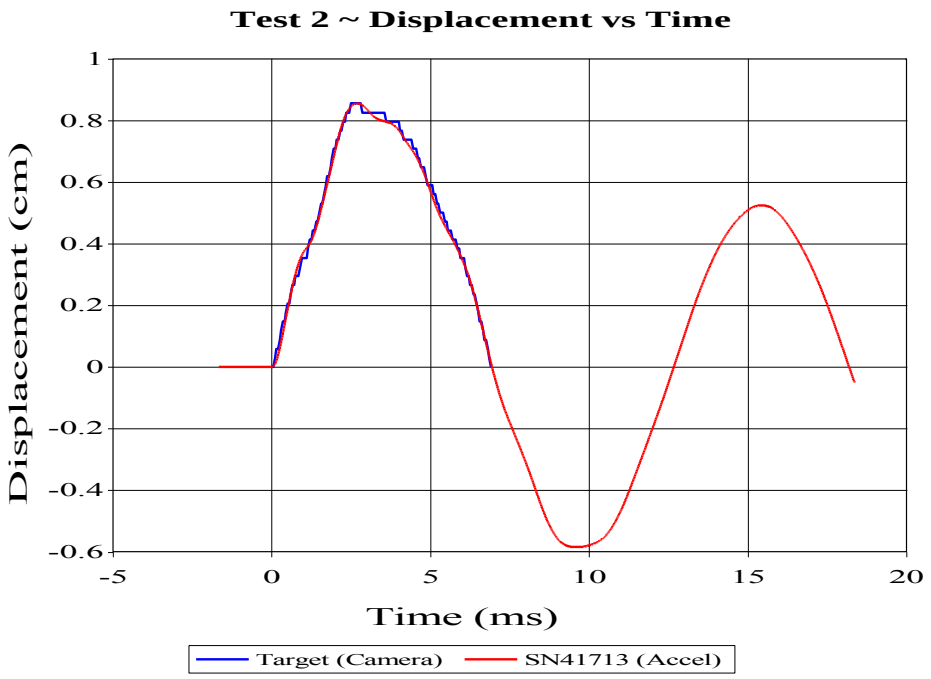

Figure 24: Example of a displacement versus time comparison for rubber mounted accelerometer

Preliminary Polyurea Beam Tests

Before going into each specific series of tests for the polyurea coated beams, it is necessary to specify how each beam will be placed in the cantilever support in relation to the oncoming projectile. The first item of note is that each beam is 25.4 centimeters long with the first 2.54 centimeters being secured in the cantilever support. The axis of the accelerometer is placed 2.54 centimeters below the tip of the beam. Each beam is placed such that the projectile fired from the gas gun hits the tip of the beam in the center of the beam width so that the beam does not twist upon impact.

A number of beam set-ups were tested to determine which face of the bar (the metal side or the polyurea side) should be contacted with the projectile. Three different scenarios were tested: projectile contacting the steel (polyurea in compression), projectile contacting the polyurea (polyurea in tension), and the polyurea at the area of contact ground off so that the projectile contacted the steel but still put the polyurea in tension. The situation of these preliminary tests is shown in Figure 25.

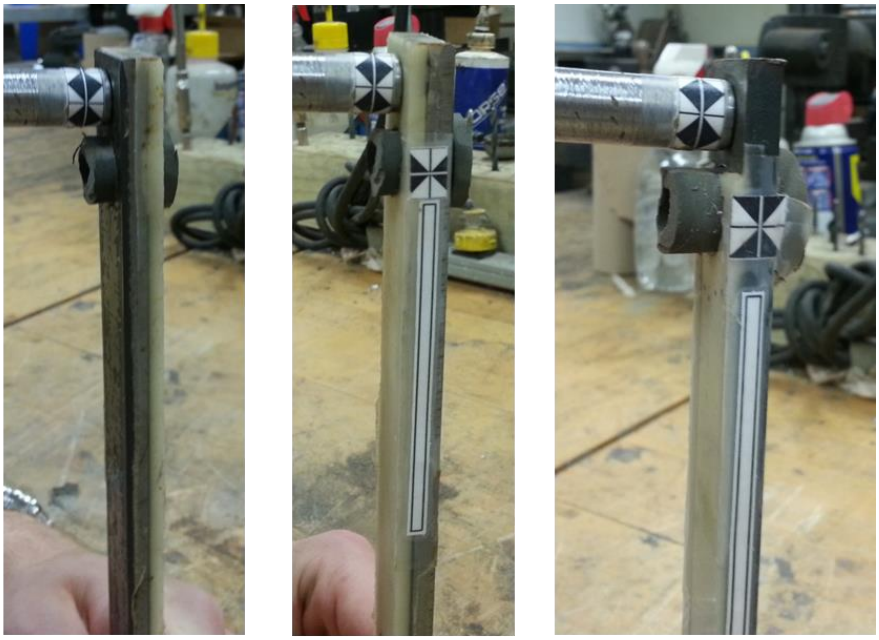

Steel side contact | Polyurea side contact | Steel contact on polyurea side

Figure 25: Contact configuration for preliminary polyurea tests

Preliminary Beam Test Results

Only the peak acceleration will all be reported for each test. The results of situating the beam in the cantilever for the three scenarios portrayed in Figure 25 are displayed in Figure 26. Each configuration was tested twice to determine test scatter. The blue bars show the values for the initial tests and the red bars give the value for the repeat test for each scenario.

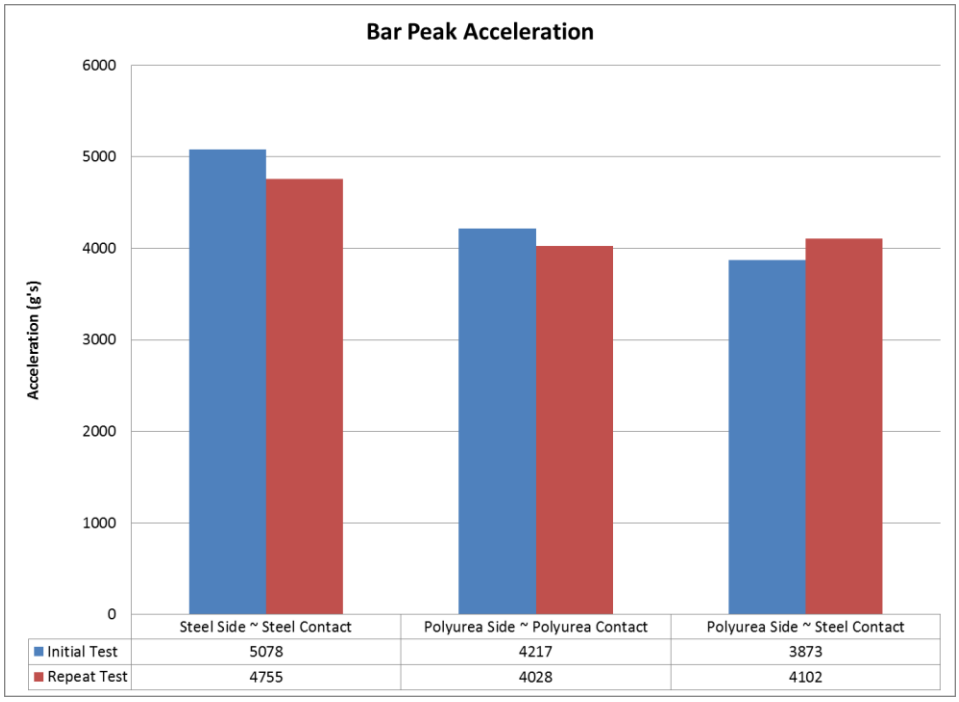

Figure 26: Peak acceleration for preliminary polyurea beam tests

From looking at the figure it is noted that situation of the polyurea side to the oncoming projectile only has a slight effect on acceleration. The slight benefit in acceleration values results from the bar being placed so that upon initial deflection of the beam, the polyurea is put into tension. There does not appear to be any effect on any test output when the polyurea at the tip of the beam is removed, resulting in a projectile to steel interaction. As such, each of the cantilevered beam tests in what follows were conducted with the polyurea side facing the projectile, without removing the polyurea from the tip of the beam.

Cantilevered Beam General Study

The first series of tests run for polyurea coated bars studied the effects of increasing polyurea thicknesses on steel beams of the same outer dimensions. Baseline tests were run with two different bare steel beams to determine the variance in behavior for two different beams of steel cut from the same bar. After these initial tests, three different thicknesses of polyurea were applied to steel beams and tested.

As a quick note, looking at Figure 25, it is seen that there is a target taped to the end of the projectile. For each test the projectile is tracked for an inch of travel using high speed video. The slope of the displacement versus time curve for the projectile is determined to be the velocity of the projectile for each test, and must be in the range of 8.4-8.6 meters per second in order for the test to be accepted. The outline of the tests for the general study is seen in Table 11. Each test is performed twice to display data scatter and repeatability.

Table 11: Test matrix for general polyurea thickness study

Test Number	Bar Number	Steel Mass (g)	Polyurea Mass (g)	Total Mass (w/ accel) (g)	Bar Thickness (mm)	Polyurea Thickness (mm)	Total Thickness (mm)
4	3	302.6	0	314.1	6.22	0.00	6.22
6	3	302.6	0	314.1	6.22	0.00	6.22
8	1	300.3	0	312.5	6.20	0.00	6.20
9	1	300.3	0	312.5	6.20	0.00	6.20
17	2	301.5	12.6	326.8	6.23	1.58	7.81
18	2	301.5	12.6	326.8	6.23	1.58	7.81
24	1	300.3	18.3	329.7	6.20	3.11	9.30
25	1	300.3	18.3	329.7	6.20	3.11	9.30
27	3	302.6	21.4	334.6	6.22	4.76	10.97
28	3	302.6	21.4	334.6	6.22	4.76	10.97

General Study Test Results

At the conclusion of the general study series of tests, as in the preliminary tests, peak acceleration was analyzed and plotted. The graph is shown in Figure 27. The figure shows a very interesting and unexpected result. The tip acceleration of bars coated in polyurea increases with polyurea thickness, and at the final thickness (with the polyurea about two millimeters thinner than the steel) the acceleration level is around 1000g's higher than the baseline steel bar.

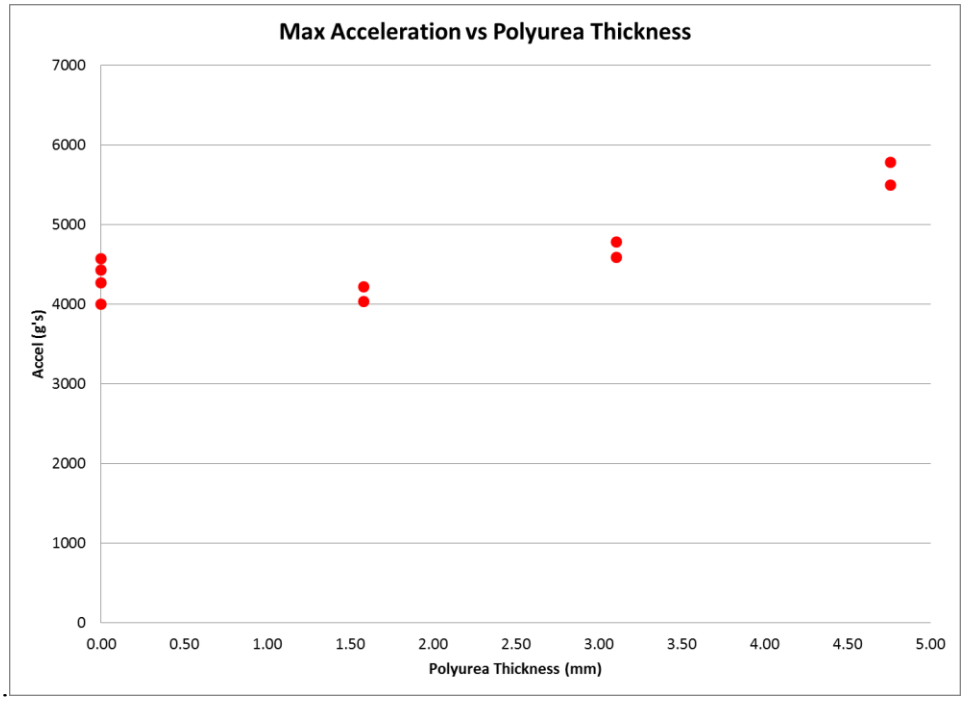

Figure 27: Peak acceleration versus polyurea thickness

Cantilevered Beam Mass Study

After having seen the unexpected trend in polyurea coated beams, it was determined that a series of tests should be run to further explore this behavior. To this end a set of tests was conducted where the mass of each bar was kept constant as the polyurea mass increased. This was performed by using a mill to shave specific thicknesses of metal off of steel beams. A polyurea coat having the same mass as the removed steel was then applied to each beam. The mass of the each beam was kept at the mass of the baseline beam from the first series of tests. The tests were run in the same configuration as the previous series of tests. The matrix of tests is seen in Table 12.

Table 12: Test matrix for polyurea beam mass study

Test Number	Bar Number	Steel Mass (g)	Polyurea Mass (g)	Total Mass (w/ accel) (g)	Mass Ratio (Polyurea/Steel)	Bar Thickness (mm)	Polyurea Thickness (mm)	Total Thickness (mm)
a	3	302.6	0	314.1	0.000	6.22	0	6.22
b	3	302.6	0	314.1	0.000	6.22	0	6.22
c	1	300.3	0	312.5	0.000	6.20	0	6.20
d	1	300.3	0	312.5	0.000	6.20	0	6.20
12	6	281.8	23.4	316	0.083	5.88	3.49	9.37
15	6	281.8	23.4	316	0.083	5.88	3.49	9.37
17	4	273.9	25.8	310.2	0.094	5.68	4.33	10.01
18	4	273.9	25.8	310.2	0.094	5.68	4.33	10.01
19	5	265.2	37.8	313.8	0.143	5.46	5.88	11.34
20	5	265.2	37.8	313.8	0.143	5.46	5.88	11.34
21	5	265.2	37.8	313.8	0.143	5.46	5.88	11.34

Mass Study Test Results

As with the other two cantilever beam studies the acceleration was analyzed at the end of each test. These values were then plotted as a function of the polyurea to steel mass ratio. The results can be seen in Figure 28. It is seen that the acceleration of the beam tip increases for increasing mass ratio, though not as smoothly as it did for the general study.

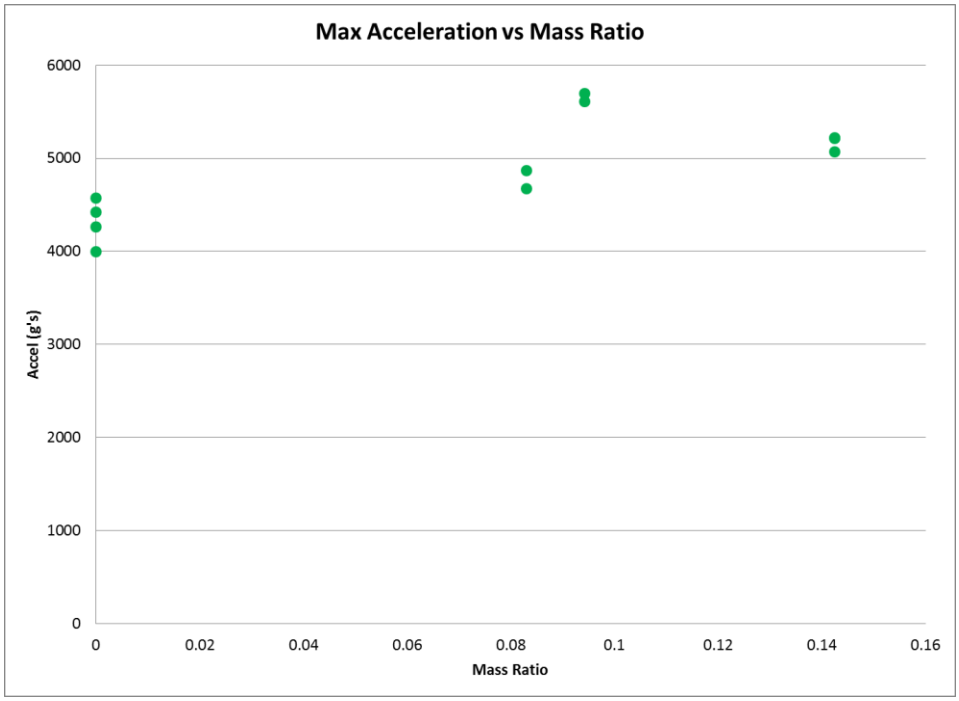

Figure 28: Peak acceleration versus polyurea to steel mass ratio

Similar Mass Ratio Cantilever Beam Study

After the completion of the polyurea-coated cylinder tests in which two plates were explosively loaded, it was seen that by coating an aluminum thin-walled cylinder with polyurea, significant benefits in the peak acceleration are realized. Referring to the results of the polyurea to steel mass ratio study performed with cantilevered beams, this positive impact of the polyurea coating on the cylinders may come as a surprise. It is seen in Figure 28 that a general increase in acceleration is expected as the polyurea to steel mass ratio of a coated beam increases.

In hopes of clarifying this result, a final series of cantilever beam tests were carried out. It was noted that the mass ratios of the beam tests and the cylinder tests were not equivalent with the beams having a polyurea to steel mass ratio in the neighborhood of .08-.15 while the cylinders had a mass ratio anywhere from one to five. To create a more equivalent series of tests, it was necessary to process cantilever beams with a mass ratio in the same neighborhood as that of the cylinders.

These beams were created by cutting the mass of the metal base of the beam by switching the metal from steel to aluminum, and also by decreasing the thickness of the metal from 6.2 millimeters to 3.18 millimeters. An uncoated beam was tested in addition to two beams with mass ratios in the desired range. The test matrix can be seen in Table 13. Each beam was tested twice to show data scatter and repeatability.

Table 13: Test matrix for similar mass ratio cantilever beam study

Test Number	Beam Number	Beam Thickness (mm)	Beam Mass (g)	Polyurea Thickness (mm)	Polyurea Mass (g)	Beam Length (cm)	Beam Total Mass w/ accel (g)	Polyurea/Steel Mass Ratio
1	1	3.18	54.81	0	0	25.4	65.93	0
2	1	3.18	54.81	0	0	25.4	65.93	0
3	2	3.18	54.81	7.77	48.1	25.4	65.93	0.88
4	2	3.18	54.81	7.77	48.1	25.4	65.93	0.88
5	3	3.18	53	14.01	95.5	25.4	159.3	1.80
6	3	3.18	53	14.01	95.5	25.4	159.3	1.80

Similar Mass Ratio Cantilever Beam Study Test Results

At the conclusion of the tests mentioned in Table 13, the acceleration is studied as a function of mass ratio. Two tests are conducted for each beam, and these results are shown in Figure 29.

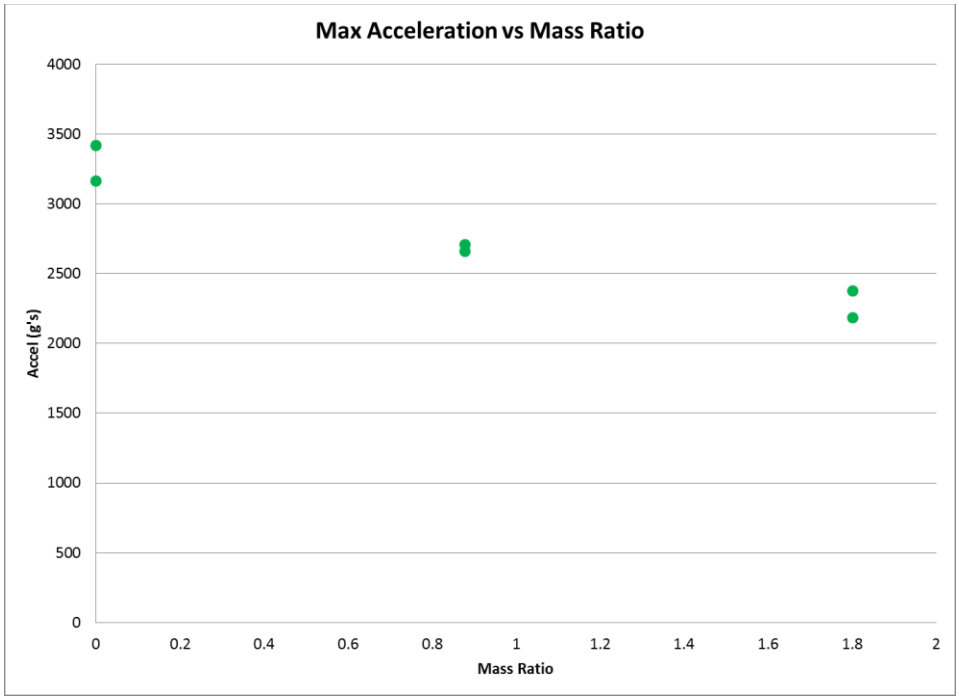

Figure 29: Peak acceleration versus mass ratio for aluminum cantilever beam tests

From viewing the previous figure and comparing it with the trends developed in the steel cantilevered beam tests, it is apparent that a completely different trend has emerged. Whereas the beams with a mass ratio much less than one see increases in the peak acceleration, the beams with mass ratios greater than one see decreases in the same parameter

To develop a better understanding of how all of the polyurea coating results line up, the acceleration values for each series of tests were normalized by setting the acceleration of the uncoated bar or cylinder as the baseline value, and dividing each acceleration value in the series by the acceleration of each test series' respective baseline value. By doing this, a plot was developed that directly compares the effect on acceleration of coating structures in polyurea. This plot is shown in Figure 30.

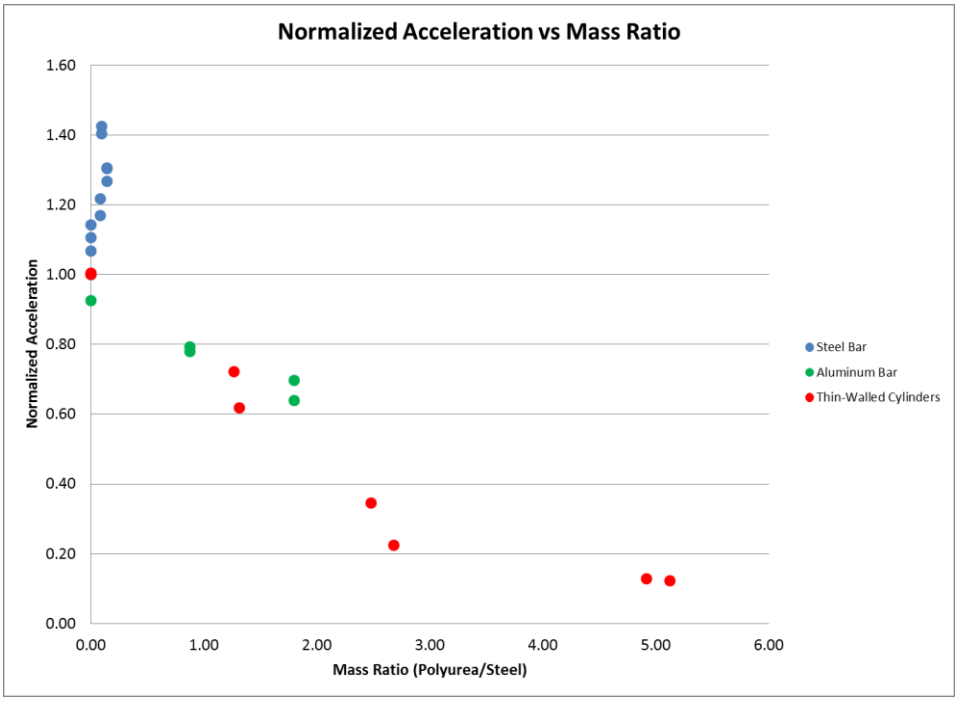

Figure 30: Normalized acceleration versus mass ratio for three test series

In Figure 30, blue is the cantilevered beam tests conducted with steel bars, the red represents the thin-walled cylinders which were blast tested, and green shows the acceleration value of the aluminum cantilevered beams. From this figure, the conclusion is made that the mass ratio of a coated structure has significant importance when considering the possibility of the coating to have an effect on peak acceleration of a structure. Very small mass ratios may indeed have a detrimental, or no, effect on the ability of a structure to effectively absorb a blast load, while a mass ratio greater than one has a positive effect. This result is of significant value as steel plates are a commonly coated material. In order for the coating to have positive effects, an extremely thick coating would have to be applied. On the other hand, when considering very light structures, such as the thin-walled cylinders used in this study, a small amount of polyurea may have a very large effect.

Polyurea-Coated Thin-Walled Cylinder Tests on a Simulated Vehicle

In this section two tests were run using the simulated vehicle set-up previously described. The first test involved connecting the hull of the vehicle to the frame with six aluminum columns. This test served as a "worse-case" scenario in which there was a rigid connection between the hull and the frame. Each column was connected to the hull and the frame. A blast test, using a 40 millimeter SOD and a ten millimeter DOB was performed in the saturated sand test bed described in the mitigation chapters.

The second and final test performed for this section used six thin-walled cylinders coated with polyurea as the connecting elements between the hull and the frame. Each thin-walled cylinder was created with .1millimeter aluminum shim-stock with a height of 38 millimeters and a 66 millimeter outer diameter. All six cylinders were coated with three grams of polyurea, resulting in an approximately one to one

polyurea to aluminum mass ratio. The cylinders were connected to both the hull and the frame so that the cylinders could crush and stretch during the test, maximizing the amount of acceleration mitigation they have to offer.

As in each of the previous simulated vehicle tests, a 4.4 gram charge is used to supply the blast load. Two accelerometers are embedded in rubber mechanical filtering mounts and four targets on the frame are used for high-speed video tracking. Pictures of the two plate set-ups can be seen in Figure 31 and Figure 32.

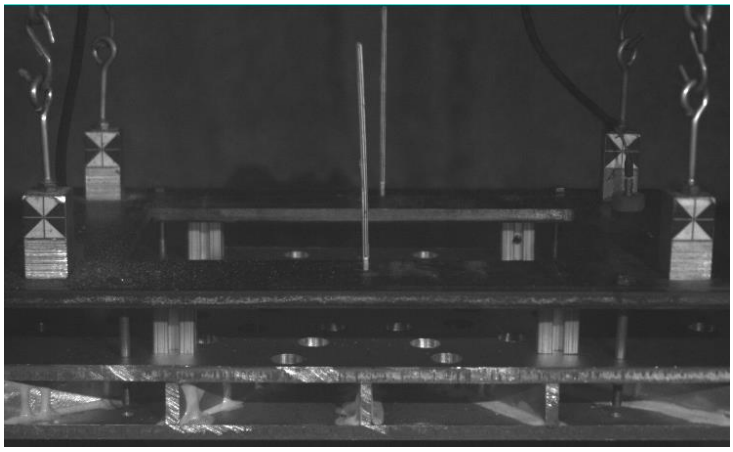

Figure 31: Plate set-up for solid column test

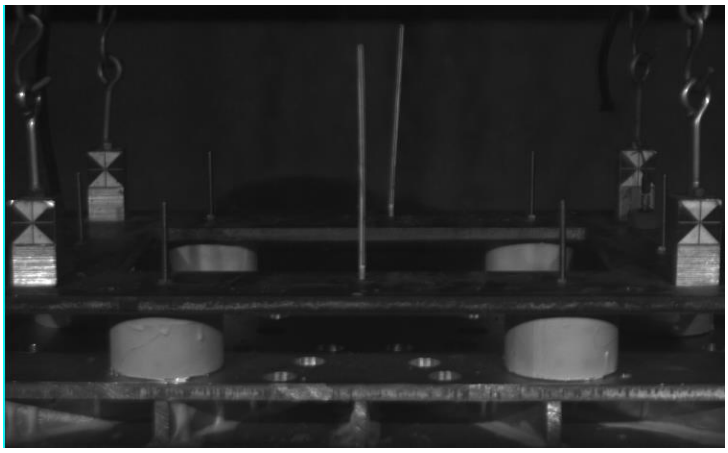

Figure 32: Plate set-up for polyurea-coated cylinder test

Polyurea-Coated Thin-Walled Cylinder Test Results

After completing each of the two tests, the initial data verification steps were taken by comparing the displacement curve developed from the high speed video to the double integrated acceleration signal. In order for the data to have been considered worthy of reporting, the two displacement signals must show strong correlation.

Once the acceleration data has been verified, it is of interest to compare the two acceleration profiles for each test. To this end, the acceleration profile was taken from the same accelerometer for each of the two tests and plotted on the same graph.

The comparison between the non-deforming column test and the polyurea-coated thin-walled cylinder test is shown in Figure 33.

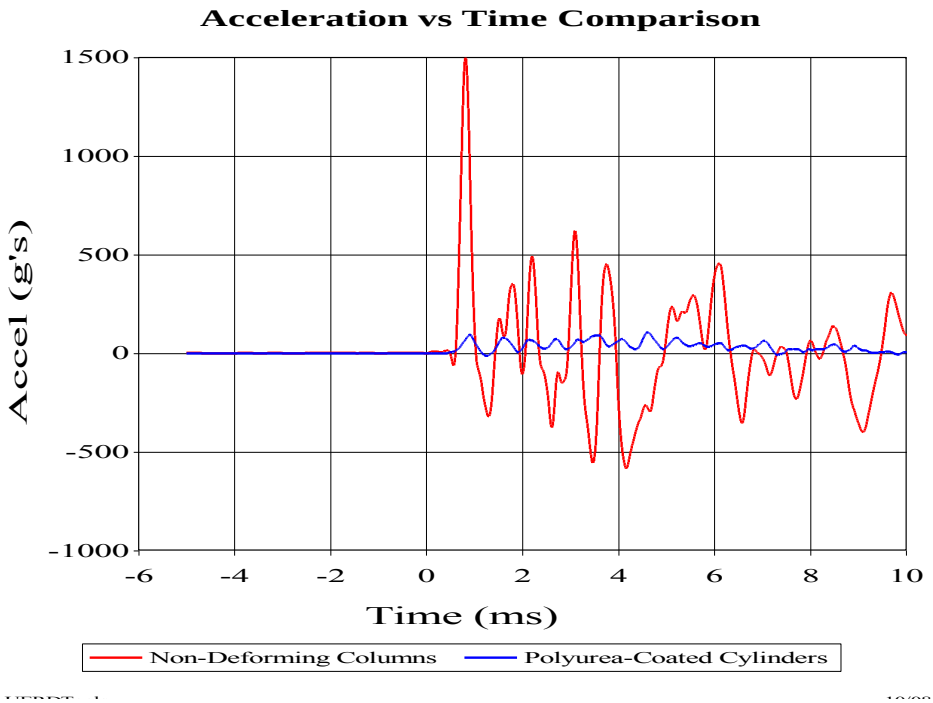

Figure 33: Acceleration versus time comparison for non-deforming columns and polyurea-coated cylinders

It is evident from viewing Figure 33 that an immense benefit comes from using thin-walled cylinders as a mitigation technique. This information however was already known from previous tests. Perhaps a more telling comparison can be made by studying how the accelerations of the simulated vehicle frame compare between the coated and uncoated cylinder tests. To perform this comparison, it is necessary to view a number of test results as a test with the cylinder number and geometry of the final test was not conducted previously in the mitigation study. As such, the information in Table 14 is presented so that a better understanding of the material may be obtained.

Table 14: Comparable test results for numerous simulated vehicle test studies

Connection Method	Number of Elements	HOT (mm)	Hull Attached	Frame Attached	Acceleration (g's)	Impulse (N-s)	Kinetic Energy (J)
Air	-	38	-	-	1458	70.56	178.00
Aluminum Cylinder	4	38	Yes	No	121.5	58.01	118.48
Aluminum Cylinder	4	38	Yes	Yes	89	51.27	89.40
Aluminum Cylinder	6	25	Yes	No	141.5	55.02	102.61
Solid Columns	6	38	Yes	Yes	1641	76.24	181.64
Coated Cylinder	6	38	Yes	Yes	108	52.96	87.65

Studying Table 14, a number of observations are made. Initially it is seen that by substituting non-deforming columns in the place of air as the material in between the hull and the frame, comparable values in terms of acceleration result. Moving

beyond these baseline comparisons, it is noted that while the polyurea coated cylinders perform admirably with extremely low acceleration, the drastic drop from the bare cylinder case is not realized. According to the tests conducted with the reduced circular plates, a 20-40 percent drop in acceleration should have occurred between the bare cylinder and the coated cylinder tests.

While slightly unexpected, the above results are not discouraging for a couple of reasons. The first reason for enthusiasm with regards to polyurea coated cylinders is due to the fact that while the bare aluminum thin-walled cylinders crushed completely during the blast tests (see Figure 16), the polyurea coated cylinders crushed approximately one-half of their height during the initial blast, and recovered over 90 percent of their initial height by the end of the blast event (see Figure 34). The relatively small initial deformation will be treated later, but at this point, the fact that the polyurea coated cylinders recover such a large percentage of their initial shape may result in a vehicle that is structurally able to drive away from a blast event.

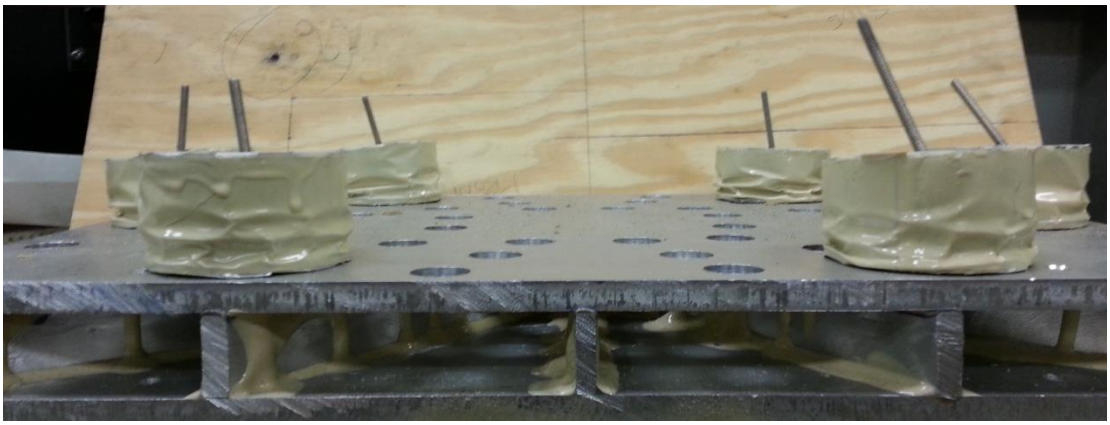

Figure 34: Recovered height of the polyurea-coated cylinders after blast testing

Looking at Figure 34, it is clearly seen that deformation of the coated cylinder occurs primarily at the lower half of the cylinder. This fact will be used in conjunction with information from the small circular plate tests to realize a further advantage of using polyurea coated cylinders as opposed to bare aluminum cylinders as a mitigation technique. The statement that needs to be made about the coated cylinder tests using the reduced-sized circular plates is that the acceleration of the baseline (uncoated cylinder) tests was dramatically greater than that of the simulated vehicle baseline (uncoated cylinder) tests. Comparing acceleration values from Figure 22 and Table 14, it is seen that the acceleration of the bare cylinder test using the circular plates and a single cylinder is in the neighborhood of 3500g's while the acceleration using bare cylinders on the simulated vehicle plates lies in the area of 100-150g's.

The increased level of loading of the smaller plates is backed up by the high speed video, in which the polyurea coated cylinders crush completely before recovering some of their height. In the case of the simulated vehicle tests, it was pointed out that the cylinders crush only partially before recovering almost all of their height. It was initially curious that a 20-40 percent acceleration drop between uncoated and coated cans did not appear in the simulated vehicle test. However, after looking at the data in its entirety, it is not that surprising, as the acceleration levels in the simulated

vehicle using bare cylinders might not be sufficient to bring out the full benefit of coating the cylinder with polyurea. The next section of the paper will study the non-linear mitigation behavior of polyurea coated thin-walled cylinders.

Nonlinear Acceleration Mitigation Benefit of Polymeric Coated Thin-Walled Cylinders

In order to tease out the previously hypothesized nonlinear acceleration mitigation benefit of polymeric coated thin-walled cylinders, a series of blast tests was run where the polyurea to aluminum mass ratio was kept constant (along with the other test parameters such as SOD and DOB) while the charge mass was varied. Tests with coated and uncoated cylinders were run to compare how the acceleration varied between the coated and uncoated cylinders as the charge size changes. The test matrix for this series of tests is shown in Table 15.

Table 15: Test matrix for nonlinear study

Test Number	Charge Mass (g)	DOB (mm)	SOD (mm)	# of Cylinders	Cylinder Material	Cylinder OD Before Coat (mm)*	Cylinder ID (mm)*	Cylinder Height (mm)*	Cylinder Mass (g)*	Polyurea Mass (g)	Mass Ratio (P/S)
1	2.2	10	40	1	Aluminum	66	65.8	38.1	5.37	2.37	0.79
2	2.2	10	40	1	Aluminum	66	65.8	38.1	5.58	2.58	0.86
3	1.75	10	40	1	Aluminum	66	65.8	38.1	5.75	2.75	0.92
4	1.75	10	40	1	Aluminum	66	65.8	38.1	5.02	2.02	0.67
5	1.25	10	40	1	Aluminum	66	65.8	38.1	5.63	2.63	0.88
6	1.25	10	40	1	Aluminum	66	65.8	38.1	5.27	2.27	0.76
7	0.75	10	40	1	Aluminum	66	65.8	38.1	5.46	2.46	0.82
8	0.75	10	40	1	Aluminum	66	65.8	38.1	5.47	2.47	0.82
9	0.75	10	40	1	Aluminum	66	65.8	38.1	3	0	0.00
10	0.75	10	40	1	Aluminum	66	65.8	38.1	3	0	0.00
11	1.25	10	40	1	Aluminum	66	65.8	38.1	3	0	0.00
12	1.25	10	40	1	Aluminum	66	65.8	38.1	3	0	0.00
13	1.75	10	40	1	Aluminum	66	65.8	38.1	3	0	0.00
14	1.75	10	40	1	Aluminum	66	65.8	38.1	3	0	0.00
15	2.2	10	40	1	Aluminum	66	65.8	38.1	3	0	0.00
16	2.2	10	40	1	Aluminum	66	65.8	38.1	3	0	0.00

A total of 16 tests were run, eight tests with cylinders having a polyurea to aluminum mass ratio of about 0.75 and eight tests with uncoated cylinders. Two tests were run for each type of cylinder at charge sizes of 0.75 grams, 1.25 grams, 1.75 grams, and 2.2 grams of explosive. The simplified hull/frame plate combination used in conjunction with a single cylinder was used to collect data. As in the other studies, in order for the data to be reported, the displacement profiles obtained from the high speed camera and the accelerometer must match.

Nonlinear Effect Results

At the conclusion of the test series to determine the non-linear acceleration mitigation effect on coating thin-walled cylinders with polyurea, two plots were created that show the effect quite clearly. In Figure 35 , the difference between the peak acceleration of the coated cylinder and non-coated cylinder is plotted for each charge mass. Figure 36 shows the final recovered height of the cylinder.

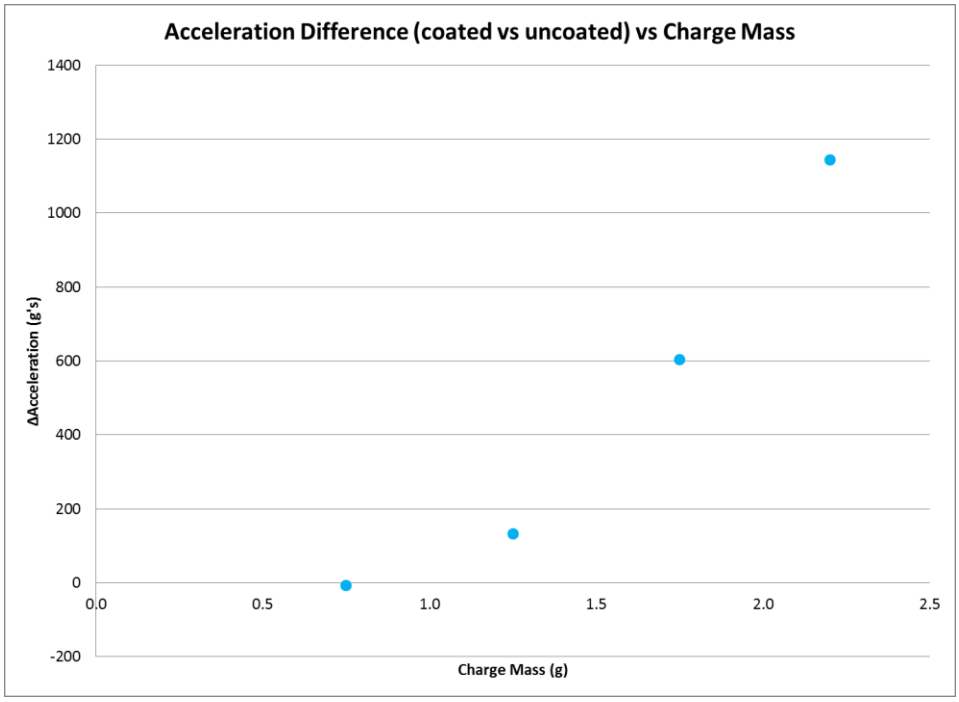

Figure 35: Difference in peak acceleration between coated and uncoated cans versus charge mass

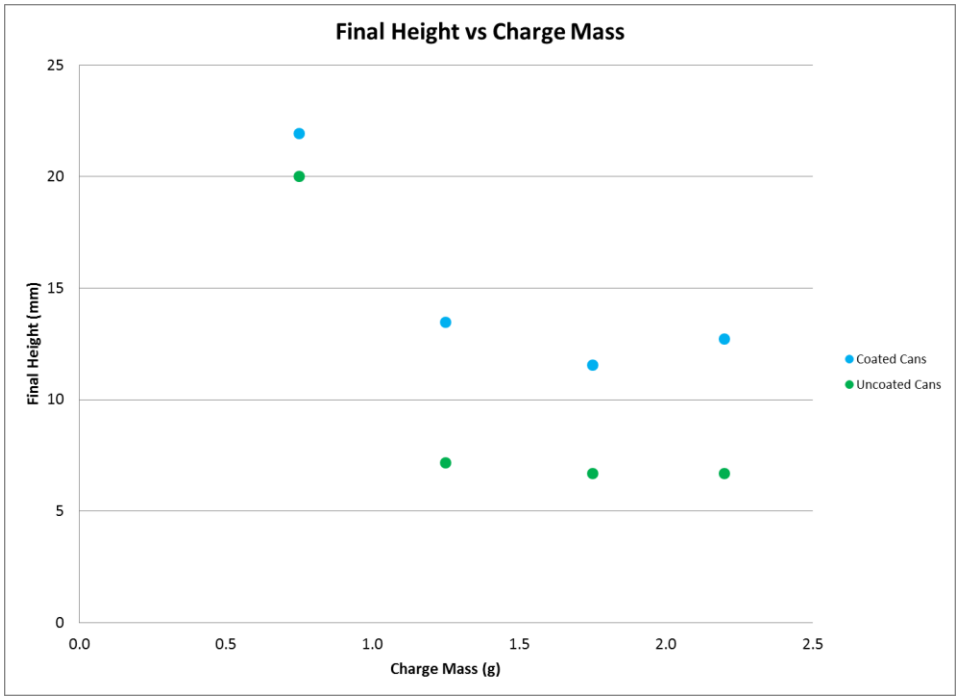

Figure 36: Final recovered height of the blast loaded cylinder versus charge mass

Looking at the previous two figures a complete picture of the non-linear effect of polymeric coatings on peak acceleration can be determined. It is seen that as charge mass increases, the recovered height of the polymeric cylinder is steadily greater than the uncoated can. It seems that during maximum crushing scenarios, coated cylinders

will recover to around a 13 millimeter height as compared with uncoated cylinders which only recover to around a seven millimeter final height. In terms of acceleration, it is seen that at smaller charge sizes, the acceleration profiles of coated and uncoated cylinders are essentially the same. However as the charge mass increases, the polyurea cylinder acts to better mitigate the acceleration of the frame.

Conclusions

At the outset of this research program a couple of broad goals were laid out. Initially it was desired to develop an effective means of acceleration mitigation for use on explosively loaded vehicles. To achieve these goals, small-scale explosive testing was conducted in saturated sand. Simulated vehicles and more simply shaped plate combinations were utilized to study the effects of various mitigation techniques.

It was shown in this paper that acceleration levels, reported at full-scale values, can be decreased from 150 g's to levels around 10 g's by application of thin-walled cylinders alone. With the addition of a polyurea coating to the thin-walled cylinders, at very high acceleration levels, an 80-90 percent decrease in acceleration may also obtained. Furthermore, numerous geometric properties of thin-walled cylinders were experimented with showing marginal differences to the baseline acceleration mitigation. It is believed that some combination of all of the best-case scenarios for each geometric condition, in addition to a polyurea coating, applied to the cylinders would result in a mitigation technique that would allow for complete survivability of an explosive event.

It was also found, though not reported in depth, that significant improvements in impulse and kinetic energy may also be made through the use of thin-walled cylinders. Previous research has been conducted in the Dynamic Effects Lab that used shaped hulls to decrease impulse on simulated vehicles to safe levels. In addition to using shaped hulls, the thin-walled cylinders may give further aid in preventing impulse related injuries to passengers in blast-loaded vehicles.

It was also desired that a greater understanding of the effects of polyurea applied to structures be developed. Some basic research was performed through the use of polyurea coated steel and aluminum cantilever beams. The cantilever beams were tested dynamically through the use of a high-pressure gas gun, and produced information leading to the following conclusion; that in the elastic range of material response to dynamic loading, bare steel has lower levels of acceleration, velocity, peak displacement, and half-wavelength time than steel bars coated with a thin layer of polyurea. For the beneficial effects of polyurea coatings to appear, the mass ratio of polyurea to metal must be increased to the order of magnitude of one or higher. It was found that at higher mass ratios, the acceleration of cantilever beams and explosively loaded plates both show similar decreasing trends as the mass ratio of the polyurea to metal increases.

Finally, a very important conclusion was made with regard to coating thin-walled cylinders with polyurea. It was seen that at low acceleration levels, polyurea coated and uncoated cylinders both mitigate acceleration equally well even if the deformation of the coated cylinder was significantly less. This minimal deformation would result in a vehicle being structurally sound enough to drive away from an

explosive event. In addition to this powerful fact, the data from a multitude of tests was used to come to the conclusion that as the explosive event becomes more violent, the polyurea coated cylinders can be expected to act to mitigate more of the acceleration, creating non-linearity in the mitigation of acceleration a vehicle by using polyurea coated thin-walled cylinders.

Bibliography

[1] Fiskum, G., Hazelton, J., Gullapalli, R., Fourney, W.L. "Animal Model of Mild Brain Injury Caused by Blast-Induced Hyper-Acceleration Relevant to IED-Targeted Military Vehicles."

[2] Nelson, N.W., Lamberty, G.J., Sim, A.H., Doane, B.M. "Blast from the Past and Present: A Review of Blast-Related Injury in Military Personnel and Veterans." *Neuropsychological Practice with Veterans* (2012): 145.

[3] Fourney, W. L., Leiste, U., Bonenberger, R., Goodings, D. J. "Mechanism of Loading on Plates Due to Explosive Detonation." Fragblast, Vol. 9, No. 4, December 2005.

[4] Genson, K. (2006). "Vehicle Shaping for Mine Blast Damage Reduction." University of Maryland: College Park.

[5] Benedetti, R., Fourney, W.L. (2010) "Mitigation of Loading on Floorboards in Light Armored Vehicles Subjected to Explosive Loading." University of Maryland: College Park.

[6] Leiste, U. (2012). "Experimental Studies to Investigate Pressure Loading on Target Plates." University of Maryland: College Park.

[7] Lamb, C., Schmidt, M., Fitzsimmons, B. "MRAPS, Irregular Warfare, and Pentagon Reform." Institute for National Strategic Studies National Defense University. Volume 6, June 2009.

[8] Alghamdi, A.A.A. "Collapsible Impact Energy Absorbers: An Overview." Thin Walled Structures, Vol. 39, No. 2, February 2001.

[9] Yuen, S.C., Nurick, G.N. "The Energy-Absorbing Characteristics of Tubular Structures with Geometric and Material Modifications: An Overview." Applied Mechanics, Vol. 69, No. 2, March 2008.

[10] Gupta, N.K., Sekhon, G.S., Gupta, P.K. "Study of lateral compression of round metallic tubes." Thin Walled Structures, Vol. 43, No. 6, December 2005.

[11] Shim, V.P.W, Stronge, W.J. "Lateral crushing in tightly packed arrays of thin-walled metal tubes." International Journal of Mechanical Science, Vol. 28, No. 10, June 1986.

[12] Gupta, N.K., Velmurugan, R. "An analysis of axial crushing of composite tubes." Journal of Composite Materials, Vol. 31, No. 13, July 1997.

[13] Palanivelu, S., Paepegem, W.V., Degrieck, J., Vantomme, J., Kakogiannis, D., Ackeren, J.V., Hemelrijck, D.V., Wastiels, J. "Comparison of the crushing performance of hollow and foam-filled small-scale composite tubes with different geometrical shapes for use in sacrificial cladding structures." Composites Part B: Engineering, Vol. 41, No. 6, September 2010.

[14] Palanivelu, S., Van Paepegem, W., Degrieck, J., Van Ackeren, J., Kakogiannis, D., Van Hemelrijck, D., Wastiels, J., Vantomme, J. "Experimental study on the axial crushing behavior of pultruded composite tubes." Polymer Testing, Vol. 29, No. 2, April 2010.

[15] Palanivelu, S., Van Paepegem, W., Degrieck, J., Reymen, B., Ndambi, J.M., Vantomme, J., Kakogiannis, D., Wastiels, J., Hemelrijck, D.V. "Close-range blast loading on empty recyclable metal beverage cans for use in sacrificial cladding structure." Engineering Structures, Vol. 33, No. 6, June 2011.

[16] Theobald, M.D., Nurick, G.N. "Numerical investigation of the response of sandwich-type panels using thin-walled tubes subject to blast loads." International Journal of Impact Engineering. Vol. 34, No.1, January 2007.

[17] Theobald, M.D., Nurick, G.N. "Experimental and numerical analysis of tube-core claddings under blast loads." International Journal of Impact Engineering. Vol. 37, No.3, March 2010.

[18] Yi, J., Boyce, M.C., Lee, G.F., Balizer, E. "Large deformation rate-dependent stress-strain behavior of polyurea and polyurethanes." Polymer, Vol. 47, No.1, January 2006.

[19] Roland, C.M., Twigg, J.N., Vu, Y., Mott, P.H. "High Strain Rate Mechanical Behavior of Polyurea." Polymer, Vol. 48, No.2, January 2007.

[20] Tekalur, S.A., Shukla, A, Shivakumar, K. "Blast resistance of polyurea based layered composite materials." Composite Structures, Vol. 84, No.3, July 2008.

[21] Ackland, K., Anderson, C., Ngo, T.D. "Deformation of Polyurea-Coated Steel Plates under Localized Blast Loading." Impact Engineering, Vol. 51, January 2013.

[22] Brodrick, T.J. "Mitigation of Frame Acceleration Induced by a Buried Charge." Diss. 2010.

[23] Fourney, W. L., Leiste, U., Bonenberger, R., Goodings, D. J. "Explosive Impulse on Plates." Fragblast, Vol. 9, No. 1, December 2005.

[24] Taylor, L.C., Skaggs, R.R., Gault, W. "Vertical Impulse Measurement of Mines Buried in Saturated Sand." Fragblast, Vol. 9, No.1, March 2005.

[25] PCB Piezotronics, Shock ICP Model: 350B04. (2013). Retrieved August 20, 2013 from <http://www.pcb.com/products.aspx?m=350B04#.UhOiuZLVAsI>

[26] RP-501 Economy EBW Detonator. (2011). Retrieved August 20, 2013 from <http://www.teledynerisi.com/products/0products_1ebw_page28.asp>

[27] HM-VK Ultra high strength handmix polyurea elastomer. (2013). Retrieved August 26, 2013 from <http://www.specialty-products.com/pdf/tech-data/polyurea/HM-VK%20Preliminary.pdf>

[28] Plunkett, R. Lee, C.T. (1968) "Length Optimization for Constrained Viscoelastic Layer Damping." Minnesota University Minneapolis Department of Aeronautics and Engineering Mechanics: Minneapolis.

[29] Bonsmann, J.M. “Small Scale Testing to Study Mitigation of Acceleration on Simulated Vehicles.” Diss. 2013.

[30] Bonsmann, J.M., Fourney, W.L. “An Examination of the Factors Affecting the Loading on a Vehicle Subjected to the Detonation of a Buried Mine.” Blasting and Fragmentation, Vol. 6, No. 3, December 2012.